CONTAIN: Integrated final results and conclusions

Deliverable D11

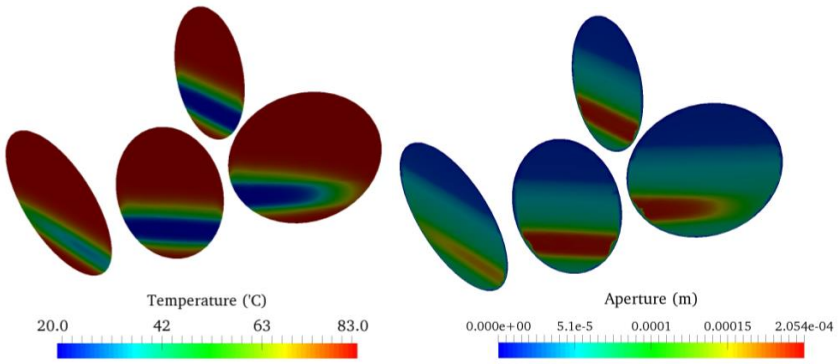

CONTAIN: Integrated final results and conclusions

DELIVERABLE D11

CONTAIN D11: Integrated final results and conclusions

Keywords

CCS; Public Perception; Reservoir Modelling; Critical State Mechanics; Reservoir; Caprock.

Front cover

Temperature and aperture distribution on faults within the reservoir layer.

Bibliographical reference

HARRINGTON, J.F., GRAHAM, C.C., DOBBS, M., CUSS, R.J., DANIELS, K.A., WISEALL, A.C., PARKES, D., PALUSZNY, A., ZIMMERMAN, R.W., SALIMZADEH, S., TSAPARLI, V., TEMPONE, P., THOMAS, R.N., XENIAS, D., AND WHITMARSH, L., 2018. CONTAIN D11: Integrated final results and conclusions. CONTAIN Report D11, 72pp.

J.F. Harrington, C.C. Graham, M. Dobbs, R.J. Cuss, K.A. Daniels, A.C. Wiseall, D. Parkes, A. Paluszny, R.W. Zimmerman, S. Salimzadeh, V. Tsaparli, P. Tempone, R.N. Thomas, D. Xenias, and L. Whitmarsh.

British Geological Survey

Imperial College

Cardiff University / Prifysgol Caerdydd

Keyworth, Nottingham British Geological Survey 2018

Foreword

This report is a deliverable for the EPSRC funded research project CONTAIN (The impact of hydrocarbon depletion on the treatment of caprocks within performance assessment for CO_2 injection schemes). The report summarises the final outcomes of the project and draws overall conclusions on the use of depleted reservoirs for the storage of super-critical carbon dioxide.

Acknowledgements

This report has been written as part of a research project funded by EPSRC (EP/K036025/1). Thanks go to the CONTAIN advisory board, who provided fruitful discussion in relation to the direction of the research over the duration of the project.

Contents

FIGURES

TABLES

Summary

Carbon capture and storage is a technology capable of reducing CO_2 outputs on a large scale; the concept usually requires CO_2 to be removed from post-combustion flue gases and sequestered in geological formations. Depleted gas fields constitute “the most important storage type for the UK” and will provide a large and important potential future offshore storage capacity (DECC, 2012). Over the last 4 years, the CONTAIN research project has focussed on the geomechanical behaviour of depleted hydrocarbon fields in response to injection with CO_2, combining a modelling and experimental approach with the public perceptions of CCS into three work packages. The project has provided a better understanding of the hydromechanical impacts of depletion on caprocks and the effect of subsequent CO_2 injection, in order to assist with the implementation of CCS in this type of reservoir.

Work package 1 outlined a phenomenological approach to assessing possible deformation during operation. Focus was placed on rock mechanics and transport experiments on material from the geologies of target formations in the North Sea, providing information that could be incorporated into numerical simulations. Work package 2 expanded this understanding by considering fractured caprock. Numerical modelling was used to study the deformation of an initially intact caprock caused by the depletion of an underlying reservoir during oil extraction. Deformation and flow were geomechanically modelled in three dimensions using a fully coupled poroelastic model, incorporating discrete fractures and faults into the caprock. Work package 3 offered new and valuable insight on future public awareness campaigns aimed at gaining acceptance of CCS. Qualitative expert interviews have been used, a CCS expert survey and a public survey across four countries to gain an understanding of perceptions of CCS risks and benefits, and has allowed for comparison of views on CCS between experts and public. In addition, the work package has explored the impact of different message framings on CCS attitudes.

The findings of each work package are summarised in this report, with each work package represented by a report chapter. A synthesis of the findings and discussion of the work as a whole follows.

1 Introduction

The capture of carbon dioxide (CO_2) from large point source emitters and storage in the form of a super-critical fluid within geological formations is a key technology in tackling anthropogenic climate change (Haszeldine, 2009, Bickle, 2009). To achieve a reduction in emissions, significant quantities of CO_2 need to be injected into suitable geological formations capable of containing the fluid for thousands of years. It has been estimated that approximately 3.2 billion tonnes (Gt) of CO_2 need to be injected annually (Zoback & Gorelick, 2012). Depleted hydrocarbon reservoirs represent a significant national resource within the UK with the potential for storing gigatonnes of CO_2 and aiding UK emission reduction targets. In 2012, the then Department of Energy and Climate Change (DECC) stated that depleted gas fields represent "*the most important storage type for the UK*", and "*provide a significant proportion of potential future capacity for the nation*" (DECC, 2012). Estimates suggest up to 9.9 Gt of UK storage capacity comes from reservoirs that have previously contained hydrocarbons extracted by the oil and gas industry (Holloway *et al.*, 2006). This form of storage site has a number of benefits, including the generally well-characterised geology and the potential for reutilisation of pre-existing infrastructure for injection activities. They also offer security of storage with an effective top-seal that previously acted as a seal to hydrocarbons, provided no deformation occurred during hydrocarbon extraction. Several demonstration projects have been conducted injecting megatonne scale CO_2 into depleted hydrocarbon reservoirs, including in the Norwegian North Sea at Sleipner (Arts *et al.*, 2008).

The use of a depleted reservoir will play a role in the performance of the storage facility. The process of hydrocarbon extraction, or depletion, can significantly affect both the reservoir involved and the surrounding rocks. During depletion, reservoir pore pressure will have lowered as hydrocarbon extraction occurred and as a result, the reservoir may have subsided. These activities, therefore, have the potential to cause deformation, movement on faults and/or damage to infrastructure, for example induced seismicity at Groningen (Netherlands; van Thienen-Visser & Breunese, 2015) and faulting at Ekofisk (North Sea; Zoback & Zinke, 2002).

The injection of super-critical fluid into a depleted reservoir will result in an increase in pore pressure, possibly resulting in heave and consequently has the potential to cause additional deformation, movement on faults and/or damage to infrastructure. The use of injection and extraction boreholes can minimise this effect, with water injected at a rate similar to the hydrocarbon extraction rate during drawdown, and extraction of aquifer water at a similar rate to CO_2 injection.

Perturbations of reservoir pore-fluid pressures occur when flow out of, or into the reservoir is initiated. These changes in pore pressure, and as a result the stress state, may lead to undesired geomechanical deformation that could affect the integrity of the reservoir and the overlying seal. The long-term impacts of such pore pressure changes, particularly when the reservoir is re-inflated during injection of CO_2, are not well understood and there is a lack of physical data for specific rock types and scenarios. Zoback & Gorelick (2012) identified the risk to security from a geomechanical point of view, while Economides & Ehlig-Economides (2010) showed that an upper pressure limit exists for carbon capture and storage (CCS), above which the seal is potentially compromised due to the formation of fractures. Verdon *et al.* (2013) examined the deformation observed at pilot injection sites and noted that the geomechanical response was: complicated and non-intuitive at Weyburn (Saskatchewan Province, Canada; e.g. Wilson & Monea, 2004); small at Sleipner due to the high permeability and large lateral extent of the reservoir (Chadwick *et al.*, 2012); and that uplift and microseimic activity was noted at In Salah (Algeria; e.g. Mathieson *et al.*, 2010). Therefore, reservoirs are evaluated on an individual basis, both in terms of their geometry and the properties of the geology present.

In order for depleted reservoirs to become a viable national resource, uncertainties must be addressed. As such, this project focussed on providing a better understanding of the impact of depletion and re-inflation on reservoir and caprock material. It involved a combined approach, using both laboratory experiments and computer simulation to improve our understanding of this aspect of storage site behaviour. The project addressed this key area with a focussed programme of work that generated a much-needed and unique dataset, new modelling tools, and a fuller understanding of the processes involved. The findings will inform regulators and aid operators in reducing the financial and environmental risks of CCS, for depleted storage sites, making the technology more likely to be used.

In addition, work was conducted examining effective communication of CCS with the public. Social acceptability represents a major potential barrier to CCS developments, as indicated by protests and moratoria in several countries. It was therefore critical to understand public attitudes and the bases of concern about CCS, and work as effectively as possible to improve understanding and engagement.

The CONTAIN (The impa**C**t of hydr**O**carbon depletio**N** on the **T**reatment of c**A**procks within performance assessment for CO_2 **I**njectio**N** schemes) project was implemented with three interlinked Work Packages. In Work Package 1 (Chapter 2), experiments were conducted on reservoir and caprock material in order to directly observe deformation associated with depletion and re-inflation; this included scenario analysis of potential reservoirs. Work Package 2 (Chapter 3) concentrated on geomechanical modelling of caprock behaviour during depletion and inflation. Finally, Work Package 3 (Chapter 4) examined the social understanding and acceptance of CCS storage proposals. Chapter 5 outlines the major conclusions and outcomes from the study, making clear recommendations for CCS implementers and regulators.

2 Work Package 1 – Impact of depletion and re-inflation on reservoir behaviour

2.1 INTRODUCTION TO WP1

The long-term feasibility of CO_2 containment in depleted reservoir formations or within targeted porous lithological units will depend on a number of factors, in particular, the hydromechanical (HM) and transport characteristics of the reservoir and caprock strata. The permeability of these materials and their reaction to the passage of CO_2 are key to the operational feasibility and long-term containment for such systems. For the purposes of performance assessment and possible site selection, it is essential to understand the coupled flow processes governing the movement of CO_2, in particular the long-term evolution of caprock behaviour in response to the depletion and subsequent re-inflation of underlying reservoir sequences. Elastoplastic models can predict when failure is likely to occur, offer insight into volumetric changes, and aid in prediction of deformation mechanisms. Critical state mechanics provides a useful framework describing the volume, and hence porosity, variation during deformation by a simple differential stress. This work package sought to understand the roles of the stress tensor, the stress path, and associated mechanical deformation on the permeability change affecting both the sealing efficiency of indurated hydrocarbon caprocks and HM response of reservoir materials during reservoir depletion and re-inflation. The British Geological Survey conducted this Work Package. Note that this report summarises the outcomes of WP1, more detail can be found in Harrington *et al.* (2018[a,b]) and Dobbs *et al.* (2018). Further scientific papers will become available.

2.2 GEOLOGY OF THE NORTH SEA

Within the UK the primary offshore oil and gas fields are located within the basins of the East Irish Sea, the Southern North Sea (SNS), and the Northern & Central North Sea (Holloway *et al.*, 2006; Bentham, 2006). Within these areas, there are a number of candidate-depleted fields that have the potential to become CCS sites in the future. For this potential to be realised, a detailed assessment of both the reservoir rocks and cap rocks is necessary. The geological setting of these formations is part of this analysis. In the CONTAIN project Deliverable 1, Parkes *et al.* (2014) gave a detailed review of the three UK offshore areas and the key geological units. These will be summarised in the subsequent sections of this report. The units discussed formed the basis of the experimental materials used, however, in some cases onshore analogues were used due to a lack of well-preserved reservoir/caprock. This is discussed in more detail in section 2.5.

2.3 SOUTHERN NORTH SEA AND EAST IRISH SEA

Within the SNS, as well as the East Irish Sea Basin, the Bunter Sandstone Formation (BSF) is a key reservoir material. The BSF is a Triassic Sandstone that is part of the Bacton Group. Figure 1 shows a stratigraphic correlation of the Triassic succession from the onshore and offshore UK across to the Netherlands sector of the SNS.

Within the SNS the BSF is a red, orange, and occasionally white sandstone. It comprises of mostly fine-grained sand, but with local areas of courser-grained sands and conglomerates. The thickness of the BSF varies across the SNS. Conservative estimates of average thickness of between 200 m and 350 m have been reported (Brook *et al.*, 2003; Williams *et al.*, 2013; Cameron *et al.*, 1992). The upper surface of the BSF has been recorded between 1 – 1.3 km depth (Noy *et al.*, 2012). The BSF is a major target in the SNS due to it containing many domal structural traps that formed due to the upwelling of the Permian Zechstein Salts beneath (see Figure 1). The Bunter Sandstone has an average porosity reported in the range 18 – 23 % (Williams *et al.*, 2013; Bentham, 2006; Cooke-Yarborough, 1991; Noy *et al.*, 2012). The primary porosity has been altered through compaction, cementation, cement-dissolution, and detrital grain-dissolution. The lowest porosities are seen

where the deposition has been greatest; the highest porosities correspond to the geological highs. The Bunter Sandstone exhibits permeability anisotropy, with the horizontal permeability (average 446 - 483 mD) being higher than the vertical permeability (average 294 - 415 mD) (Noy *et al.*, 2012). The onshore equivalent of the BSF is the Sherwood Sandstone Formation (SSF).

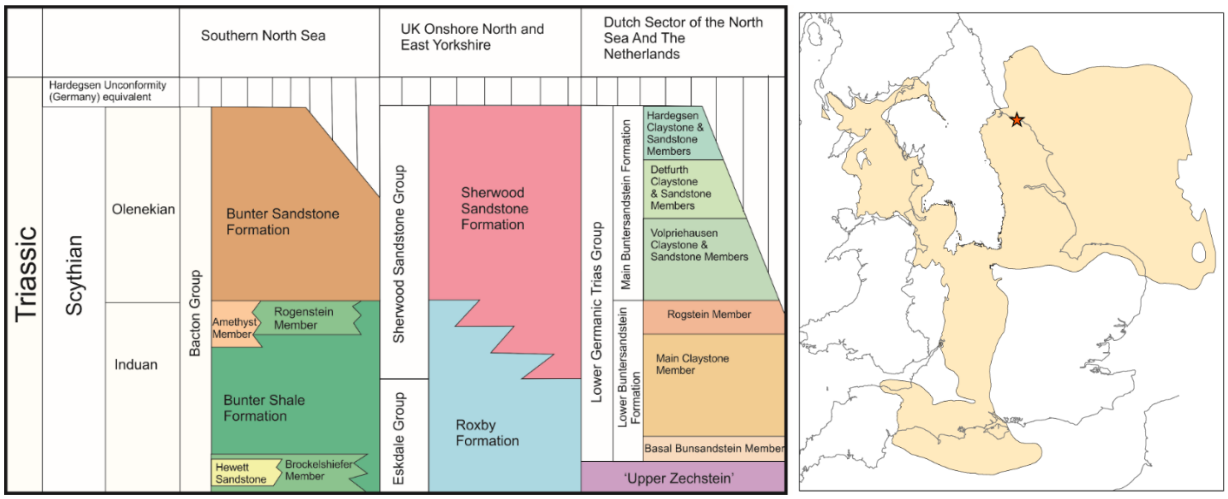

Figure 1 – A) Triassic stratigraphy showing onshore and offshore UK basins, B) Onshore and offshore extent of the Bunter Sandstone in the UK. Red start shows location of Staithes borehole (Parkes *et al.*, 2014).

The BSF has both a basal seal, the Triassic Bunter Shale, and an upper seal, formed by the Haisborough Group. The location within the SNS determines which of these dominates. The onshore equivalent of the Haisborough Group is the Mercia Mudstone Group (MMG). The upper seal includes the Rot Halite Member, the Dowsing Dolomite and the Solling Claystone. Parkes *et al.* (2014) give a detailed description of both the upper and lower seal as well as the Mercia Mudstone Group.

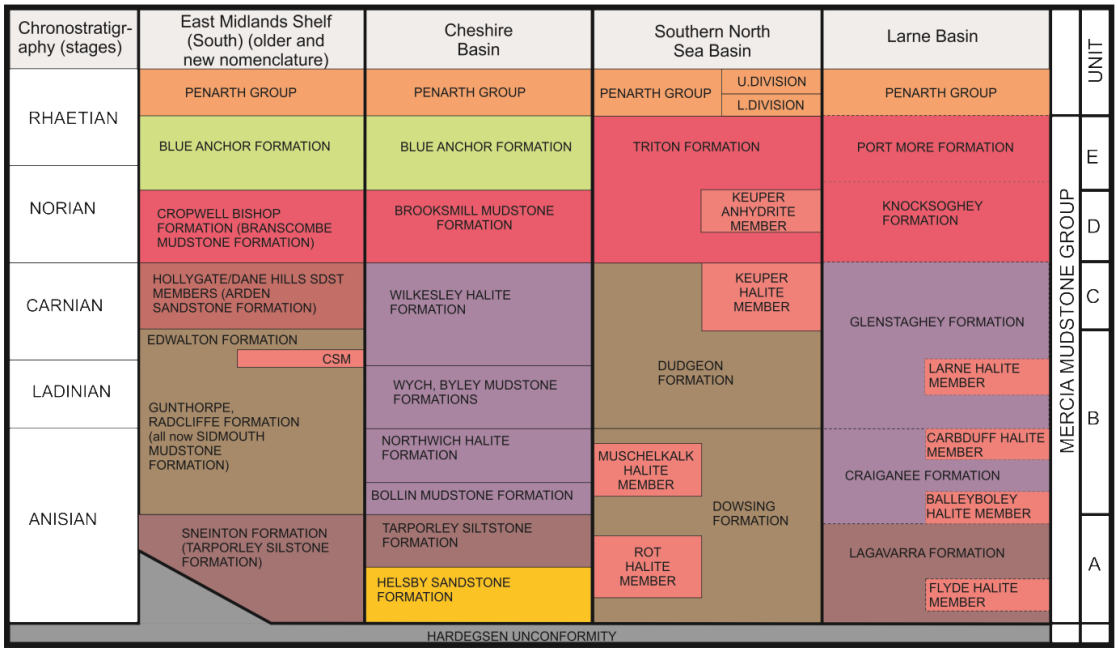

Figure 2 - Stratigraphy of the Mercia Mudstone Group in UK basins (Parkes *et al.*, 2014).

The MMG is a fine red mudstone/siltstone from the mid-late Triassic containing layers of grey and green mudstone/siltstone. The key characteristics of the MMG are observed to vary stratigraphcially (Figure 2; Hobbs, 2002). Present are sulphates, courser sandstones as well as halite in the periphery of the basin. Detrital clays are ubiquitous throughout the group, whilst authigenic clays are only found in the middle section. The carbonate content of the MMG is usually

up to 30 %, although locally it can be as high as 50 %; dolomite and calcite form the cement, with dolomite being the dominant carbonate (Hobbs, 2002). Armitage *et al.* (2013) observed that the porosity and permeability of the Mercia Mudstone were variable dependent on the mineralogical composition (specifically the clay content, the amount of cementation, and the cement and detrital mineral composition). The porosities were also as much as 10 % lower than expected, given the burial history, which could be due to a combination of a high initial detrital clay and silt content prior to compaction, and, where clay contents were lower, the growth of carbonate or gypsum cements in the granular pore space.

2.4 NORTHERN NORTH SEA

Within the Northern North Sea, two fields with particular potential for CCS are the Goldeneye and Captain Fields (Figure 4). The Goldeneye Field is a depleted reservoir in the Outer Moray Firth, south of the dominant Halibut Horst and at the northern edge of the South Halibut Basin (Parkes *et al.*, 2014). The Captain Sandstone forms the reservoir rock. This is early Cretaceous in age and makes up part of the Cromer Knoll group, which can be subdivided into the Rødby, Carrack, Valhall, and Wick Formations (Parkes *et al.*, 2014). The Rødby Formation is the youngest of these formations and forms the seal for the Captain Sandstone. The stratigraphy of the Cromer Knoll Group is described in Figure 3.

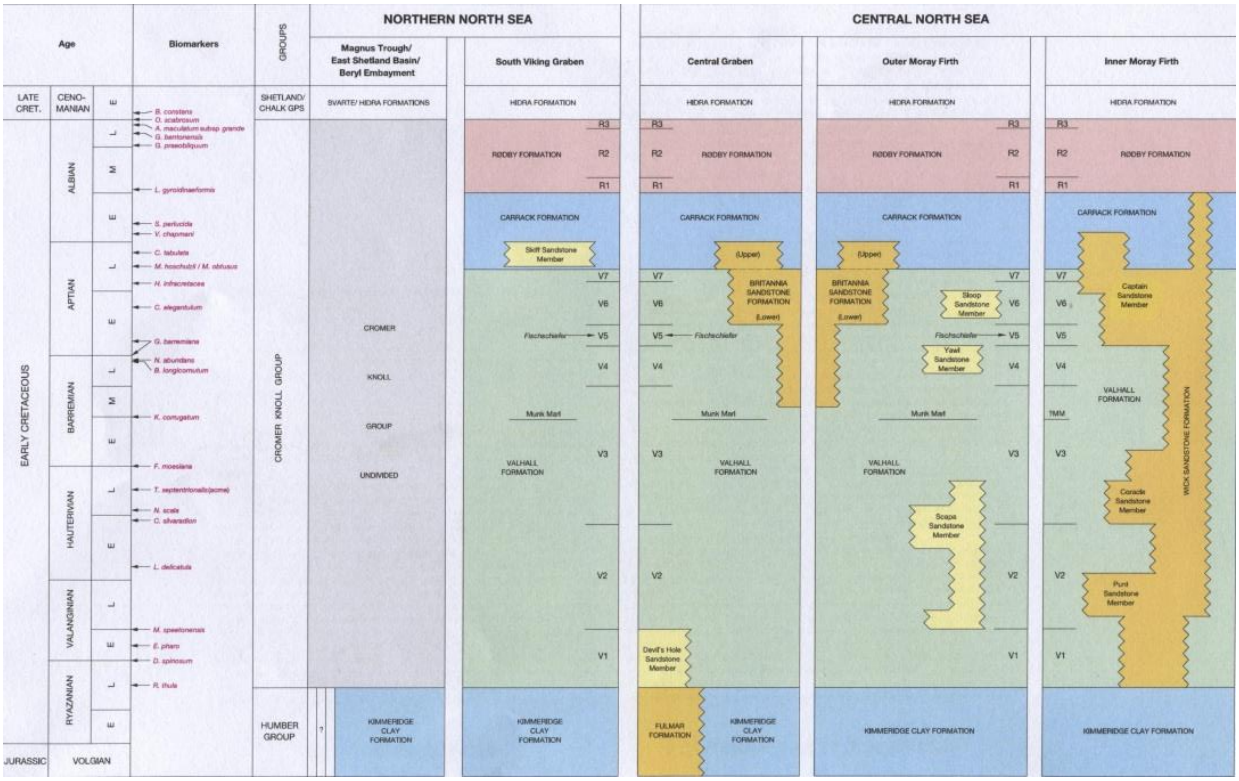

Figure 3: Stratigraphy of the Northern North Sea showing Captain Sandstones and Rødby Formation.

The Captain Sandstone is a high energy mass-flow-produced sediment with a high porosity and permeability. The sandstone extends into Western Moray Firth Basin, where it also forms the primary reservoir rock for the Captain Field (Figure 4).

The Captain Sandstones were formed from the collapse of high-density turbidity currents causing a rapid deposition of sediment (Parkes *et al.*, 2014). The Captain Sandstone is sand-rich, clean, blocky and massive (Rose, 1999), forming thickly bedded (up to 100 m), stacked and amalgamated, moderately sorted sequences of mostly medium-grade subarkosic sandstones (Pinnock & Clitheroe, 1997). It has been divided into the Upper and Lower Aptian Captain Sands. These are turbidite sand reservoirs, which are poorly consolidated and have a high porosity and

permeability (Parkes *et al.*, 2014). In both the Goldeneye and Captain Fields, the Mid Captain Shale, a thin layer of interbedded silts, sand and tuff, splits the Upper and Lower Aptian Captain Sands (Parkes *et al.*, 2014). The Upper Captain Sandstone is slightly less arkosic than the Lower Captain Sandstone, is more laterally continuous and has a higher lithic component (Pinnock & Clitheroe, 1997, Rose 1999, Parkes *et al.*, 2014). The Upper Captain is also courser, with fine to medium sand, as compared to the fine to very fine sand of the Lower Captain. Whilst the Upper sandstone member has very good reservoir properties across its entirety, the Lower sandstone is variable. Thin-bedded, fining-up, rippled, cross-stratified sandstones are located at the upper boundary transition to the overlying claystones (Pinnock & Clitheroe 1997, Parkes *et al.*, 2014).

The overriding mudstones of the Rødby and Carrack Formations have been identified as the primary seal formations for the Goldeneye and Captain Field. However, in places these have been eroded and the Captain is overlain by the Upper Cretaceous Chalk Group (SCCS, 2015). The Carrack Formation directly overlies the Valhall and is late Aptian to early/mid Albian in age. It is composed of firm to hard, blocky fissile, non-calcareous mudstones and sandstones, rich in pyrite, mica and carbonate. The upper most seal is known as the Rødby Formation. This overlies the Carrack Formation, being mid to late Albian in age. It is composed of calcareous and chalky mudstones, thin beds of argillaceous limestones. The Rødby generally varies between 30-100 m thick depending on the height of the depositional environmental, but can reach up to 150 m (Johnson *et al.*, 2005) in depocentres and is 200 m thick in the Viking Graben (Iskasen & Tonstad, 1989).

The reservoir and caprocks of the southern and northern North Sea that have been briefly summarised here represent likely candidates for any future CCS industry in the UK. As such, this project has, where possible, aimed to understand the hydro-mechanical characteristics of these formations. However, analogue formations have been necessary, due to the scarcity of appropriate, well-preserved samples. Section 2.5 of this report summarises the rocks used and, where appropriate, their relation to the rocks described here.

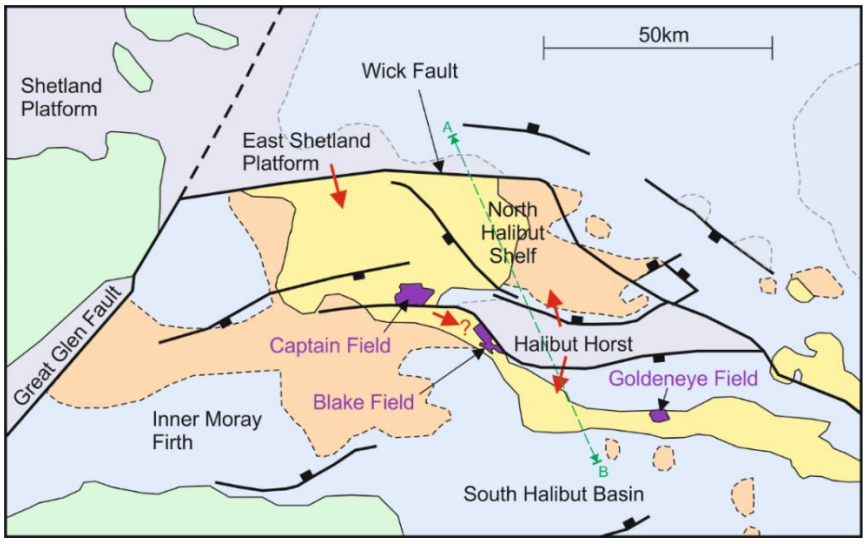

Figure 4 - Location of Captain and Goldeneye Fields and local structural geology.

2.5 SELECTION OF SAMPLES

WP1 aimed to test the hydro-mechanical properties of reservoir and caprock formations of particular interest to the UK CCS industry. However, in some cases the use of the exact formations described in Section 2.4 was not possible. Analogue formations that were more readily available were, therefore, used instead. The analogues were assessed against a number of criteria, which are described in Parkes *et al.* (2014).

Potential core material from the Triassic BSF was identified at the National Geological Repository of the British Geological Survey. However, due to extensive slabbing and sub-sampling of these cores it was not possible to obtain samples of appropriate dimensions for experimental testing. As such, the Staithes Sandstone from the Chester Formation (part of the Sherwood Sandstone Group), was selected as the onshore analogue. It was decided that the material from the Staithes No.20 Borehole (NZ71NE/14;E476024, N0517997) would be appropriate. This core gave access to the Sherwood Sandstone Group between 650 - 925 m below ground level. This will be referred to as SSG1.

The Haighsborough is the offshore stratigraphic equivalent of the Mercia Mudstone Group (MMG). Samples from the MMG were collected from a depth of 57 m in the Carrickfergus salt mine, near Larne, Northern Ireland. The Larne Basin (see Figure 2) contains a Triassic sequence of various red beds of the Mercia Mudstone Group that have been interbedded with evaporates, siltstones, and some sandstone beds (Downing *et al.*, 1982). The experimental material belongs to the upper Knocksoghey Formation, a homogeneous, fine-grained, well-consolidated, reddish-brown mudstone, with abundant bluish-green patches of mudstone containing reduced iron. The lithological descriptions of the other formations in the basin do not significantly vary from the Knocksoghey Formation supporting the use of the material from Larne as an analogue for the Mercia Mudstone Group. However, the sample's petrographic description is less closely matched, suggesting that at a smaller scale the formation is more heterogeneous, which makes comparisons within the Larne basin and across the UK more complicated (Parkes *et al.*, 2014).

In terms of the Northern North Sea material the Bestwood Sandstone, part of the Chester Formation of the Sherwood Sandstone Group, was selected as an analogue material for the Captain Sandstone. Nine samples of sandstone were prepared from blocks obtained from the Bestwood No. 2 Quarry located outside Papplewick, approximately 10 km north of Nottingham. The blocks were cut from approximately 30 m below ground level. This will be referred to as SSG2.

Another reason for the selection of the Staithes Sandstone (SSG1) and the Bestwood sandstone (SSG2) is their suitability as two end members of reservoir formations. Figure 5b shows a plot from Noy *et al.*, in which porosity is shown against vertical air permeability for a number of sandstones. The Staithes Sandstone (SSG1) and the Bestwood Sandstone (SSG2) are plotted as lines at their measured porosities. As can be seen the Staithes Sandstone (SSG1) represents one end member as it has a relatively low porosity and therefore permeability. Whereas, the Bestwood Sandstone (SSG2) has a very high porosity and therefore plots as the opposite end member. Being able to measure hydro-mechanical data on two opposing end member reservoir rocks allows us to draw conclusions on the way in which a large range of reservoirs may behave during CO_2 sequestration.

In terms of the Rødby Formation a separate North Sea caprock was chosen as an analogue. The Våle Shale from the Ormen Lange field was selected, core was supplied by Shell as a good representation of caprock material. This is a Palaeocene age (Danian to Thanetian) sedimentary unit that forms the seal for the Ormen Lange and Egga fields. It is a shale consisting of marls, claystones with interbedded limestones, sandstones, and silttones. It is normally less than 100 m thick. The rock provided for this project came from a depth of approximately 2,900 m and was well-preserved in glycerol to ensure it did not dry out.

Further analogous shale rocks are discussed to draw further comparisons from our results; these are the Boom Clay and the Callovo-Oxfordian Claystone.

The Boom Clay is the youngest unit in a sequence of marine clays deposited in the north European sedimentary province during the middle Oligocene (Tertiary) period ca 28 to 34 Ma years ago. The clay content of the formation varies between 23 and 60 % and is comprised illite, smectite, and kaolinite, with an average porosity ranging from 39 to 40.6 % (Wiseall *et al.*, 2015).

The Callovo-Oxfordian Claystone is a Late Jurassic formation which Wenk *et al.*, (2008) describe as having a clay content of 25-55 wt%, 23-44 % carbonates and 20-31 % silt (essentially quartz + feldspar). Clay minerals are reported to include illite and illite-smectite with subordinate kaolinite and chlorite.

2.6 TESTING METHODOLOGY

The experimental programme utilised a number of apparatus and testing protocols. The following section only briefly outlines the tests performed.

Geotechnics: Basic geotechnics were determined for all test rock types following ISRM standards where appropriate (Ulusay & Hudson, 2007). For reservoir rocks, density (dry and saturated) and porosity were determined using saturation and buoyancy techniques. Particle size analysis was undertaken using the dry sieving method (BSI, 1990). For caprock materials, samples were weighed in their initial state and after oven drying. This gave the water content of the clay-rich material. This was used in conjunction with the bulk density of the rock and the assumed grain density to give measures of porosity, voids ratio, and saturation.

Point load (PL): the simple Point Load test is a standard geotechnical measure of rock strength (e.g. Ulusay & Hudson, 2007). Regular samples were loaded between two hardened stainless steel conical platens and were loaded by use of a hydraulic ram. The maximum load prior to failure was recorded for each specimen.

Uniaxial compressive strength test (UCS): The UCS test is an industry-standard measure of strength. It is performed on cylindrical samples loaded axially, with no lateral confinement of the sample, i.e. $\sigma_1 > \sigma_2 = \sigma_3 = 0$. Two pieces of apparatus were used. 1) The MTS apparatus (e.g. Dobbs *et al.*, 2018) uses cylindrical samples of 54 mm diameter and ~108 mm length up to a maximum axial stress of 1.1 GPa. The apparatus is a servo-controlled system that can perform complex stress histories meaning that strain rate can be lowered close to the point of ultimate failure. This can yield considerable insight into the deformation of rocks. The system measures axial stress, axial strain, and circumferential strain. 2) a simple loading press was used to perform UCS tests on samples of 37 mm diameter and ~70 mm length (e.g. Harrington *et al.*, 2017[a]). The samples were subjected to a constant strain rate throughout the test until failure (unlike the MTS experiments). Axial load, axial displacement, and radial displacement in three locations approximately 120° apart were recorded using a load cell and four displacement devices.

Isotropic testing: The isotropic, or hydrostatic, testing configuration is one where a confining pressure is applied to a rock sample of equal magnitude on all faces of a cylindrical sample, i.e. $\sigma_1 = \sigma_2 = \sigma_3$. It is used to define the consolidation properties, relationship of permeability with stress, or the onset of deformation through loading alone. Two pieces of apparatus were used in isotropic arrangements. 1) The BGS custom-designed isotropic permeameter (IsoP; e.g. Harrington *et al.*, 2017[b]) uses cylindrical samples of 50 mm diameter and ~50 mm length up to a maximum confining pressure of 70 MPa and a pore pressure of 26 MPa. Teledyne-ISCO syringe pumps mean that the pore-pressure system has microlitre volume accuracy and can resolve steady state flow rates of a microlitre per hour. Similarly, the syringe pump attached to the confining circuit had microlitre volume resolution. 2) A custom-built modification to the BGS permeameter that included a metal syringe arrangement of 50 mm diameter and ~50 mm length filled with unconsolidated sand. This allowed 1-d (K_0) deformation of lose sand to be investigated by monitoring the pore volume within the syringe during changes of confining pressure.

Triaxial compression testing: The triaxial compression test is similar to the isotropic testing arrangement with the addition of a greater stress imposed axially along the cylindrical sample, ie. $\sigma_1 > \sigma_2 = \sigma_3$. It is used to define the strength and permeability of rocks under realistic *in situ* stress conditions. In the current study, three pieces of triaxial apparatus were used. 1) the MTS apparatus (e.g. Dobbs *et al.*, 2018) uses cylindrical samples of 54 mm diameter and ~108 mm length up to a

maximum confining pressure of 140 MPa, axial stress of 1.1 GPa, and pore pressure of 70 MPa. The apparatus is a servo-controlled system that can perform complex stress histories. It allows axial and circumferential strain of samples to be recorded. Additional acoustic sensors measure P- and S-wave velocity, giving dynamic elastic constants. A pulse-decay permeability test is possible on rocks with relatively high permeability (i.e. reservoir rocks). 2) the BGS designed triaxial apparatus (TriAx; Harrington *et al.*, 2017[b]) uses samples of 37 × ~70 mm up to a maximum confining pressure of 70 MPa, axial stress of 212 MPa, and pore pressure of 26 MPa. This system is a simple one that can increase boundary conditions in either steps, or pressure ramps. It has a sensitive pore pressure system designed to investigate steady-state flow in low permeability rocks, particularly shale and is able to resolve microlitre changes in pore volume. 3) the BGS designed Stress Path Permeameter (SPP; Cuss *et al.*, 2014) uses samples of 56 × ~80 mm up to a maximum confining pressure of 70 MPa, axial stress of 98 MPa, and pore pressure of 26 MPa. The SPP is an evolution of the TriAx system and includes additional sensitive radial strain measurements capable of observing microstrains. All three triaxial systems can be operated in either drained or undrained configurations.

Sample preparation: Test materials were prepared with the utmost of care to ensure that no damage occurred to them that would adversely influence results. Where necessary, samples were over-cored using diamond-tipped core barrels. These were finished by machine lathing to the desired diameter within a tolerance of 20 μm. The samples were trimmed along their length using a rock saw and the ends where completed on the lathe to create parallel ends. The samples were generally prepared along the borehole length and were approximately perpendicular to bedding. Samples were vacuum-packed and stored under refrigeration until required. This minimised drying, biological, and chemical degradation of the test material. Where available, off-cuts of material provided geotechnical data.

2.7 RESERVOIR PROPERTIES

Reservoir rock is directly impacted by the extraction of pore fluids (hydrocarbons/saline) and the subsequent injection of super-critical CO_2. The law of effective stress in porous rocks states that the force felt by the rock is equivalent to the mechanical load minus the pore pressure. A reduction in pore pressure during extraction therefore increases the effective stress felt by the reservoir rock. Injection of pore fluid increases the pore pressure and therefore lowers the effective stress. Rocks at depth can generally be thought of as at a state of limiting equilibrium with everywhere at the point of shear failure according to Byerlee's rule (Engelder, 1992). Therefore, any change of stress regime, such as pore pressure perturbations due to CCS activities, could potentially result in deformation. An early assessment of geomechanical performance during depletion and reinjection can be used as a screening tool to identify viable candidate reservoirs prior to investment in more costly examination. Such an assessment is also key in the selection of optimum operational limits.

Of primary interest in the case of reservoir rocks is the stress condition at which deformation is first induced. In Work Package 1 (WP1) sandstone was the reservoir rock investigated. Sandstone is an elasto-plastic material. It behaves linear-elastically, with fully-recoverable strain, up to the condition of "yield", which is the stress condition capable of creating permanent, non-recoverable (plastic) deformation through a number of microscale mechanisms. Yield-envelope assessment was therefore adopted as an appropriate approach for this study (Figure 5). For the purposes of WP1, yield is defined in the effective mean stress (P') versus differential stress (Q) space. Only stress states within the grey shaded area are achievable. Within this region the rock deforms elastically. When stress changes are sufficient the yield envelope is intercepted. If this occurs in the brittle regime (red line) deformation in sandstone will be through shear-enhanced dilation and the formation of shear fractures/zones. This results in an initial permeability increase due to dilation and increased porosity, but with extended deformation and the formation of a fine-grained gouge within the shear zone can result in a decrease in permeability. Should deformation occur at a stress-state greater than the brittle-ductile transition (blue line) then distributed shear-enhanced

compaction occurs through the cataclastic deformation of grains. Here a concomitant reduction in permeability and porosity occurs. In both conditions, once yield has occurred the stress-state will track towards the critical state (red circle). It should be noted that deformation will result in a change in the size of the yield envelope and so this stress-path also tracks into and out of the plane of the diagram through changes in porosity and grain size.

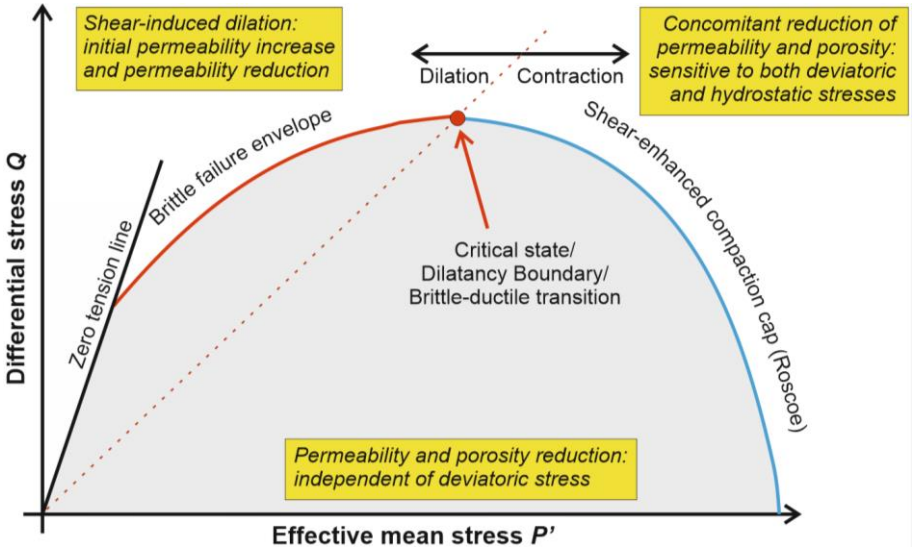

Figure 5 – Yield envelope concept. Modified from Zhu & Wong (1997).

In rocks that do not show an initial perfect linear response, as is commonly found, the identification of yield can be somewhat ambiguous. Determining yield is not always straightforward and more easily defined properties of strength and failure, such as peak strength (peak stress condition), have become the commonly reported strength parameters. However, yield is of significance to carbon capture and storage as it represents the stress state at which a permanent change of the reservoir or caprock occurs. Considerable deformation of a reservoir may occur at a stress state greater than the yield condition, but less than peak strength.

Since the onset of yield is not straightforward to determine, several approaches have been developed, including monitoring of volumetric dilation, acoustic emissions (e.g. Wong *et al.*, 1997), porosity (e.g. Baud *et al.*, 2006), or permeability (e.g. Zhu & Wong, 1997b). Cuss *et al.* (2003) determined yield from stress-strain results by fitting a linear trend to the elastic-region and setting a threshold at which a deviation from the linear-elastic response defines yield; this approach was used in the current study to allow direct comparison with the well-constrained data from that study.

Geomechanical data for the Southern North Sea (SNS) basin is not readily available. Consequently, it is difficult to make a reasonable early assessment of reservoir-specific geomechanical performance. Offshore drilling for new borehole core for testing is often prohibitively expensive, particularly at such an early stage of CCS development. Consequently, testing of existing borehole core is the most economical way to obtain geomechanical parameters for early reservoir viability assessment. Two sandstones were investigated with the aim of defining the yield envelope and deformation behaviour of significantly differing rock. As discussed in Section (2.5) Sherwood Sandstone Group (SSG1) was investigated as an analogue of the Bunter Sandstone Formation (BSF) of the SNS, with the SSG being a close onshore equivalent of the BSF in terms of porosity, grain size, and diagenetic history. It represents one end member as it represents the lower porosity, low permeability section of the Bunter Sandstone (Figure 6b). SSG2 was selected as the end member of potential Bunter Sandstone behaviour, representing a high porosity variant, as shown in Figure 6b. The results for these two sandstone varieties were compared with 27 datasets of yield found in the literature for other sandstone varieties.

2.7.1 Sandstone variability

Sandstone is often viewed as a homogeneous rock type that deposits in thick sequences. As shown in Figure 6, the results from the current study show this not to be the case. A total of 39 tests were conducted on material from the Staithes No.20 borehole for SSG1. Figure 6a shows the results obtained for dry density, saturated density, particle density and effective (connected) porosity. Dry density varied from 2.16 to 2.43 Mg m^{-3}, with an average of 2.28 Mg m^{-3} and standard deviation of 0.06 Mg m^{-3}. Saturated density varied from 2.33 to 2.53 Mg m^{-3} with an average of 2.43 Mg m^{-3} and standard deviation of 0.04 Mg m^{-3}. Particle density varied from 2.62 to 2.71 Mg m^{-3} with an average of 2.68 Mg m^{-3} and standard deviation of 0.02 Mg m^{-3}. The effective porosity of the test samples ranged from 10.3 to 17.5 % with an average of 14.9 % and a standard deviation of 1.7 %. These ranges reflect the true variability within the lithological succession. These geotechnical properties are also described in Appendix 2 (Table 1). Figure 6b shows field data reported by Noy *et al.* (2012) for the BSF in the SNS. Porosity ranges from effectively zero to greater than 30 %, with permeability ranging over six orders of magnitude. Therefore, it has to be emphasised that formation-scale deposits of sandstone are highly variable in physical properties. Mechanical testing tends to be bias towards competent parts of the sequence, skewing results. This degree of variability could not be fully explored in the current study, but has to be borne in mind when interpreting results.

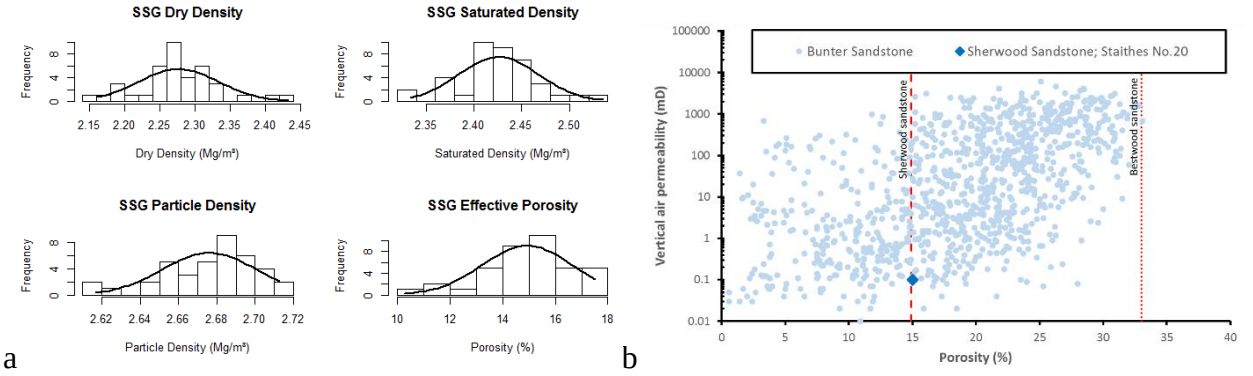

Figure 6 – Sandstone physical property variability. a) Histogram and density plot for dry density, saturated density, particle density and effective porosity of the Sherwood Sandstone Group from the Staithes No. 20 borehole (SSG1); b) Vertical air permeability versus porosity for the Bunter Sandstone Formation (from Noy *et al.*, 2012).

2.7.2 Sandstone deformation

Sherwood Sandstone Group 1 (SSG1): Figure 7ab summarises the results from the compression tests for SSG1. A progression from brittle to ductile deformation was seen with increasing confining pressure. Examination of the final test samples suggested that the transition occurred at about 60 to 80 MPa confining pressure. All samples showed a peak in stress prior to strain-softening; generally, this peak stress increased with confining pressure, as described by a power law relationship (Figure 7b). However, the test conducted at 140 MPa confining stress, had a lower peak stress (303 MPa) than the test at 120 MPa (325 MPa). This may be due to differences in the effective porosity of the test samples, with the stronger test sample having a porosity of 14.8 %, compared with 16.5 %, or due to earlier onset of yield. Post-peak stress behaviour also showed a clear transition from brittle to ductile behaviour. Samples tested at lower confining pressures (20 and 40 MPa) underwent Type II brittle failure; samples tested at intermediate confining pressures (60, 80, and 100 MPa) showed (sometimes considerable) post-peak strain-softening; samples tested at higher confining pressures (120 and 140 MPa) showed a transition to strain-hardening after an initial phase of post-peak strain softening. Strain results show that increasing confining pressure resulted in greater axial and volumetric strain at peak stress, with the exception of axial strain at 140 MPa, which is slightly lower than that at 120 MPa.

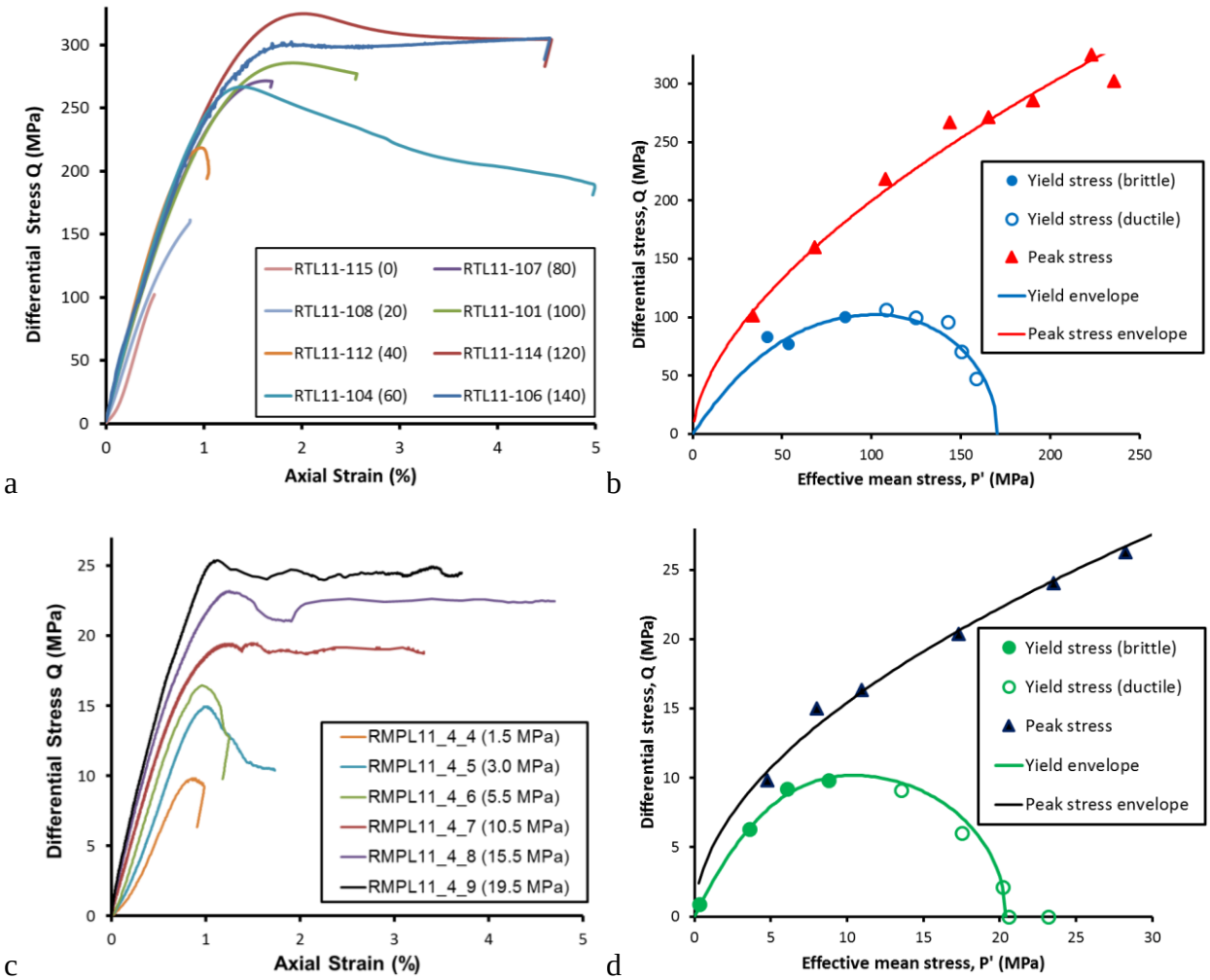

Figure 7 - Results for triaxial compression testing of the Sherwood Sandstone Group (SSG1 and SSG2). a) stress-strain results for SSG1; b) yield and peak stress for SSG1 in *P´ – Q* space; c) stress-strain results for SSG2; b) yield and peak stress for SSG2 in *P´ – Q* space. Note: open yield stress markers denote deformation on the ductile side of critical state line and closed markers deformation on the brittle side.

Sherwood Sandstone Group 2 (SSG2): Figure 7cd summarises the results from the triaxial compression tests for SSG2. As with SSG1 a transition from brittle to ductile deformation was seen with increasing confining pressure, occurring at about 10 MPa confining pressure, much lower than seen in SSG1. Most samples showed a peak in stress prior to strain-softening, with the exception being test 7, which showed almost perfect elastoplastic behaviour. This suggests that 10.5 MPa corresponds with the brittle-ductile transition. Figure 7d shows that peak stress increased with increasing confining pressure, as described by a power-law relationship. On the ductile side of deformation, samples did not show any sign of strain-hardening even at elevated strains. This suggests that this sandstone variety can accommodate significant volumetric strains with relative ease. Inspection of stress-strain data at low confining pressures indicated Type II brittle failure. Figure 7d also includes data from the two hydrostatic tests conducted, giving grain-crushing pressures (yield stress in a hydrostatic stress regime) of 20.6 and 23.2 MPa.

For both sandstones, Young's modulus increased with confining stress, although there is scatter within this relationship. Poisson's ratio was relatively constant throughout the pressure range with values between 0.16 and 0.2 (see Appendix 6.2 Table 2 for more detailed hydro-mechanical properties). For SSG1 at the lowest confining pressure a much higher Poisson's ratio of 0.35 was observed. This however, may be attributed to a high effective porosity of the sample (17.5 %), compared with the other test samples that ranged between 14.1 and 15.4 %. Mohr-Coulomb and

Hoek-Brown (Hoek *et al.*, 2002; Hoek & Diederichs, 2006) failure envelopes and corresponding failure criterion parameters were calculated for the triaxial and uniaxial compression tests, using the peak stress as peak strength and providing values for cohesion (c) and friction angle (Φ).

2.7.3 Yield envelopes

Yield was determined for each uniaxial, hydrostatic, and triaxial compression test. Yield was considered to be at the onset of significant stress deviation (more than 1 MPa for SSG1 and 0.1 MPa for SSG2) from the tangent of the elastic region of the stress-strain curve. Error in determining yield was not significant and generally varied by less than 10 % when different sections of the stress-strain curve were considered linear.

Figure 7d,b shows the results for yield and peak strength when plotted in the differential (Q) versus effective mean stress (P') space. Differential stress was calculated as the difference between axial (σ_1) and confining stress (σ_3). Effective mean stress was defined as $^1/_3(\sigma_1 + 2\sigma_3) - P_p$, where P_p is pore-pressure. As seen, the peak strength data for both SSG1 and SSG2 follow a curved trend with strength continually increasing with mean stress as a power-law. Yield showed a curved form similar to that shown in Figure 5. For tests that displayed shear-localisation in hand specimen (dilatant behaviour), the data fall on the portion of the curve with a positive slope. For tests with pervasive cataclastic flow (contraction), the data fall on the portion of the curve with a negative slope. The apex of the yield envelope signifies the condition of isovolumetric deformation, also referred to as critical state deformation or the brittle-ductile transition.

The post-test observations of failure mode showed that the transition from brittle to ductile deformation occurred between 60 and 80 MPa for SSG1 and around 10.5 MPa for SSG2. On the brittle side, purely brittle deformation was seen with sample failure by shear localisation. Around the brittle-ductile transition a more distributed series of localised deformation features formed. At elevated confining pressures the samples appeared to have undergone distributed ductile deformation with the test sample clearly barrelling. These observations are consistent with those of Wong *et al.* (1997) and Cuss *et al.* (2003). For SSG1 it should be noted that the brittle-ductile transition at such a pressures represents a depth greater than 2.5 km in the Southern North Sea, which is deeper than the depth of most potential storage sites in the area. Therefore, SSG1 is not likely to undergo distributed cataclastic flow (contraction) and that deformation would be brittle (dilatant), or at the brittle-ductile transition (isovolumetric). However, for SSG2 the brittle-ductile transition represents a depth of less than one kilometre and therefore deformation would be possible by either dilation or contraction under a variety of stress conditions.

Limited yield data is available in the literature, particularly for weak sandstone varieties. However, data from 27 individual studies covering Adamswiller, Berea, Benteim, Bestwood, Bleurswiller, Boise, Darley Dale, Diemelstadt, Hollington, Kayenta, Penrith, Rothsbach, Sherwood, and Tennessee sandstone varieties was found in papers by Baud *et al.* (2004, 2006), Cuss *et al.* (2003) Fortin *et al.* (2006), Klein *et al.* (2001), Louis *et al.* (2009), Rutter & Glover (2012), Wong & Baud (2012), Wong *et al.* (1997) and Zhu *et al.* (1997).

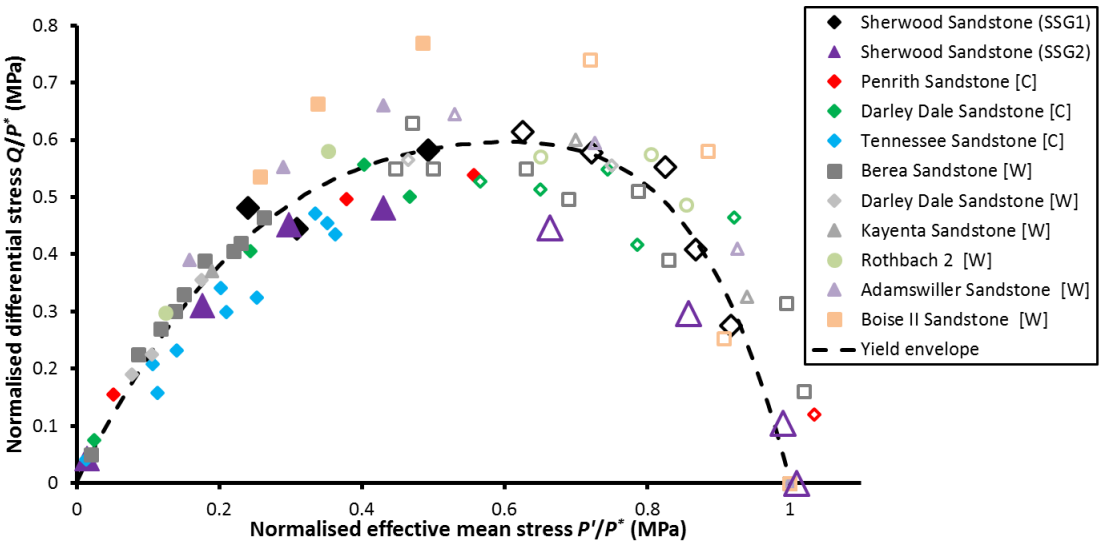

Figure 8 - Critical state envelope calculated for 11 sandstone varieties, normalised by the grain crushing pressure (*P). As seen, all data approximately correspond to a single yield envelope with brittle deformation below *P´/P** = 0.5 and ductile deformation above. [C] refers to Cuss *et al.* (2003); [W] refers to Wong *et al.* (1997); open symbols denote ductile deformation; closed symbols denote brittle deformation.**

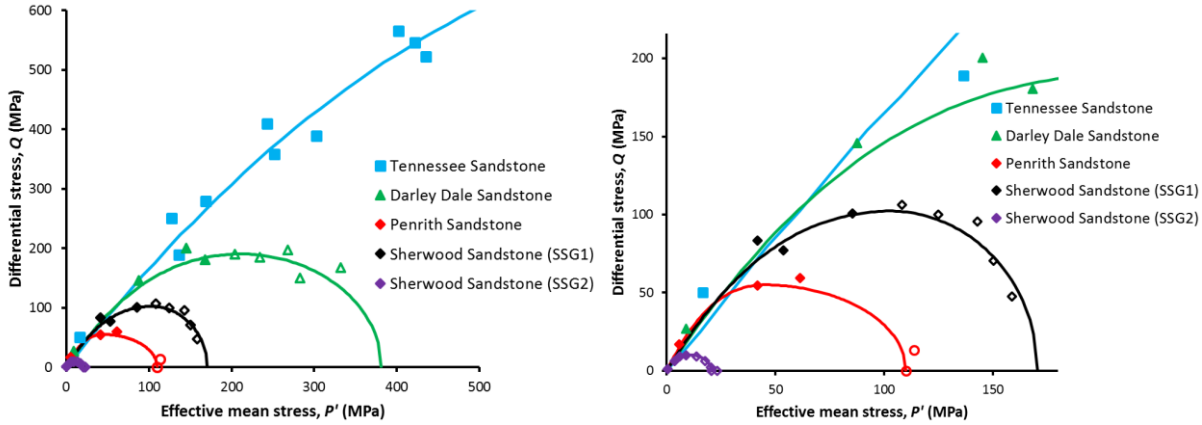

Figure 9 - Comparison of the current test data (Sherwood Sandstone Group SSG1, SSG2) with Penrith, Darley Dale and Tennessee sandstone (from Cuss *et al.*, 2003). Open symbols denote ductile deformation; closed symbols denote brittle deformation, solid lines represent the calculated yield envelopes.

Figure 8 shows data from the current study compared with the results presented by Cuss *et al.* (2003) and references therein. Wong *et al.* (1997) showed that sandstones when normalised by their grain crushing pressure (P^*) have a similar, singular, yield envelope. The grain crushing pressure is the condition where yield occurs under purely hydrostatic conditions and in a *Q-P* plot occurs along the abscissa. This was achieved in SSG2, but was greater than that rating of the apparatus for SSG1. However, the grain crushing pressure can be determined from the Hertzian contact model (Wong *et al.*, 1997), which states P^* scales with the grain radius (R) and porosity (ϕ), such that:

$$P^* \propto (\emptyset R)^{-\frac{3}{2}} \quad [1]$$

Average grain diameter and porosity were determined to be 215 µm and 15 % respectively using scanning electron microscopy. This gave a predicted P^* of 173 MPa, allowing the current study to be normalised and plotted in Figure 8. The current data correspond well with the findings of Wong *et al.* (1997) and Cuss *et al.* (2003). This is further emphasised in Figure 9 where the current data for SSG1 and SSG2 are compared with Penrith, Darley Dale, and Tennessee Sandstone varieties

(from Cuss *et al.*, 2003). SSG1 is intermediate in strength between Penrith and Darley Dale Sandstone, whilst SSG2 is the weakest of the five rock types.

4.1.1 Refinement of the yield envelope

Wong and co-workers showed that sandstones of varying properties have similar yield envelopes when plotted in the differential stress versus effective mean stress space. It would be possible to fit a polynomial to the data shown in Figure 8, but this approach would not allow definition of any parameters based on physics. Wong *et al.* (1997) observed that most of their normalised data on the ductile side are bracketed by the elliptical cap model (DiMaggion & Sandler, 1971) given by:

$$\frac{\left(\frac{P}{P^*}-\gamma\right)^2}{(1-\gamma)^2}+\frac{\left(\frac{Q}{P^*}\right)^2}{\delta^2}=1 \qquad [2]$$

with peaks at (γ, δ) = (0.5, 0.5) and (0.5, 0.7). Therefore, for the ductile side of the yield envelope (from P/P^* = 0.5 to 1.0) the above relationship can be used to estimate yield. A yield envelope was constructed with the ductile side defined by the DiMaggio & Sandler model with a peak of (0.5, 0.5) and for the dilatant side, a polynomial least-squares best fit was applied through all the data shown in Figure 8.

The form of the yield envelope is further defined by two parameters. The slope of the critical state line (M) defines the position along the abscissa where the peak of the envelope occurs. As shown in Figure 8, the best fit through all the data suggests the peak occurs at P/P^* ~ 0.6, therefore introducing asymmetry to the envelope. As shown by Wong *et al.* (1997) the data are generally bound by the δ parameter between 0.5 and 0.7, this defines the height of the yield envelope.

A macro was written in Microsoft Excel to optimise the fit of the recorded data to the yield envelope by adjusting three parameters; P^*, M, and δ. This gave the results presented in Figure 8-Figure 11. The slope of the critical state line varies between 0.77 and 1.25, although for the latter the envelope was fitted to only five data points. For all five sandstone types a good fit is achieved to the data, see Figure 10.

An alternative approach was also introduced by Sheldon *et al.* (2006). In this case, the yield surface was described differently above and below the effective pressure at the critical state point (P'_{cr}) such that:

$$(Q)^2-\frac{Qp^*M}{2}\left[1-\left(\frac{P'}{P'_{cr}}-1\right)^2\right]=0 \qquad \text{for } P'\le P'_{cr}$$

$$(Q)^2-\left(\frac{Mp^*}{2}\right)^2\left[1-\left(\frac{P'-P'_{cr}}{P^*-P'_{cr}}\right)^2\right]=0 \qquad \text{for } P'\ge P'_{cr} \qquad [3]$$

where $P'_{cr}=\beta p^*$ and β is a material constant. M is generally seen to fall in the range of 0.8 – 1.5 and β varies between 0.45 and 0.55.

2.7.4 Yield envelope asymmetry and variation

The grouped data in Figure 8 correspond well with the observed general trend, but when individual rocks are considered, the fit is not perfect. For instance, Boise II plots much higher than the general trend. Furthermore, Berea sandstone displays ductile behaviour at P/P^* = 0.45, whereas SSG1, Penrith, and Boise II observe dilatant behaviour. SSG2 generally plots lower than the rest of the sandstone data. This is emphasised in Figure 11 where data from 29 rock varieties are plotted in a uniform colour. The distribution of data about the general trend is considerable.

Figure 10 shows five example envelopes along with a comparison plot. SSG1 and SSG2 are shown in Figure 10a,b. Darley Dale Sandstone is shown as an example of an envelope with a much higher form. In contrast, Hollington, Berea, and SSG2 all have a lower form. Berea is an example of a yield envelope with a skew to the left, while Hollington Sandstone is an example with a skew to

the right. The Hertzian contact model shows that the overall size of the envelope is dictated by the product of the porosity and the average grain diameter. It was hypothesised that the skew (related to M) and elevation (related to δ) would also relate to petrological properties. However, the availability of such data is incomplete for all 29 studies. That which is available has been determined in a number of ways. Therefore, no link was found between porosity, grain size, or roundness with M or δ. This requires further investigation.

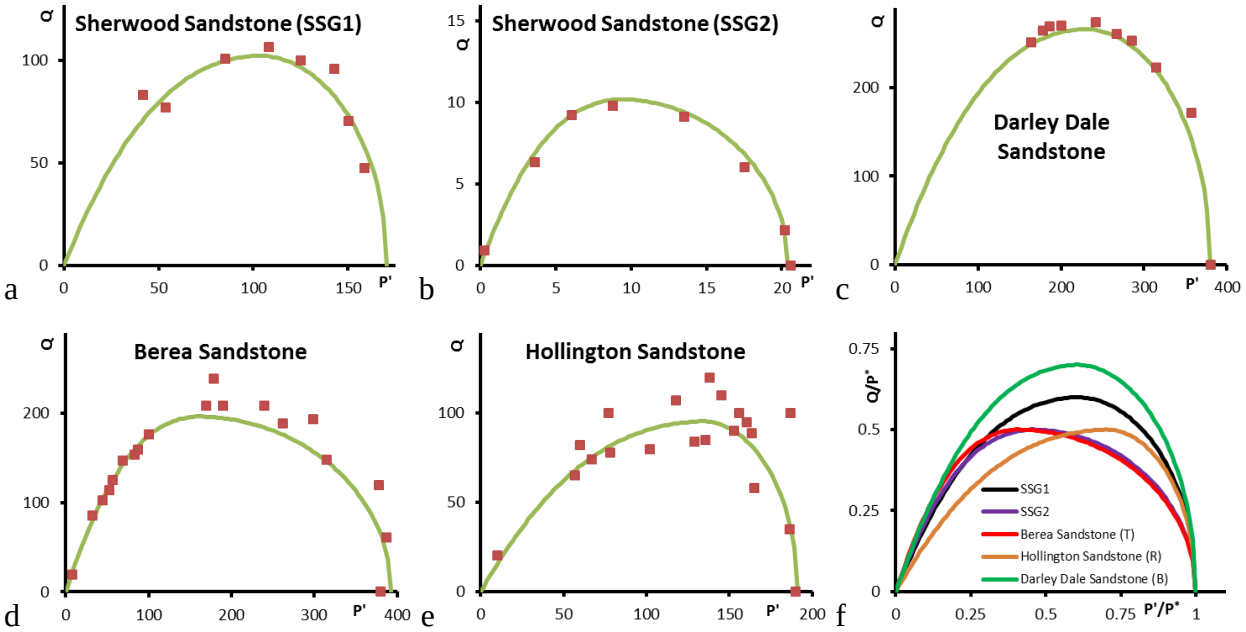

Figure 10 – Yield asymmetry displayed in best-fit envelopes for sandstone. a) Sherwood Sandstone Group (SSG1); b) Sherwood Sandstone Group (SSG2); c) Darley Dale Sandstone (Baud *et al.*, 2006); d) Berea Sandstone (Wong & Baud, 2012); e) Hollington Sandstone (Rutter & Glover, 2012); f) comparison of yield envelopes.

2.7.5 Simple and expanded yield analysis

The yield approach offers a simple preliminary screening tool for assessing viability of carbon sequestration. As outlined, a unified yield envelope has been defined for sandstone. The size of this envelope is dictated by the grain-crushing pressure, which in turn is related to the porosity and average grain diameter of the rock. The following statements can be made about the yield approach in the presence of variable available data:

1. In order to fully understand the deformation of a reservoir, a full uniaxial/hydrostatic/triaxial deformation campaign is preferable. This will define the yield and strength of the rock. In addition, petrology gives insight into the behaviour of the rock. This option is costly.
2. If only limited core is available, the yield envelope can be determined from a single hydrostatic test. This could be conducted on loose sand material derived from drilling chippings, but ideally should be conducted on competent core. This will determine P^* and define the envelope assuming the sandstone in question follows the general form of sandstone yield and that the specimen reflects bulk reservoir behaviour.
3. If no core material is available, the yield envelope can be constructed from petrophysical borehole logging tools. These can be used to estimate porosity and grain size of the sandstone. This can then be used to estimate P^*, which in turn determines the yield envelope. This approach uses the most assumptions and conservatism is necessary due to the errors associated with determining petrophysical parameters from geophysical borehole tools.

Figure 11 shows all available yield data for sandstone. It displays considerable spread about the average yield envelope. A significant number of data fall within a stress regime that the average envelope would predict to be stable. For instance, the average approach greatly overestimates the

yield of SSG2. For a conservative estimate of yield the 80 % fit line has been shown (green line). Here the vertical extent of the envelope has be scaled by a factor of 0.8, while the horizontal extent has been scaled by 0.9. Here, few data plot within the stable area of the envelope.

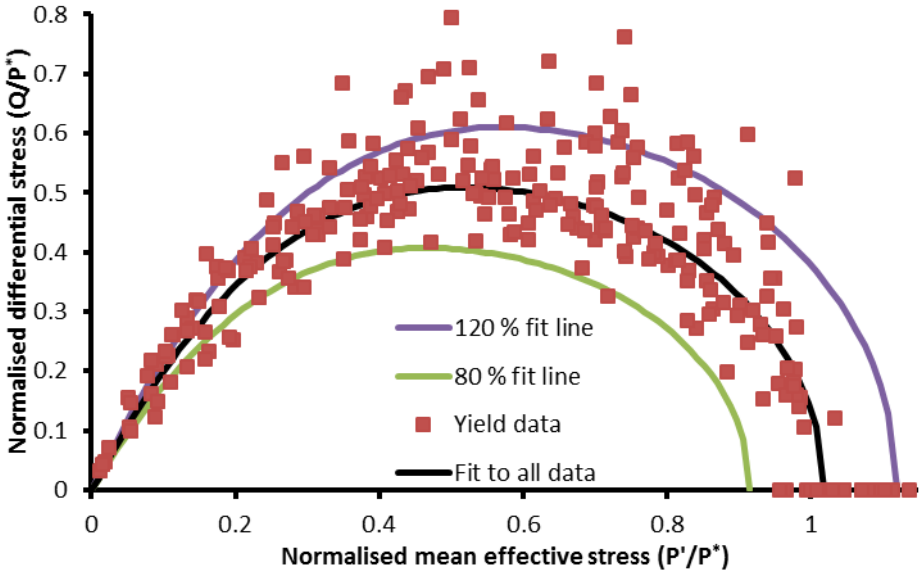

Figure 11 – Errors in yield prediction. Considerable spread is seen in yield estimate about the average yield envelope. In the absence of complete data it may be necessary to adopt the 80 % fit to ensure that yield is not over-estimated.

For condition (1) above where a full experimental study is conducted, a yield envelope can be determined and used to model the behaviour of the sandstone in question. For conditions (2) and (3), considerable care is required and the 80 % fit line is necessary to fully ensure that the yield envelope is not over-estimated. For sandstone varieties such as Darley Dale, which was given as an example with a "high" yield response, this would represent a significant difference between the conservative estimate from the 80 % fit and the actual rock strength. Furthermore, it should be noted that the Hertzian contact model can result in significant under- and over-estimates of P^*. Therefore, condition (3) requires greatest conservatism and may render perfectly viable reservoirs as being vulnerable, or could result in a significant reduction in carbon volume by limiting pore pressure changes. Condition (3) should only be considered as a preliminary screening tool and should progress to Condition (1) or (2) if a reservoir is deemed viable.

Given the paucity of available geomechanical data from depleted hydrocarbon reservoirs (due to commercial confidentiality, historical emphasis on presence of hydrocarbons, permeability, and porosity) and lack of readily available borehole core (due to predominance of open hole drilling, core slabbing, commercial confidentiality, poor curation, and prohibitively cost of offshore drilling to acquire new core), it is difficult to make a reasonable early assessment of reservoir-specific geomechanical performance. Testing of material from an onshore analogue, such as SSG1 or SSG2, is therefore a cost effective and desirable way to obtain geomechanical parameters to access reservoir viability, and hence to use as an early stage screening tool prior to investing in significantly more costly investigation for design purposes.

2.8 CAPROCK PROPERTIES

To assess the impact of depletion and re-inflation on caprock a similar yield envelope approach has been adopted. However, whilst superficially the yield envelope appears the same, the yield behaviour of clay-rich rocks is markedly dissimilar to sandstone in the brittle regime. Experiments therefore were conducted in a similar manner to those described for reservoir rocks, with the addition of careful tests to define the consolidation and hydraulic behaviour of shale in response to the prevailing stress field. The question of interest in the caprock is whether a change in reservoir

pressure is transmitted to the caprock of sufficient magnitude to result in volumetric deformation, which could result in the formation of shrinkage cracks, or to increase hydraulic permeability sufficiently to result in leakage of the seal. Experiments were conducted on three formations; Mercia Mudstone Group (MMG), Callovo-Oxfordian mudstone (COx), and Våle Shale (VS). The yield behaviour and influence of effective pressure cycling on their hydromechanical properties were investigated.

2.8.1 Critical state soil mechanics

Critical state theory proposed by Roscoe *et al.* (1958) provides a framework by linking volume change of a material to both effective stress (P') and differential stress (Q). Here, the onset of permanent deformation (yield) occurs in an isotropic medium at a critical specific void ratio (e_c) and a critical specific volume:

$$v_c = 1 + e_c \quad [3]$$

Yield is considered to occur as a combination of effective stress and specific volume, coinciding with a state boundary surface. Experimentation has shown that, when sheared, a deforming material will tend towards criticality, a state where large shear distortions will occur without any further changes in P', Q, *or* v (Schofield & Wroth, 1968). The Critical State Line (CSL) is the locus of all possible critical states in P'–Q–v space. In critical state soil mechanics (CSSM), the change of state of a medium can be represented by its progression along a given stress path, allowing deformation history of the material to be described, as well as its current state.

The yield surface can be described in terms of the zero-tension cut-off surface, the Hvorslev surface and the Roscoe surface (Figure 12b). These surfaces are analogous of those described for yield in sandstone (Figure 5). The Roscoe surface is identical to the shear-enhanced compaction cap and the zero tension line appears in both definitions. Differences occur in the brittle failure regime. In the case of sandstones (and other lithified rocks) failure is described by a brittle failure envelope. In CSSM brittle deformation is described by the Hvorslev surface.

The zero-tension cut-off is defined in P'-Q' space as the transition from compressional to tensional deformation, occurring at:

$$Q = 3P' \quad [4]$$

Heavily overconsolidated sediments or those that have been unloaded by either increasing pore pressure or total stress reduction, deform along the Hvorslev surface (Hvorslev, 1937), which is described as:

$$Q = HP' + (M - H)exp\left(\frac{\Gamma - v_f}{\lambda}\right) \quad [5]$$

where H and M are intrinsic material properties, -λ is the slope of the virgin consolidation line (VCL) in the v-P' space and Γ is the specific volume intercept of the CSL at a reference pressure P'_r. For a porous rock, this region of P'-Q' space is associated with deformation by shear localisation and dilatancy.

Finally, the Roscoe surface is defined as the state boundary along which normally consolidated sediments deform and can be described by:

$$Q = MP'\left(\frac{p'_c}{P'} - 1\right)^{0.5} \quad [6]$$

where p'_c is the preconsolidation pressure of the clay. For a porous material, this region of P'-Q' space is associated with shear-enhanced compaction/cataclasis resulting in compactive strain.

In the P'-Q' space, the projection of the CSL (Figure 12b) can be defined as:

$$Q = MP' \quad [7]$$

and meets the Roscoe surface at its maximum value (Figure 12b).

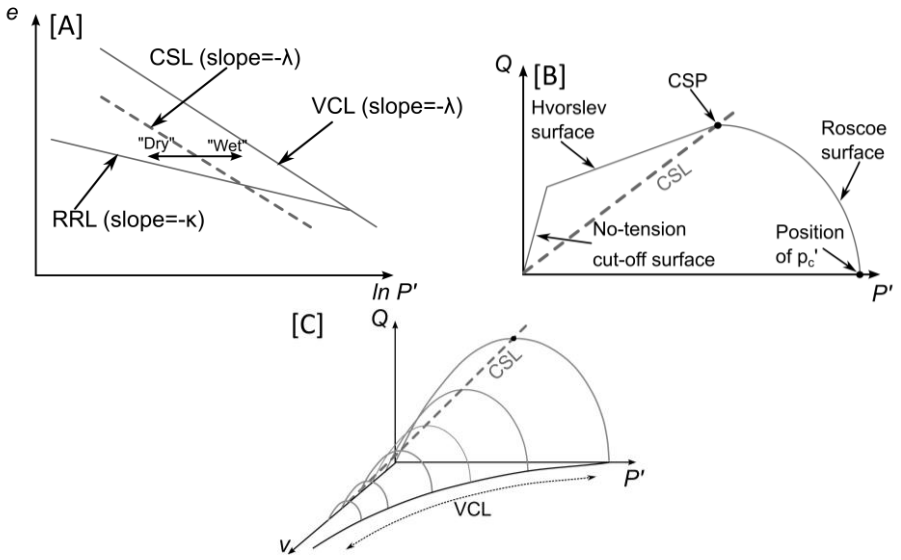

Figure 12 - Idealised yield behaviour of porous materials (soils) as a function of void ratio (*e*), effective pressure (*P´*), and differential stress (*Q*). a) for a clay in *e*-ln *P´* space (after Horseman *et al.*, 1993); b) for a clay in *P´* - *Q´* space; c) Idealised behaviour of a lithified sediment in *P´*-*Q´*-*v* space, showing the modified envelope of Sheldon *et al.* (2006). CSP = Critical State Point, CSL = Critical State Line, VCL = Virgin Consolidation Line, and RRL = Rebound/Recompression Line.

The main differences between the yield envelope/surface approach for reservoir (sandstone) and caprock (clays and shales) are within the brittle deformation region (Hvorslev for shale and brittle failure envelope for sandstone) and the behaviour of unlithified clays resulting in a greater importance in consolidation behaviour and changes in porosity during deformation. However, both approaches require a detailed description of yield under hydrostatic and triaxial stress conditions. Alternatively, the consolidation behaviour can define the intercept of the yield envelope with the abscissa and the virgin consolidation line can define the yield surface in three dimensions.

The following sections describe the deformation of Våle Shale (VS), giving a fully defined yield envelope, and the consolidation behaviour of Mercia Mudstone Group (MMG), Callovo-Oxfordian mudstone (COx), and VS. An approach is introduced to define the yield envelope/surface from the consolidation data. Finally, hydraulic behaviour is introduced.

2.8.2 Shale deformation

Figure 13 summarises the results from the compression tests for Våle Shale (VS). A total of 7 undrained triaxial tests were conducted, with a single uniaxial compression test. Results are shown in Table 1 and Table 2 of Section 6.2. All post-test samples showed the formation of a fracture at between 30 - 40° to the loading direction. This is also borne out in the stress-strain data, with all tests showing a reduction in stress. However, the nature of the stress-drop and the final fracture formed varies with increasing confining pressure. At low effective stresses an instantaneous stress drop is seen with a clear fracture forming at between 30-34˚ to the long axis. At the lowest confining pressure the fracture caused significant damage to the sample. This is characteristic of classic brittle behaviour. At elevated confining pressures the sample shows more elasto-plastic deformation with strain softening after the attainment of peak stress. The final test samples also displayed a degree of barrelling. This resulted in the formation of a thin fracture through the sample. It has been interpreted that the triaxial test conducted at the lowest confining pressure (9 MPa) is characteristic of brittle deformation, the two tests conducted at 19 and 29 MPa are representative of transitional behaviour, with the test at 39 MPa representing ductile deformation.

However, the latter was taken to sufficient strain that barrelling occurred and the sample fractured. The tests conducted at confining pressures greater than 49 MPa underwent yield during pressurisation to a starting stress greater than the preconsolidation stress.

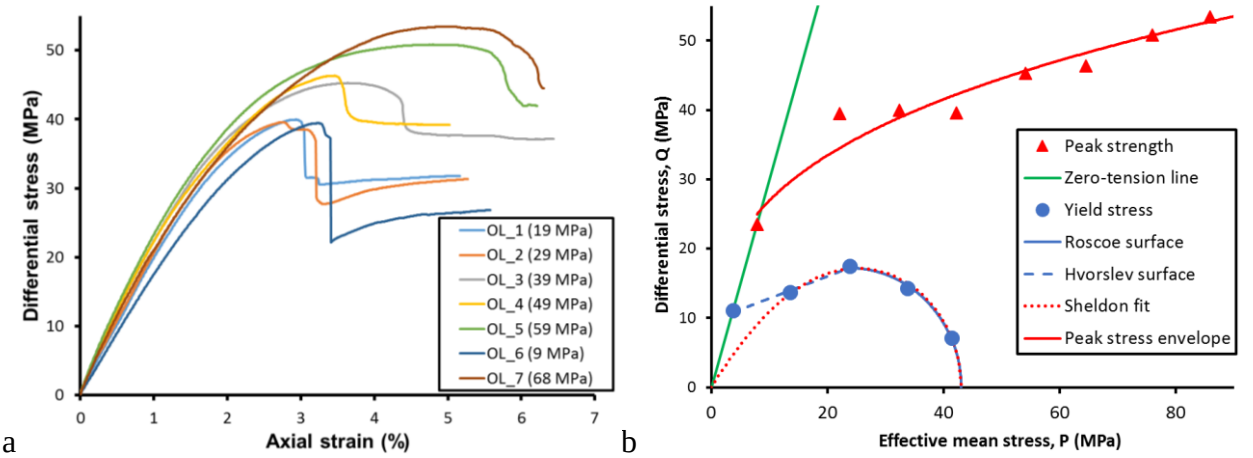

a b

Figure 13 - Results for triaxial compression testing of the Våle Shale (VS). a) stress-strain results for VS; b) yield and peak stress for VS in *P´* – *Q* space.

2.8.3 Yield envelopes (Critical State Soil Mechanics, CSSM)

Yield was determined for each uniaxial and triaxial compression test. Yield was considered to be the onset of volumetric deformation, as observed in the volume of the confining fluid. Figure 13b shows the results for yield and peak strength when plotted in the differential (Q) versus effective mean stress (P') space. As seen, the peak strength data follow a curved trend with strength continually increasing with mean stress as a power-law. Although the fit is not perfect as the three tests conducted at the lowest confining pressures all show near-identical peak strengths. The fit of the data including the uniaxial compressive strength suggests that the two tests conducted at 9 and 19 MPa confining pressure showed uncharacteristic strength. This, however, is not seen in the yield strength and may suggest that the damage created by the formation of the shear fracture in a relatively short sample is influencing results post-yield.

Yield data have been approximated using a linear fit for the Hvorslev surface, and a Roscoe surface using Eq.6 (Figure 13b). The Hvorslev has a slope of 0.32 and an intercept of 9.63 MPa, while the Roscoe surface equates to a slope of the critical state line (M) of 0.73 and a preconsolidation stress (p'_c) of 43.03 MPa. The fit suggests the brittle-ductile transition occurs at 23.7 MPa, at a critical differential yield stress of 17.2 MPa. Peak stress data were also fit in the Mohr-Coulomb approach, giving a shear strength of 16.5 MPa, an angle of friction of 5.5 °, and a fault angle of 42.2°. Analysis of all experiments has shown that brittle failure generally occurred after 3 – 3.5 % strain, Poisson's ratio was approximately 0.22, and Young's modulus increased with confining pressure from about 1.7 to 2.5 GPa. Figure 13b also has the Sheldon yield envelope plotted. This describes well the Roscoe surface, but considerable differences are seen in the brittle regime when considering the uniaxial strength result.

The Våle Shale (VS) samples used came from the Ormen Lange field and were taken at 2.9 km depth. This would equate to an effective stress of 37.1 MPa assuming a typical vertical gradient of 23 MPa/km (Zoback, 2010) and a hydrostatic pore pressure gradient of 10.2 MPa/km. This corresponds well with the estimate for p'_c and therefore suggests that the over consolidation ratio (OCR) of the VS is 1.14, meaning the samples were lightly over-consolidated.

2.8.4 Consolidation response

As with sandstone deformation, the yield envelope is bound by an important parameter that needs careful definition. In the case of sandstone this is the grain crushing pressure (yield under purely

hydrostatic stress conditions) and in the case of shale the bounding parameter is p'_c. Therefore, this is seen as a fundamental parameter of interest in the study of caprock behaviour.

The transport properties of rocks and sediments are intrinsically interlinked with fabric and porosity. These characteristics are directly related to burial and exhumation history, particularly in weaker materials such as mudstone. As a sediment is buried, the resulting increase in effective pressure leads to consolidation, by way of compaction and dewatering processes, and a reduction in void ratio, which in turn impacts hydraulic conductivity. A previously loaded sediment will therefore, retain a 'memory' of prior loading up to the previously experienced pressure.

The void ratio (e) is defined as the ratio of the volume of voids to the total volume of the sample. It is related to porosity (ϕ) by:

$$\phi = \frac{e}{1+e} \quad [8]$$

where e and ϕ are dimensionless. In soil mechanics, conventionally, the consolidation response of a clay is considered in terms of the change in void ratio resulting from a change in the logarithm of effective pressure, P' (Schofield & Wroth, 1968; Atkinson & Bransby, 1978). In e-ln P' space, the response of an unconsolidated clay to loading can be described in terms of consolidation along the 'Virgin Compression Line' (VCL) and unloading along the 'Rebound/Recompression Line' (RRL) (Figure 12a). A clay that has been previously consolidated, will plot below the VCL, until it is loaded above the maximum effective pressure it was previously subjected to (preconsolidation pressure, or p'_c).

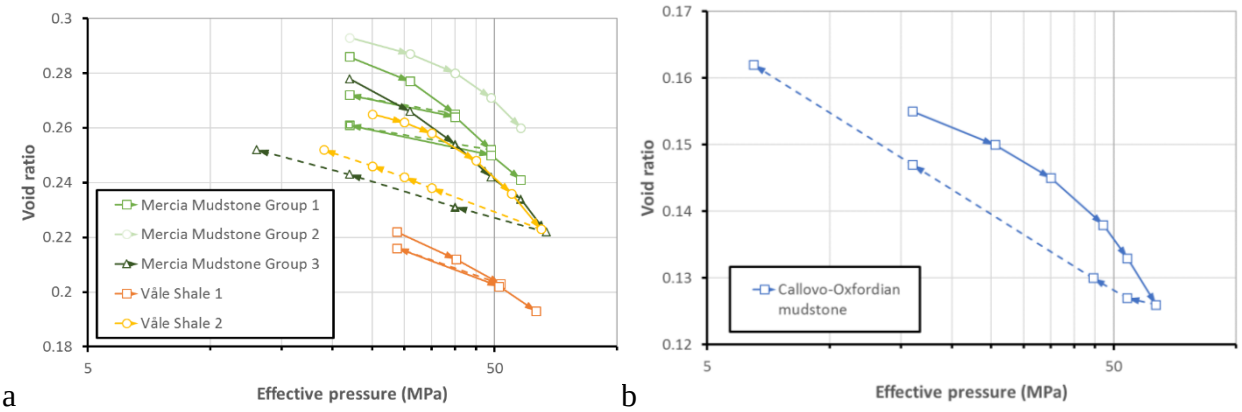

a b

Figure 14 - Void ratio versus effective pressure data. a) Mercia Mudstone Group and Vâle Shale test samples; b) Callovo-Oxfordian mudstone.

The consolidation responses for three Mercia Mudstone Group (MMG) samples, one Callovo-Oxfordian mudstone (COx) and two Vâle Shale (VS) samples are shown in the *e-ln P'* space in Figure 14. The solid lines represent the behaviour of the samples when confining pressure is increased and backpressure held constant, while the dashed lines represent the behaviour of the samples when confining pressure is decreased. These curves can be represented by the expressions

$$e = e_0 - \lambda \ln\left(\frac{P\prime}{P'_0}\right) \quad \text{[for the VCL]} \qquad e = e_0 - \kappa \ln\left(\frac{P\prime}{P'_0}\right) \quad \text{[for the RRL]} \quad [9]$$

where -λ and - κ are the slopes of the VCL and the RRL respectively, e_0 is the void ratio intercept at an effective pressure P'_0 = 1.0 MPa (Schofield & Wroth, 1968). Average values for the VCL ranged 0.52 – 0.60 for MMG and 0.040 – 0.069 for VS. Average values for the RRL were 0.011 – 0.018 for MMG, 0.020 for the COx, and 0.023 for the VS. Examination of the data indicates:

- The clear differences in estimated slopes for Mercia-3 as compared to the other MMG samples are likely related to its selection from a different lithofacies within the MMG.
- COx is more indurated than other materials thus explaining its non-yielding nature. Thus, it exhibits a much lower void ratio.

- VS samples exhibit a more variable initial void ratio as compared to MMG. The limited VS samples did not allow more test to be conducted and without additional measurements it is not possible to put limits on the variation of void ratio.

2.8.4.1 PRECONSOLIDATION PRESSURE (P'_C), COEFFICIENT OF VOLUME CHANGE (M_V) AND THE COEFFICIENT OF CONSOLIDATION (C_V)

While the consolidation response is well-defined in almost all tests, there are insufficient data points during yield to accurately identify the tangent line and thereby employ Casagrande's method for determining the preconsolidation pressure in most tests (Scott, 1980). However, it was possible to apply this approach to test Mercia 1, giving a preconsolidation stress of 35 MPa. As such, we propose a simpler approach based on the projection of the rebound-reconsolidation and virgin consolidation lines, defining the preconsolidation pressure as the point of intersection between the two lines (see Figure 15 to see this construction for samples Mercia 1 and Våle Shale 2). These values should be treated with caution as the projection of the virgin consolidation line depends on the number of selected points for interpolation. Using this approach, values for the effective preconsolidation pressure of 30 – 37.1 MPa (~2.5 km depth) for MMG, and 33.8 – 36.3 MPa (~2.7 km depth) for VS were determined. The latter give good agreement with the depth that the samples were extracted. The Ormen Lange field is in 1 – 1.2 km of water, with samples extracted from 2.9 km depth. Assuming an average vertical stress gradient of 23 MPa/km and pore pressure gradient of 10.2 MPa/km, this would give an effective stress of 37.1 MPa. This demonstrates that Våle Shale is close to being normally consolidated at depth.

Since many materials exhibit overconsolidated behaviour, it is convenient to define the *e*-ln P' curve in terms of the coefficient of volume change (m_v) also known as the coefficient of compressibility (Scott, 1980; Horseman *et al.*, 1996). This parameter is defined as the change in unit volume (dV) per unit change in effective pressure:

$$m_v = -\frac{1}{V_o}\frac{dV}{dP'} \qquad [10]$$

where V_o is the initial volume of the sample. The coefficient of consolidation c_v [m^2/year] can be derived from analysis of the consolidation transients, Figure 16a. In Taylor's square root of time method, as described by Scott (1980), outflow is plotted versus the square root of time, as shown in Figure 16. When viewed in this way, the early part of this curve is approximately linear. The intersection of this line with the asymptote $y = \max(\text{outflow})$ defines a value $\sqrt{t^*}$ that can be used to determine the coefficient c_v as:

$$c_v = \frac{\pi d^2}{4t^*} \qquad [11]$$

where d is half the length of the sample. The coefficient of consolidation for each sample is presented in Figure 16c. Note: it is important to observe that these values are approximate as not all test stages reached asymptote, i.e. reach 100% flow expelled (Figure 16a), even after 33 days. In some stages, this is a coarse assumption, and thus, the derived consolidation coefficients should be considered as indicative only. This phenomenon may result from secondary compression or creep, not represented in Terzaghi's consolidation theory, which forms the basis of Taylor's root time analysis method (Whitlow, 2001). However, the fact that a number of responses do reach well-defined asymptotes, suggests that possible leakage from the apparatus plays a negligible role in the total response of the sample during testing.

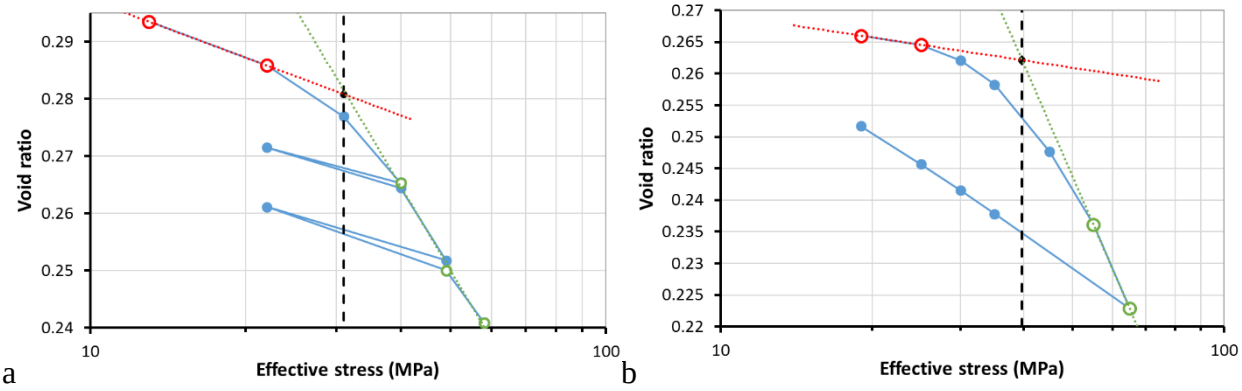

Figure 15. Void ratio versus effective pressure data, showing approach taken to define values for the preconsolidation pressure for samples (a) Mercia 1 and (b) Våle Shale 2.

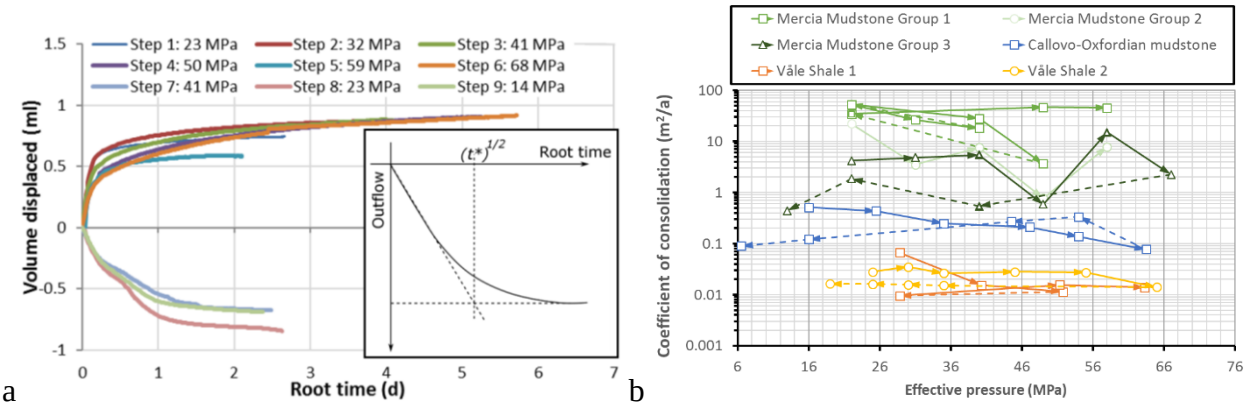

Figure 16 – The coefficient of consolidation. a) Transient outflow data for test Mercia 3 showing volume displaced against root time in days; (inset) schematic technique used to derive the coefficient of consolidation; c) coefficient of consolidation for each sample and test stage.

2.8.4.2 Sensitivity of specific storage, bulk modulus and hydraulic conductivity to pressure

From Horseman *et al.* (1996), the specific storage of a material is given by:

$$S_s = \rho_w g \left[\frac{1}{B} + \frac{\phi}{B_w}\right] \quad [12]$$

where ρ_w is the pore-water density (kg/m^3), g is the acceleration due to gravity (9.81 m/s^2), B the drained bulk modulus (defined as $1/m_v$), and B_w (= 2.2 GPa) is the bulk modulus of water. As such, specific storage therefore depends on two variables, the current porosity (or void ratio) and the bulk modulus (linking volume change to effective pressure). A weak correlation was seen between the experimentally-determined values for specific storage and the applied effective pressure. The small increase in storage coefficient may be an artefact of the calculation approach related to increased deformation as the samples undergo yield and consolidation in the normally consolidated domain. Experimentally derived data indicate:

- All specific storage values lie within the same order of magnitude. This is regardless composition and induration.
- For MMG and VS samples, there is some evidence suggesting that as yield is being approached the specific storage increases with permanent deformation. This is because the sample undergoes larger deformation at yield and thus, a larger volume of fluid is expelled. When unloading, however, deformation is within the elastic domain. Hence, strains are much smaller yielding an apparent reduction in the specific storage values.
- In the case of COx, deformation remains predominantly in the elastic domain.

It is also possible to estimate the hydraulic conductivity (K) and hydraulic permeability (k) of the sample for a change in effective pressure, using the simple relationships:

$$K = m_v c_v \gamma_w \qquad \text{and} \qquad k = K \frac{\mu}{\rho_w g} \qquad [13]$$

where γ_w is the unit weight of water (9,810 N m^{-3}) and μ is the viscosity of the fluid (Pa.s).

Inspection of the permeability data in MMG indicates significant scatter, with no consistent pressure trends obvious in the data. Permeability values range from ~2.1 × 10^{-18} to 8.4 × 10^{-21} m^2 (2.1 × 10^{-3} to 8.5 × 10^{-6} mD), indicating a reasonably good capacity as a sealing formation, despite the higher values being somewhat more permeable than many caprocks. These values are comparable with those reported by Armitage *et al.* (2016), though extending to one order of magnitude lower. A number of possible explanations may account for this. Samples in this study were fully resaturated before testing, whereas in Armitage *et al.* (2016) specimens were oven-dried first. Whilst the samples were reported to be free from smectite, the response of the much lower-swelling illite and chlorite fractions cannot be discounted out of hand and may have been impacted by this process, though the reasonably well-cemented nature of the material may have acted to counter this effect somewhat. Alternatively, the use of a pulse decay method for measuring permeability may have resulted in an over-estimation of these values (Boulin *et al.*, 2013; Egermann *et al.*, 2006). However, clearly the natural mineralogical variability within the MMG is a key control on these values and the more dolomitic horizons may potentially be of lower permeability as a result of cementation processes.

2.8.5 Hydraulic behaviour

With increasing effective stress, the permeability of shale decreases, as seen in Figure 17. For COx (Figure 17b) a clear relationship is seen, whereas VS has a less well defined relationship (Figure 17c). MMG shows a complex relationship of stress-dependent permeability (Figure 17a), although this is most probably related to noise associated with the calculation of permeability from the in- and out-flow of water from the sample. In general, a reduction in permeability is seen. The range of measured permeability values are shown in Table 2 (Appendix 6.2). Differences, however, are seen during the reduction in effective stress. In both VS (Figure 17c) and COx (Figure 17b) the permeability shows an increase with a relationship similar to that seen during the increase in effective stress. This suggests that the permeability variation is merely the elastic response of the porous network to the changing stress field and that the preconsolidation stress has not been exceeded during the experiment. The exception is MMG, which during reducing effective stress generally shows no change in permeability. A reduction is seen at the lowest effective stress, although this may be simply noise in the measurement. The non-recovery of permeability suggests that MMG has undergone permanent deformation during the experiment and has surpassed its yield stress.

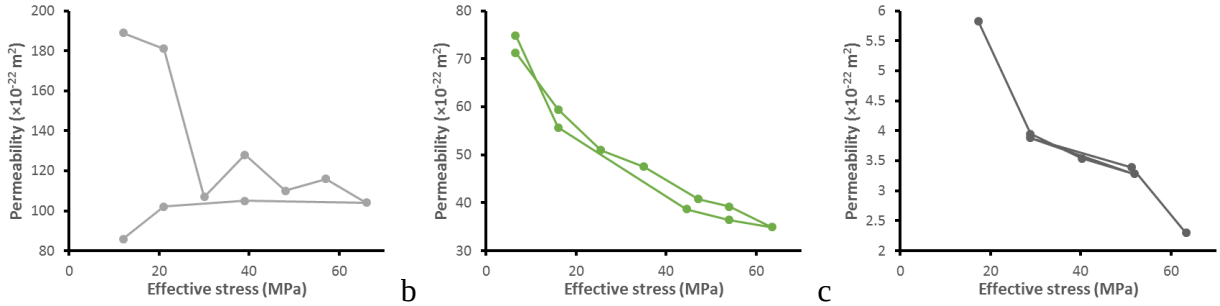

Figure 17 – Stress dependent permeability of shale. a) Mercia Mudstone Group; b) Callovo-Oxfordian mudstone; c) Våle Shale.

The hydraulic data suggest that a caprock experiencing changes in effective stress in the elastic region will show a change in permeability. For an increase in effective stress this will result in a

reduction in permeability. Should the change in effective stress result in the permanent deformation of the cap then permeability will not change during a reduction in effective stress. Therefore exceeding the yield point of a caprock will not necessarily have a detrimental influence on the sealing capacity.

2.8.5.1 NUMERICAL INTERPRETATION

The experimental results were modelled numerically to determine permeability (k) and Young's modulus (E). The fluid flow through a compressible porous medium is governed by the Biot's model (Biot, 1941). In this model, the governing equation for flow is obtained by combining Darcy's law with the mass conservation equation. The classical Biot's model assumes an elastic deformation of the matrix. Under the assumption of small strains and assuming an isotropic linear elastic material, the effective stress tensor can be determined. Following standard procedures, equations were discretized in space using the finite element method and in time using the finite difference method. Due to the nature of the problem, a two-dimensional axisymmetric finite element model was used. Regarding the time discretization, the backward Euler scheme was employed.

As shown by Horseman *et al.* (2005), the linear elastic model is unable to represent multiple testing stages from a single set of material values. Thus, each consolidation stage was treated as separate tests and the previous numerical procedure was used to fit E and k at each stage. Theoretical Young's moduli predicted by Biot's model were in good agreement with the experimental results, especially in those cases where the confining stress increased. Therefore, all three caprocks investigated as described by classical theory.

2.8.6 Summary of caprock properties

Three shales were investigated as direct or analogues of potential reservoir caprocks likely in Carbon Capture and Storage (CCS); namely Våle Shale (VS) from the Ormen Lange field of the southern Norwegian Sea, Mercia Mudstone Group (MMG), and Callovo-Oxfordian mudstone (COx). These ranged in induration, from a normally consolidated clay (VS and MMG) through to over-consolidated and highly indurated shale (COx). The triaxial testing of VS showed that the classical Critical State Soil Mechanics approach can describe yield in caprocks. A clear Hvorslev and Roscoe surface can be described, bound by the uniaxial compressive strength, slope of the critical state line, and the preconsolidation stress (P'_c). As with reservoir sandstone, the intercept with the abscissa is a critical parameter that can be used to estimate the complete yield surface. Therefore, p'_c is a fundamental property of mudrocks.

The consolidation behaviour of shale can be used to determine p'_c. However, considerable differences were found in the methodology used when compared with the triaxial test data. This may result from the limited capacity of the experimental test system and the fact that the samples were not taken to sufficiently high load. Therefore we highlight that determining p'_c in reservoir rocks requires care when interpreting results.

The stress-dependent behaviour (strain, porosity, storage, compressibility, Young's modulus, permeability) was investigated. For VS and COx the stress conditions investigated resulted in a reduction in permeability with stress, with almost full recovery during the reduction of effective stress. In contrast, MMG underwent permanent deformation and permeability was not recovered during the reduction of effective stress.

The study defined the yield envelope for shale and the volumetric deformation, and consequences thereof, once yield occurred. This approach can be used to consider a number of scenarios relevant to CCS, as outlined in the following section.

2.9 SCENARIO TESTING

The resulting yield envelopes for sandstone (Section 2.7.5) and mudrocks (Section 2.8.3) provide a tool with which to assess the mechanical response of these rocks to a depletion history scenario. Parkes *et al.* (2014) summarised the available *in situ* data for the Esmond, Gordon, Forbes, Hewitt, and Goldeneye fields in the North Sea, with additional information in Bentham *et al.* (2017) on production history. Differential horizontal stress data is not always reported, therefore the same proportion of differential stress as recorded at Goldeneye (Shell, 2011) was assumed for all fields, consideration was also made of the likely range of differential stresses seen in basins. A depletion of 10 MPa pore pressure was considered, this being a likely drawdown during exploration. For all yield envelopes, P' was taken as the effective mean stress, equal to $^1/_3$ (σ_1 + 2σ_3) - P_p, where P_p is the porewater pressure. The resulting change in differential stress is less well constrained. Zoback (2010) describes the relationship between P' and Q, for a chosen stress path, as:

$$Q \sim j\Delta P' \quad [14]$$

where j is a constant equal to $^2/_3$. This correction accounts for poroelasticity and includes the Poisson effect and Biot's coefficient. However, Ruistuen *et al.* (1999) highlight that during depletion the influence of pore pressure on differential stress is variable, citing examples where j varies between 0.1 and 1.0 and manifest as shallower or steeper stress paths in P'- Q space, respectively.

Figure 18 shows the scenarios for reservoir sandstone. The Sherwood Sandstone Group (SSG1) can be seen to be within the elastic region of deformation for all of the five fields considered. It can be emphasised that depletion to a condition of zero pore pressure will not result in failure. Therefore, SSG1 can be viewed as competent rock that will not result in deformation of the reservoir. In contrast, SSG2 has a different outcome. This sandstone has properties that mean it is not able to sustain the pressures present in the Gordon, Forbes, or Goldeneye fields prior to draw down. In the Esmond field yield would occur after 2 MPa pore pressure reduction, whilst Hewitt would yield after 7 MPa reduction. At yield the deformation would be in the form of pervasive cataclasis and the yield envelope would increase in size as a response of the concomitant reduction in average grain size and porosity. It can be concluded that deformation of the reservoir rock is likely to be restricted to the reservoirs, or sections of the sequence, that are high in porosity and have large grain-size.

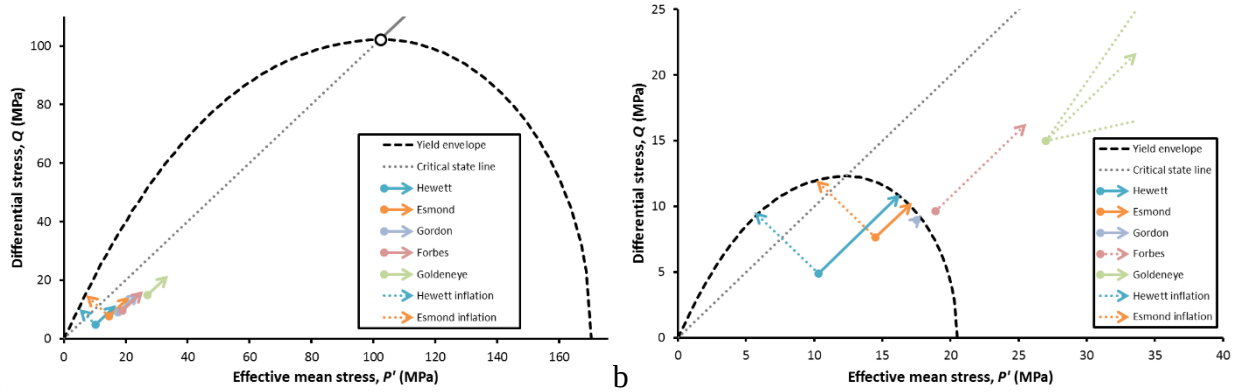

Figure 18 – Scenario analysis for reservoir rocks. a) Sherwood Sandstone Group (SSG1); b) Sherwood Sandstone Group (SSG2). Depletion scenarios for the Forbes, Esmond, Hewett, Gordon, and Goldeneye fields with a drawdown pressure of 10 MPa. Note green dotted lines for Goldeneye in (b) represent j = 0.1, 0.66 and 1; these are not shown for all scenarios.

It is expected that re-inflation of the reservoir during CO_2 injection would result in an increase in pore pressure to a magnitude that is less than the starting pore pressure of the field, i.e. if a reservoir is depleted by 10 MPa it will be re-inflated by a maximum of 9 MPa. This is likely to result in a stress path that follows that seen during depletion. As the pore pressure is likely to be less than

that seen before depletion it is therefore unlikely that the yield envelope will be intercepted. In contrast, injection of CO_2 into saline aquifers requires the raising of pore pressure above that seen *in situ*, this is necessary to induce flow into the aquifer. This scenario would result in failure of the reservoir after 6 MPa and 5 MPa in Hewett and Forbes respectively. Of note is the deformation mode. At Esmond deformation would be close to the brittle-ductile transition, whereas at Hewitt it would be purely brittle. This would result in the formation of localised shear zones. Deformation would be possible in this scenario in SSG. Raising pore pressure by 8 MPa would result in failure at Hewett, whereas 11 MPa would cause Esmond to fail. In both of these cases the deformation would be brittle.

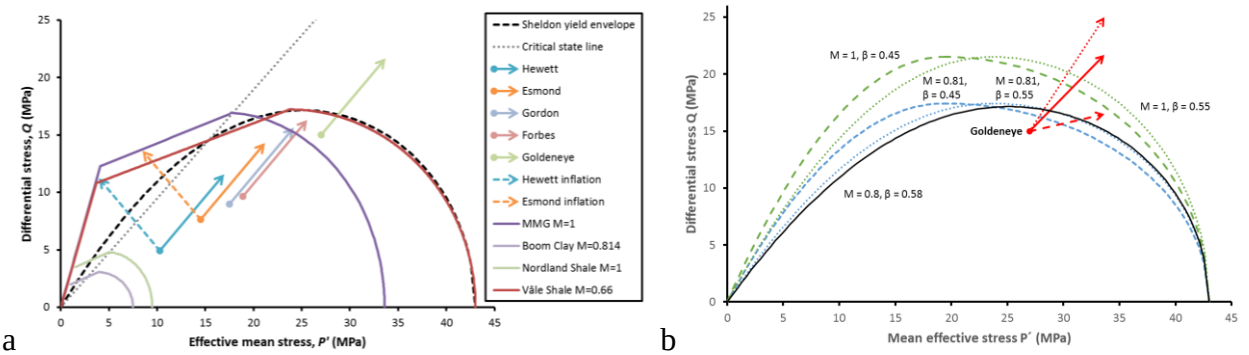

Figure 19 – Scenario analysis for caprocks. a) Mercia Mudstone Group and Våle Shale. The measured yield envelope for VS is compared with the Sheldon yield (dashed line). Depletion scenarios for the Forbes, Esmond, Hewett, Gordon, and Goldeneye fields with a drawdown pressure of 10 MPa are shown; b). Example Sheldon yield envelopes for Våle Shale with varying *M* and *β* and stress path for Goldeneye with varying *j* (0.1, 0.66 and 1).

Figure 19a shows the scenario analysis for caprock material. This shows that the Våle Shale is a competent caprock and that failure in the scenarios investigated would only approach failure for Goldeneye given a pore pressure depletion of 3 MPa. This would result in failure at the Roscoe surface, with distributed shear deformation. Failure could be induced in Esmond if it was a virgin aquifer and pore pressure was raised by 7.5 MPa. This would result in a shear localisation failure mechanism. Finally, Hewett could be taken to extensile failure if pore pressure was raised from a virgin state by 9 MPa.

Figure 19a shows a postulated yield envelope for Mercia Mudstone Group with M = 1 and a Hvorslev of similar slope to that measured in Våle Shale. This shows that failure would be induced with a drawdown of 10 MPa in Gordon and Forbes, with the starting stress regime greater at Goldeneye than the strength of MMG. In all three cases the deformation would be through distributed shear localisation. As with MMG, failure could be induced in Esmond and Hewett if it was a virgin aquifer and pore pressure was raised by 9 and 9.5 MPa respectively. In both cases, shear localisation failure would be induced.

Figure 19a shows a comparison of caprock materials assuming a common form of the yield envelope. This includes Norland Shale (Harrington *et al.*, 2007) and Boom Clay (Harrington *et al.*, 2017[a]). As shown, these two weak mudrocks, including a reservoir caprock, are not sufficiently strong enough to accommodate the *in situ* stresses of the fields investigated. Deformation is likely to be in the form of distributed consolidation.

Figure 19b illustrates the variability and uncertainty in the yield envelope approach. The properties of the caprock will vary based on M and β. As described for sandstones, these parameters describe the height and asymmetry of the envelope. Four possible envelopes are shown for Våle Shale with the expected range of M of 0.81 and 1. In addition, yield is shown for M = 0.8, as measured for VS. Envelopes are also shown illustrating the asymmetry of β between 0.45 and 0.55. This illustrates that in the absence of directly determined parameters, the selection of parameters based on knowledge of other mudrocks can introduce marked uncertainty on the yield envelope. Figure

19b also illustrates the uncertainty in the direction of the stress path. Zoback (2010) states that a change in pore pressure results in a change in differential stress because of poroelasticity and Biot effect. Three stress paths are illustrated for j = 0.1, 0.66, and 1. Experience of clay-rich materials at BGS suggests that pore pressure changes are seen equally in all directions, i.e. the path is parallel with the x-axis. Further research is needed to determine the direction of the stress path.

It has to be noted that many of the rocks reported here are normally consolidated for the depth that the samples were acquired. Therefore, correction should be made to the size of the yield envelope to realistically predict how the caprock will behave at the depth of the reservoir of study. Therefore, the analysis stated above is not a full analysis of the behaviour expected at each individual reservoir and only gives a flavour of the approach given the limited data available. In order to fully describe deformation the full yield envelope is required along with estimates for the over consolidation ratio and depth of investigation at each reservoir.

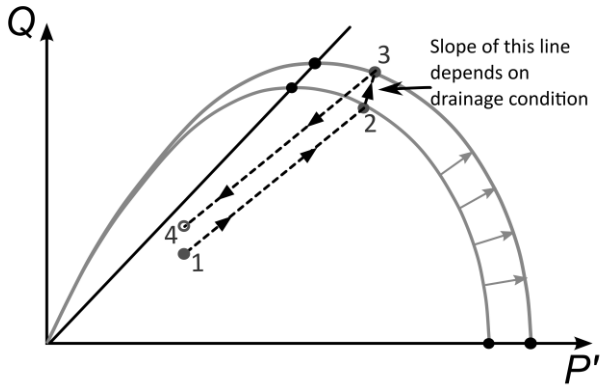

Figure 20 – Critical state envelopes in P'- Q (effective-differential stress) space. A schematic highlighting the stress path taken during (1-2) depletion pre-yield, (2-3) depletion post-yield, (3-4) pore pressure recovering resulting from injection of CO_2. The envelope will grow in response to yield.

In cases where yield on depletion occurs, inelastic deformation will also impact the return stress path on injection of carbon dioxide (Figure 20). The initial stress path will be followed (1) until the yield envelope is intersected (2). At this stage, stress levels above the yield surface cannot occur and begin to converge towards the critical state point. However, as shown during consolidation testing, yield will result in a reduction in the void ratio, reflected as a migration along the third axis of the critical state envelope, the specific volume. In P'- Q space this will be manifest as an increase in the size of the critical state envelope (3), as the rock responds to the changing stress conditions. The amount of deformation experienced during this stage will be dependent on the slope of the envelope in Q - v space, as well as the total reduction in pore pressure allowed during this phase, and will control the degree of hysteresis experienced when pore pressure again increases during injection of CO_2. Any hysteresis will lead to a greater chance of intersecting the dry-side of the envelope as pore pressures are elevated to their original values. Also of importance will be the drainage condition of the rock during these changes, which will impact the stress path slope between stages (2) and (3). Undrained conditions are more likely to lead to brittle behaviour, whilst improved drainage will encourage ductile deformation. The full draw down experienced by the reservoir will primarily impact on the caprock at the interface with the reservoir, whilst propagation into the caprock will be limited by its transport characteristics. As such, the impact of stress path changes will be dependent on the thickness of the seal and its initial permeability.

2.9.1 Four potential scenarios

There are four possible reservoir conditions that may be encountered during CCS;

1. Strong reservoir overlain by a strong caprock: In this case it is likely that perturbations of pore pressure will not induce deformation in either the reservoir or the caprock. All bulk deformation will be elastic and recoverable.
2. Strong reservoir overlain by a weak caprock: Here, the reservoir elastically deforms and is unaffected by changes in pore pressure. However, the transmission of pore pressure change to the caprock may result in deformation. This is likely to result in the consolidation of the caprock in response.
3. Weak reservoir overlain by a strong caprock: In this case the reservoir sandstone reaches yield, resulting in cataclasis and compaction of the reservoir. Porosity and permeability will reduce and impacts the bulk transport properties of the reservoir. The strong caprock is generally unaffected by the pore pressure change, but does need to accommodate the compaction seen in the reservoir. This will result in the formation of flexural forces with the cap, which could result in the formation of faults as the reservoir subsides.
4. Weak reservoir overlain by a weak caprock: As with (3), the reservoir will subside in response to cataclastic deformation of the sandstone. If the reservoir area is large and the caprock is close to being normally consolidated, the cap is likely to accommodate these strains without significant deformation. Any deformation in the cap is likely to result in consolidation and not the formation of fractures.

It should be noted that the four scenarios above are simplistic. In reality, considerable variation is likely to be seen in the properties of individual layers within both the cap and reservoir. Therefore, it can be concluded that the weakest layers will fail first. This may lead to compartmentalisation in the reservoir rocks and differential deformation in the cap.

2.10 DISCUSSION

The critical state mechanics (CSM) approach provides a robust framework with which to assess the performance of both reservoir systems and caprock formations. It is able to predict the onset of yield and the deformation that follows, should it occur. In this way, it is able to represent both depletion and inflation scenarios.

As with any model approach, the predictions of the CSM are dependent on the quality of the input data. Availability of core may limit the number of tests which can be used to define the failure envelope. In reality preserved core from both reservoir and caprock sequences of sufficient quality and quantity is unlikely to be available. Therefore, compromises need to be made and the consequences of these will be discussed.

2.10.1 Sandstone reservoirs

In general, all sandstones can be described using a single yield envelope form that is bound by the intercept of the abscissa (grain crushing pressure, P^*). This parameter has been shown to be easy to measure from either whole core or drill chippings. Alternatively, this parameter can be estimated using the Hertzian contact model if porosity and average grain size are known. However, this approach can introduce significant error in defining the size of the envelope, but in the absence of test material this is seen as an acceptable approximation.

The height and asymmetry of the yield envelope is not fully captured by using the single envelope approach based on P^* values. This can introduce a second error which requires conservatism on pore pressure variation based on sandstone varieties that are weak in shear, see Figure 11 green line.

To limit uncertainty a full suite of triaxial experiments would be preferable from either the reservoir or analogue material. Should this not be possible, estimates of P^* made from chippings assuming a common yield envelope, provides the next best option but requires conservatism. Finally, estimating P^* from petrography could be used but could introduce significant error.

2.10.2 Mudrock caprocks

Similarly to sandstones, mudrocks can be described by the critical state mechanics approach with a yield envelope bound by the preconsolidation stress (p'_c). Differences occur in the form of the envelope on the brittle side of the critical state where a linear Hvorslev surface exists. Unlike sandstones, normalisation of the yield envelope in mudrocks may be more complicated, Figure 19.

One approach to defining the yield envelope is described by Sheldon *et al.* (2006). This describes the Roscoe surface (ductile deformation) well but differences are observed in the brittle regime (Hvorslev line). Therefore, should stress paths intercept the yield envelope in the ductile regime the Sheldon approach provides an adequate representation. On the other hand, if deformation is in the brittle regime, the Sheldon approach predicts a weaker caprock response. This is only likely to be an issue in the inflation of 'virgin' aquifers.

Accurate definition of the preconsolidation stress can also be problematic. Differences were observed between isotropic and triaxially derived values, though the reason for this remains unclear. The interpretation of consolidation curves in 'creeping' materials presents significant challenges and is time consuming if done correctly.

Ideally, a full suite of triaxial measurements is required to reduce uncertainty in the definition of the yield surface. Should this not be possible, estimates of p'_c can be made from a single consolidation test and then assuming a unified yield envelope. Finally, estimating p'_c from an understanding of reservoir burial history can also be made but may introduce significant error, especially if the caprock material has undergone diagenesis.

2.10.3 Post-yield deformation

Based on this study, the change in stress caused by drawdown generally results in ductile deformation once the yield surface is reached. The exception is Goldeneye if the caprock was Våle Shale, even then the deformation is likely to be transitional between brittle and ductile regimes. In the ductile regime, deformation will result in consolidation of both reservoir and caprock reducing porosity/void ratio. This will increase the size of the yield envelope and reduce permeability, enhancing caprock seal capacity, but reducing storage capacity of the reservoir.

The transition to the new envelope is difficult to define and requires careful focussed experiments that were outside the scope of this study. An alternative method would be to condition core to greater burial depths and repeat the suite of triaxial tests. However, in ultra-low permeability rocks drainage times may be prohibitive and the availability of core problematic. From a spatial modelling perspective, such information would be necessary to predict the formation response.

The direction of the stress path during depletion and inflation is not accurately known. In the absence of data the approach of Zoback (2010) was adopted. However, the assumption of poroelasticity may be questionable applied to typical reservoir rocks. As the Roscoe envelope tends to be symmetrical the magnitude of the pore pressure change is not significantly altered if the direction of the stress path varies.

2.10.4 Scenario analysis

Four scenarios were considered as part of this study (Figure 21): (i) strong reservoir – strong caprock, (ii) strong reservoir – weak caprock, (iii) weak reservoir – strong caprock, and (iv) weak reservoir – weak caprock. To test these scenarios, five production histories were selected. Condition (i) all bulk deformation will be elastic and fully recoverable with no impact on reservoir management. Condition (ii) deformation limited to the caprock, which consolidates enhancing seal performance. As deformation in the reservoir is elastic no change in storage capacity is likely in both conditions (i) and (ii). In condition (iii) production leads to a loss of reservoir volume which will impact the amount of CO_2 that can be sequestered. As the caprock is strong deformation is only likely if reservoir compaction is significant leading to flexure of the caprock. The final

scenario (iv) leads to deformation of both reservoir and caprock, leading to compaction and consolidation respectively. Scenarios (iii) and (iv) can lead to subsidence at the sea floor if compaction of the reservoir is significant.

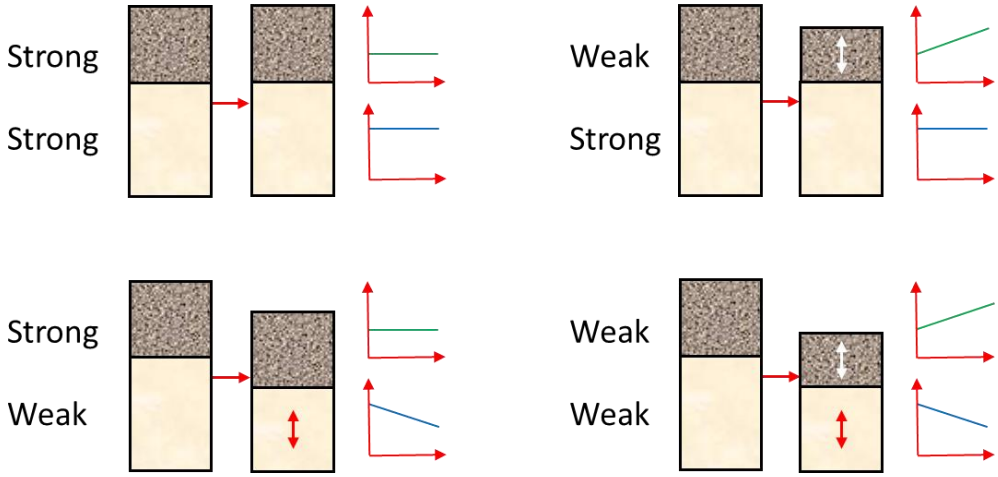

Figure 21 – Models of reservoir response to a reduction in pore pressure. Note: blue line represents storage capacity, green line represents sealing capacity.

The ideal scenario for CO_2 sequestration is a strong reservoir with a strong caprock. However, most reservoir rocks are close to failure at depth and therefore this is an unlikely situation. In reality, in weak reservoirs deformation will result in differential earth movements and flexure of caprocks. These combined effects may cause strong caprocks to fracture/fault, potentially lowering sealing capacity. Weak caprocks will deform plastically and over the time scales of depletion can accommodate significant strain without forming open fractures. Counterintuitively, weak caprocks appear preferable as seals for sequestration sites as deformation results in a reduction of permeability.

2.10.5 Additional considerations

The above scenarios consider reservoir and caprock as homogenous media. In reality, physical properties will vary considerably, with the weakest parts of the sequences deforming first. When considering CCS sites the complexity of the sequence stratigraphy needs to be incorporated. This will result in multiple yield surfaces that can be defined from the full critical state envelope in 3D.

It has been assumed that pore pressure changes in the reservoir are transmitted into the low permeability caprock. This is questionable over the timescales of a production and inflation history. However, pore pressure changes drive deformation and if not transmitted far into the caprock it will not result in deformation. Therefore, this analysis can be viewed as a ‘worse case’ scenario.

The approach presented here makes no consideration of pre-existing or induced discontinuities (fractures, faults, joints, bedding planes etc.). The implication of these features is considered in Section 3.

2.11 CONCLUSIONS

The critical state mechanics approach provides a robust framework that can be used to predict the onset of deformation in response to pore pressure changes during depletion and/or inflation. The framework also allows deformation mode and the resulting volumetric changes to be estimated. For reservoir rocks (sandstone), a single, unified, yield envelope is appropriate, which is bound by the grain crushing pressure (P^*). In detail, the height and asymmetry of the envelope needs to be considered. For caprocks (mudrocks), the yield envelope is different in the brittle regime (Hvorslev region), and non-uniqueness is seen within this region. Therefore, a unified yield approach is only

appropriate if the stress-path is likely to intercept the yield envelope in the ductile (Roscoe) regime. Our analysis has shown that depleted reservoirs are only likely to result in distributed ductile deformation (Roscoe) and therefore a unified surface can be used for depletion. Inflation of virgin aquifers may result in brittle regime deformation and care should be taken on yield envelope approach in this case. The unified envelope for mudrocks is bound by the pre-consolidation stress (p'_c), which is a straightforward measurement using standard experimental apparatus.

Four scenarios have been introduced based on strong/weak reservoir and caprocks using drawdown and inflation scenarios for five North Sea fields. The results show that both strong reservoirs and caprocks do not fail. In the case of weak reservoir rock, this consolidates reducing storage capacity and reduced flow properties. For weak caprocks, when failure occurs it will be through distributed shear deformation, increasing seal capacity. Counterintuitively, weak caprocks are favourable as they can accommodate deformation, whereas strong caprocks over a subsiding reservoir are subject to flexure forces that may result in fractures/faulting. For CCS in virgin fields as pore pressure is raised above *in situ* pressures (saline aquifers), when deformation occurs this is likely to be through localised shear processes (fractures/faults).

This study has devised a methodology for reservoir assessment considering varying degrees of core and data that are likely during reservoir assessment. The ideal case would be to perform a suite of triaxial tests on well-preserved core material (or alternatively analogue core material) to define the yield envelopes. If sufficient core material is not available, alternative approaches are necessary. For sandstones, a grain-crushing (P^*) test can be used to bound an idealised yield envelope from either a single test sample or from chippings. In mudrocks, a single core sample can be used to perform a test to define the pre-consolidation stress (p'_c). A unified yield envelope can then be assumed, although if deformation is likely in the brittle regime this could introduce errors in the prediction of yield. If core material is not available from the field in question or an appropriate analogue, P^* can be estimated from estimates of petrology (porosity and average grain size), whilst p'_c can be estimated from burial history of the reservoir. It has to be considered that uncertainty will increase as data/core availability decreases. This may lead to conservative estimates for safe pore pressure variation that ultimately reduces the utilised storage capacity of the reservoir.

The current study has highlighted three knowledge gaps that require further investigation. 1) The influence of fractures on the behaviour of the CSM approach has not been considered. 2) The transmission of pore pressure from the reservoir to the caprock is uncertain in its magnitude and depth of penetration. 3) The assumptions in Zoback (2010) and the influence pore pressure changes have on the direction of the stress-path require experimental verification.

Work Package 1 has greatly advanced our knowledge on the sealing capacity of caprocks during depletion and inflation histories. The use of the CSM approach allows description of deformation and identification of safe operational limits for CCS sites.

3 Work Package 2: Geomechanical modelling of injection/depletion scenarios

3.1 INTRODUCTION

CONTAIN has focussed on the study of injection of CO_2 into depleted reservoirs. In particular, caprock integrity during CO_2 injection into depleted reservoirs was studied in the presence of geological discontinuities at the reservoir-caprock interface. Caprock integrity was studied during two geomechanical phases: depletion and re-injection, with a particular focus on quantifying the effect of geomechanical discontinuities. WP2 of CONTAIN considered the growth of pre-existing fractures and faults, and investigated the effects of depletion and reinjection on the potential growth of pre-existing discontinuities. This section of the report is organised into three sub-sections: (1) Developed methods, (2) Effects of depletion on caprock integrity, and (3) Effects of CO_2 injection on caprock integrity. Subsequently, the report discusses work on upscaling and interaction mechanics, and summarises the main contributions. Poro-elastic effects on fluid-filled and fluid-driven fractures were investigated; growth of fractures and normal faults during depletion and re-injection was assessed, as well as significantly developing and validating our simulation capabilities during the project. The work package has involved three post-doctoral researchers, one PhD student and several undergraduate students, who have all contributed to the following report.

Work Package 2 has led to a variety of publications, including papers in the journals *Geothermics*, *International Journal of Greenhouse Gas Control*, and *Journal of Geophysical Research: Solid Earth*. Two conference papers for the *American Rock Mechanics Association* also describe the development of new modelling techniques. An additional manuscript is currently being written, which will review geomechanical studies for depleted reservoirs and their impact on social perception. Simulations presented in these publications have focused on realistically modelling reservoir and caprock properties, in order to understand the geomechanical effects arising before, during, and after CO_2 injection. Our capabilities to simulate sub-surface fluid injection have been greatly enhanced during the CONTAIN project. Several collaborations, such as with Bergen University and ENSTA Paris Tech have also emerged due to the capabilities developed at Imperial College during CONTAIN.

3.2 DEVELOPED METHODS

The in-house simulator, Imperial College Geomechanics Toolkit (ICGT), has been significantly enhanced during the course of this project, in order to incorporate the fully-coupled simulation of thermo-poro-mechanical deformation and its effects on fracture growth. In the present approach, fractures are modelled as surface discontinuities in a three-dimensional matrix. Flow through the fractures is modelled separately from the flow through the matrix; thus, five interacting conceptual models are considered: (i) mechanical deformation, (ii) flow through the matrix, (iii) flow through the fracture, (iv) heat transfer through the matrix, and (v) heat transfer through the fracture. The numerical solution has been developed using standard finite elements, with spatial discretisation achieved using the Galerkin method, and temporal discretisation using finite differences. Geometry is discretised using volumetric and surface meshes, a combination of triangle and tetrahedral isoparametric quadratic elements. In addition, the exchange of fluid and heat between the fracture and matrix is modelled using a three-dimensional leak-off model. The simulator now has the ability to handle multiple material domains, such as geological layers. During CONTAIN, we have implemented the ability to handle anisotropic permeability and elastic anisotropy. The handling of the geometry of fractures and the computation of exact aperture distributions has been significantly improved during this project. Furthermore, the poro-thermo-elastic deformation cycle has been coupled to a contact deformation module of the simulator that allows us to study

deformation under compression, alongside flow and growth analyses under compression. The details of the equations and specific validations have been published in a series of four papers.

As originally proposed, the following tasks were undertaken during work package 2. During the first two years, the focus was the extension, integration, and validation of existing flow and propagation kernels. The key developed aspects were the incorporation of the poro-elastic terms to the simulator, integration of the fluid-pressure term into the fracture propagation kernel, and incorporating a stress- and time-dependent permeability model. Permeability variation with stresses was investigated as a function of fracture aperture variability within fractures in the caprocks, as opposed to bulk material property variations. This project utilised the ICGT (Imperial College Geomechanics Tookit) and also CSMP (Complex Systems Modelling Platform), two C++ object-oriented finite-element based libraries specialised in simulating fracture growth and complex multi-physics processes, respectively. Upscaling of fracture effects within the geomechanical context was partially addressed, primarily focusing on improving the costly relationship between model size, geometric complexity, and run-time expense. Upscaling and complexity reduction is an on-going task, that relates to multiple simulation aspects. Specifically, the accuracy and efficiency of thermo-hydro-mechanical deformation of the fractured rocks was examined for monolithic and iterative solutions of the coupled equations. These are still both considered for field scale scenarios, but monolithic approaches were found to be best suited for poro-elastic scenarios albeit requiring the inversion of a larger matrix. Due to the elevated cost of friction resolution, multiple computational strategies were investigated to model the effect of *in situ* stresses on the thermo-hydro-mechanical deformation of the rock. Due to computational restrictions, most of the published approaches during CONTAIN compute compressive stresses only once, or sparsely during the simulation; in contrast to fluid-driven injection/depletion stresses which are much more frequently computed throughout the simulation (initial transient steps of 10,000 seconds, increasing by a factor of 1.1 or 1.2 during the simulation). Several depletion scenarios, consistent with Goldeneye depletion campaigns published by Shell, where taken as depletion scenarios. Generic re-injection scenarios based on Goldeneye were considered at later stages of this project. Depletion was studied in 5-year spans, followed by 5 years of equilibration. Reinjection scenarios were studied for 160-year span periods.

Two papers document the validation of the poro-elastic (HM) component of the simulator, in the context of single and multiple fracture growth (Salimzadeh *et al*., *IJSS* 2017, *IJRMMS* 2017). The third paper describes the thermal effects on fracture aperture distributions during the injection of relatively cool CO_2 into relatively warm *in situ* fractures (Salimzadeh *et al*., *Geothermics* 2018). This paper focusses on the deformation of the discontinuity wall, which translates into accurate aperture distributions. Alongside the development of the coupled thermo-poro-elastic model, we have investigated fracture and fault interactions, developing a method for quantifying the interaction between fractures (Thomas *et al*., *JGR* 2017), while observing the changes in geometry arising from interacting fluid-driven fractures (Salimzadeh *et al*., *IJRMMS* 2017).

An additional four papers document the application of these methods to the analysis of the geomechanical effects of deflation and re-inflation in depleted reservoirs. In early stages of the project, we experimented with combining discrete fracture and damage models (Defoort *et al*., *ARMA* 2016) for application to the Goldeneye reservoir, performing simulations of distributed damage due to reservoir deflation (Defoort *et al*., *ARMA* 2015). The damage model upscales the effect of distributed micro-fractures, while preserving the anisotropy and poro-elastic effects provided by a discrete fracture representation. Initial deflation simulations did not take into account thermal effects, but rather focused on the effects of deflation on stress redistribution along pre-existing fractures, and how they may lead to growth at early stages of growth. This is described in the report “Deliverable 2 Report: Initial Modelling Results”. Two further papers describe our study of re-inflation of the reservoir due to CO_2 injection. The injection of CO_2 is modelled using a coupled thermo-poro-elastic formulation. Non-isothermal flow is considered within the fractures and rock matrix, and the two flow domains are coupled through a mass transfer term. A full-scale

field case geometric model, based on the Goldeneye reservoir, has been developed, and is used for simulations. The third paper in this series applied the caprock integrity methodology to the Goldeneye North Sea reservoir. It studied the effect of a pre-existing fault distribution on the potential breach of the caprock (Salimzadeh *et al.*, *IJGGC* 2018). The paper also investigates flow paths into the caprock and the role of temperature and pressure on aperture distribution within fractures and faults. An additional paper studies the effect of CO_2 injection on a wider network of fractures, in this case, applied to a different depleted reservoir (Paluszny *et al.*, *ARMA* 2017).

3.3 EFFECTS OF DEPLETION ON CAPROCK INTEGRITY

Full-scale models with dimensions 50 × 20 × 8 km were run at large scales based on the field data from the UKCCS report (shown in Figure 22). The effect of faults on depletion was quantified by comparing models with and without the major mapped faults in the reservoir and caprock. Models containing faults included thirty faults in the reservoir and caprock, seventeen of which were solely within the reservoir layer. The large-scale models are used to quantify the effect of depletion on subsidence, and when the effect of faults were included, the models were able to reproduce the subsidence observed in the UKCCS report. Smaller-scale models (10 × 6 km) focused on the major faults order to examine the change in the state of stress at their tips in detail, revealing significant differences in how faults are stressed across the reservoir.

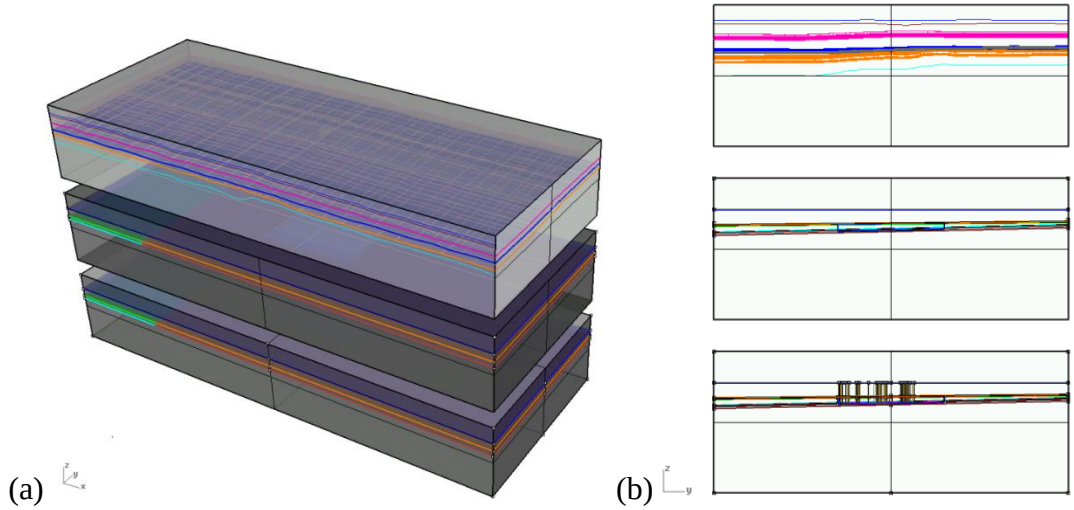

Figure 22 - Reservoir models constructed from UKCCS field data, shown in 3D (a) and side view (b). The top model shows the actual field, the middle shows a simplified model, and the bottom shows the simplified model with faults. Each model has dimensions of 50 × 20 × 8 km. The depicted are NURBS surfaces representing the layers of the model. It is merely a sketch depicting the complexity of the layers, and the relative positioning of the simulated faults. Details of he layers can be found in the UKCCS report.

Depletion of the reservoir is simulated by prescribing the pressure at a well located in the centre of the reservoir, decreasing linearly over five years. The resulting depleted pressure in the reservoir ranges from 3 to 10 MPa, which is consistent with measured reservoir data reported in UKCCS. Figure 23 shows the resulting displacement of the reservoir and caprock in the faulted model. The simplified full-scale model, without discrete faults, predicts a maximum displacement of 12.3 cm above the reservoir in the caprock layer. This in turn predicts a sea floor subsidence of less than 8 cm. The displacement in the caprock is asymmetric as a result of the change in thickness and dip of the layers. When faults are included in the full-scale model, their higher permeability enhances the pressure drop on one side of the well. Displacement concentrations are observed along the fault as well as its tips, which produce shear and tensile stress concentrations. By incorporating faults into the model, the maximum displacement is reduced to 11.6 cm.

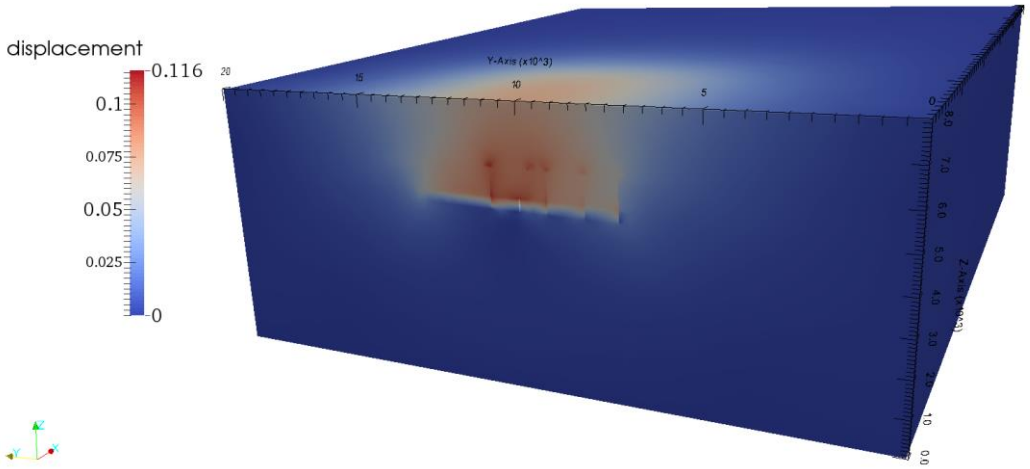

Figure 23 - Total displacement of the caprock at the end of production in the small-scale models containing discrete faults.

Profiles of the displacement at the reservoir-caprock interface and at the top of the model, demonstrating the vertical (*z* direction) subsidence that occurs due to depletion are shown in Figure 24. Fractures are aligned perpendicular to the *y* direction therefore the horizontal subsidence at the reservoir-caprock interface show displacement jumps due to discontinuities.

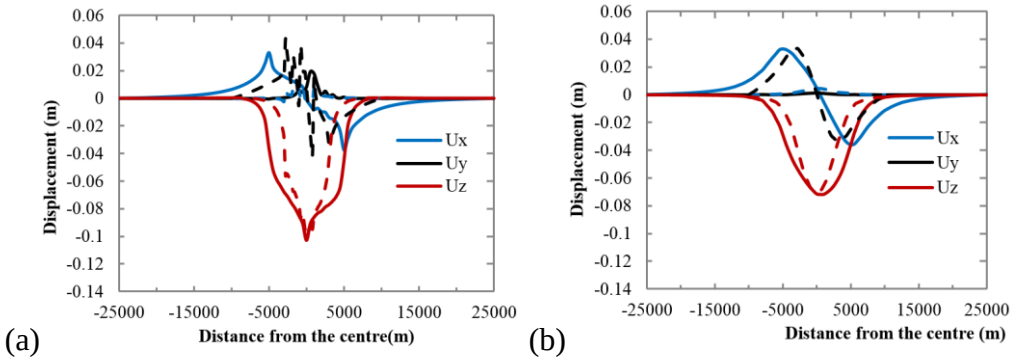

Figure 24 - Profiles of displacement in the *x*, *y*, and *z* directions at the top of the reservoir (a), and at the top of the model (b).

Small-scale models examined the stress at fault tips using Stress Intensity Factors (SIFs). SIFs quantify the energy at the fracture tip contributing towards failure in three modes: opening (mode I), in-plane shear (mode II), and out-of-plane shear (mode III). Therefore, they quantify the type of failure that may occur, and the direction of fault growth. The faults were limited to the caprock layer in order to investigate whether the potential direction of growth is towards the reservoir or away from the reservoir. After five years of production simulation, the maximum predicted displacement is now 8.44 cm, which is much closer to the actual UKCCS measurements (around 9 cm) than were the predictions of the larger-scale models. The reduction in the displacement is mostly attributed to the now fixed boundary conditions for vertical displacements.

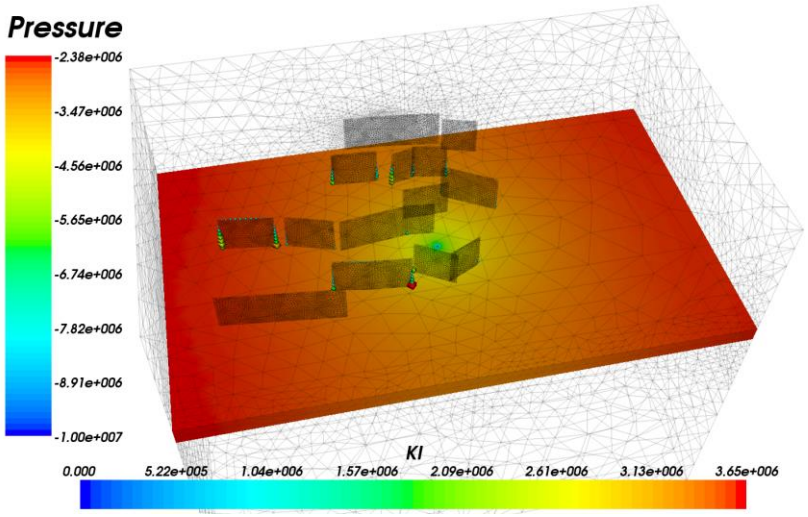

(a) Mode I

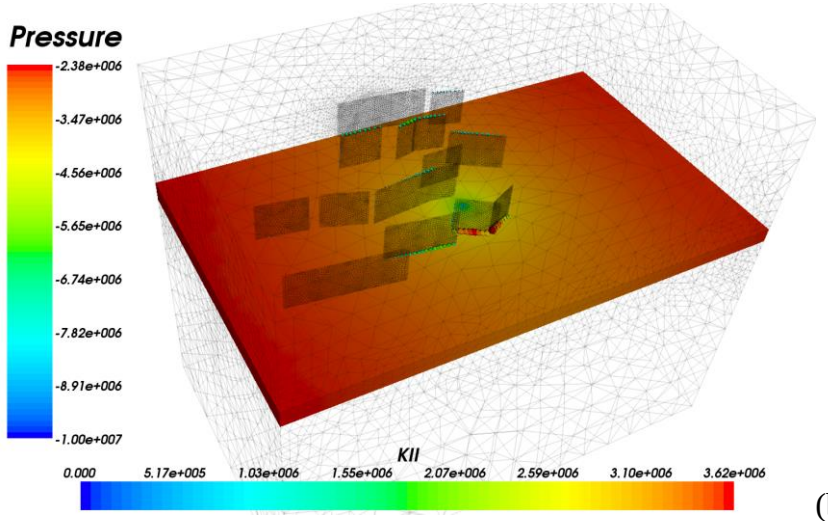

(b) Mode II

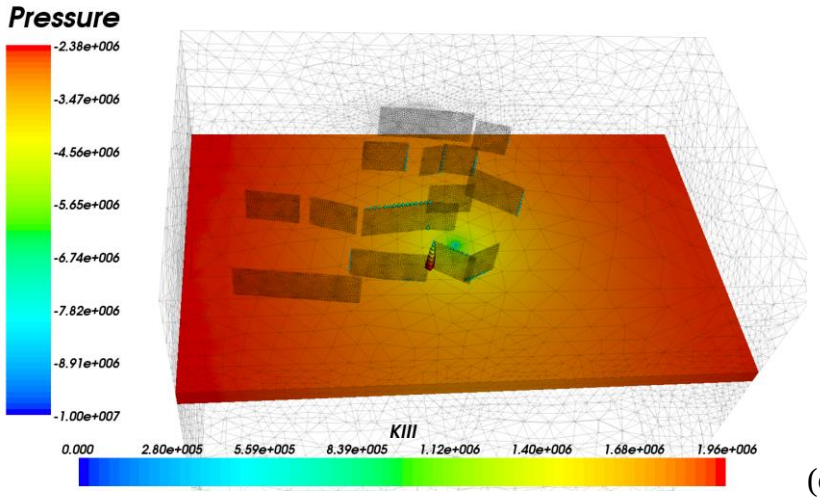

(c) Mode III

Figure 25 - Stress intensity factors (Pa $m^{1/2}$) at the end of production in the small-scale model. The scalar field represents the fluid pressure in the reservoir, and the points at the edges of the fractures show the *magnitude* of each SIF mode. (a) shows the opening mode (I), (b) shows the in-plane shear mode (II), and (c) shows the out-of-plane shear mode (III).

The distribution of SIFs across the faults was studied during the five-year injection period and the subsequent two years, to investigate changes in stress during and post production. Figure 25 shows the distribution of the SIFs at the end of production (after five years). Faults had larger SIFs at the

reservoir-caprock contact. Faults close to the well experienced mostly shear stress (K_{II} and K_{III}), and relatively lower opening mode stress (K_I) due to the compressives stress in the region. However, far from the well, faults acquired larger K_I values. When production ends and pressure equilibrates, the magnitudes of the SIFs reduce, particularly for modes II and III. Peak values of K_{II} and K_{III} migrate to the top boundary of faults and away from the reservoir.

A third type of model was investigated, focused on the upper 4 km of the Goldeneye reservoir-caprock region. Faults were replaced by finite fractures with a radial dimension of 100 m. Fractures were positioned in the lower part of the Ekofisk layer close to the Rødby caprock. Total displacement distribution at the end of five years of production is shown in D2. The maximum displacement is 8.76 cm, a slight increase with respect to the previous model. This is attributed to the inclusion of Rødby caprock layer, which is softer than the Ekofisk unit.

Higher values of K_I are found on almost all of the fractures, whereas in the previous case with faults, only a few faults showed considerable values of K_I. On the other hand, large values of K_{II} and K_{III} are restricted to few fractures. This is due to the fact that the fractures are moved away from the reservoir layer, and the relatively softer layer of Rødby caprock dissipates the shear stresses.

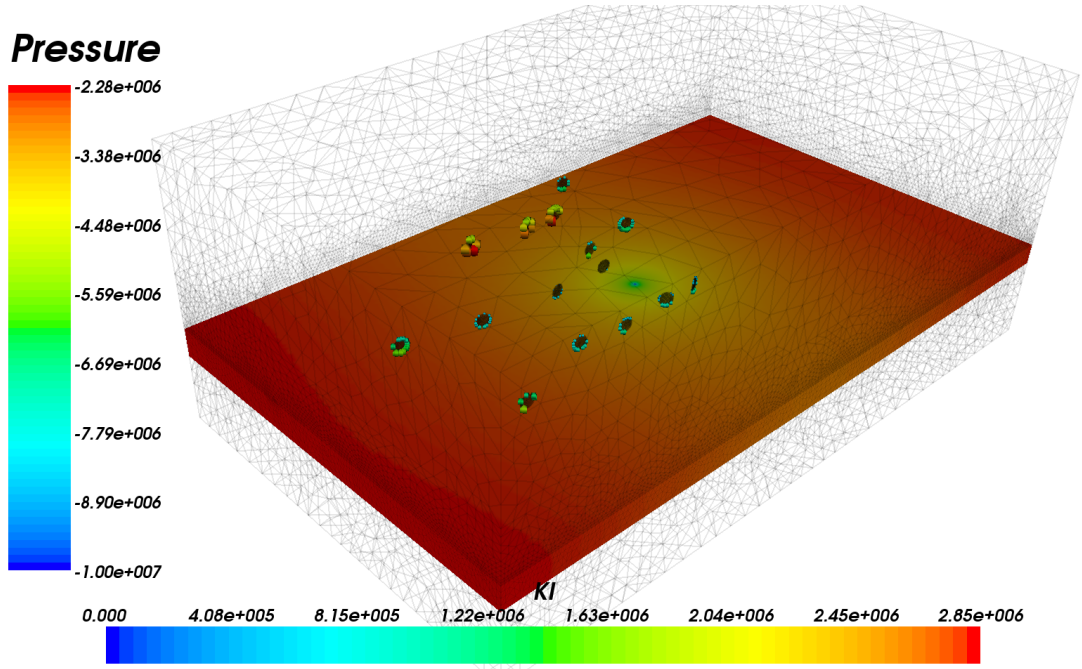

Figure 26 - Mode I stress intensity factors on circular 100 m fractures in a 4 km model of the Goldeneye reservoir.

These models provide significant insight to the pre-injection status of the caprock and reservoir. The SIF magnitudes can be used to quantify where fractures would fail, given the fracturing toughness of the *in situ* reservoir and caprock.

3.4 EFFECTS OF CO_2 INJECTION ON CAPROCK INTEGRITY

The second phase of CONTAIN was focused on the simulation of the geomechanical effects of the injection of CO_2 on the integrity of the caprock.

This study examines the geomechanical deformation of the Goldeneye reservoir during injection of CO_2. It assumes that there is a temperature contrast between the injected CO_2 and the host rock, and it considers the pressure increase in the reservoir due to the fluid injection. We vary the temperature contrast between the injected fluid and rock, the Young's modulus of the rock, and the sizes of the initial faults. The most significant result is the observation that fracture aperture distributions during cold injection are strongly regionalised, and are strongly influenced by the

inhomogeneous material properties that result from rock material property contrasts. This observation has significant relevance beyond the scope of this project, as it contributes to understanding the limits of injection pressure and its effect on regional permeability increases due to crosscutting discontinuities. Moreover, it highlights the fact that although a fracture may appear to have a continuous geometric shape, the aperture distribution is the effect of the interaction between deformation induced by fluid-driven flow and deformation of the surrounding matrix.

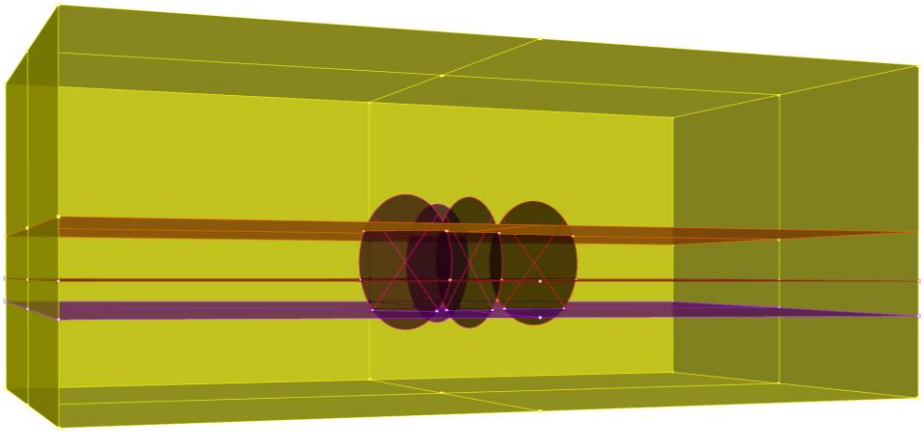

Figure 27 - Geometry of the pre-existing faults that are assumed to penetrate from the reservoir into the caprock. In this case, we investigate the worst-case scenario of a fracture completely crosscutting the reservoir and intruding into the caprock. Further cases considering smaller discontinuities were also investigated.

A specific case is investigated, which assumes that there is a pre-existing set of faults. *In situ* faults are modelled discretely as discontinuous surfaces in a three-dimensional matrix, with four geological layers; see Figure 27. The faults are assumed to be initially of low permeability, with the same permeability as the caprock. However, simulations show that their apertures (and as a result their permeability) vary due to the thermo-poro-elastic effects of the injection of the relatively cold CO_2. The change in the apertures is mainly due to thermal loading, but is also affected by the re-inflation of the reservoir. Four cases are simulated: (i) injection temperature T_{inj} = 20^{o}C and Young's modulus E = 20 GPa, (ii) injection temperature T_{inj} = 40^{o}C and Young's modulus E = 20 GPa, (iii) injection temperature T_{inj} = 20^{o}C and Young's modulus E = 10 GPa, and (iv) an isothermal case with Young's modulus E = 20 GPa. The simulations are performed for 160 years. An example output of the simulations is presented in Figure 28. A summary of the resulting apertures of the corresponding geomechanical simulations is presented in Figure 29. Apertures are indicative of the extent of the deformation of the fracture surface during injection. These cases explore specific cases of scenarios analysed in WP1. In particular, it investigated two of the four possible reservoir conditions that WP1 postulated could be encountered during CCS (see Section 2.9.1). Case 1, a strong reservoir overlain by a strong caprock, is investigated by assuming 20 GPa Young's moduli for both rock units. Case 4, a weak reservoir overlain by a weak caprock, was investigated by assuming a relatively lower 10 GPa Young's moduli for both rock units.

These values are both assumed to be higher than the realistic MMG values, and can be assumed to be realistic for sandstone units. As MMG Young's moduli were not measured in this project, the 10-20 GPa approximations were assumed as a generic value. These generic values are in line with other CO_2 sequestration modelling studies. Although it is expected that actual MMG Young's moduli values are lower than 10-20 GPa, WP2 chose higher Young's moduli order to capture potential increase in Young's modulus due to confinement stresses. This is in line with the findings

from WP1, that for tested rocks Young's moduli are significantly increased for higher confinement stresses.

The temperature of the injected CO_2 was varied in order to investigate several permeability changes and growth scenarios specific to Goldeneye. As shown in Figure 29, the effects of Young's modulus on the aperture distributions of the faults are more pronounced for stronger rocks than for weaker rocks. Thus, for the case in which both reservoir and caprock are weak, apertures in the pre-existing faults are around thirty percent smaller, thus yielding less overall deformation of the fractures. This is consistent with WP1 findings. In addition, this work shows that when considering the potential growth of pre-existing fractures, poro-elastic effects do have an important effect on the predicted permeability changes, fracture paths as well as affecting fracture extension and fracture curving.

These simulations are instrumental in understanding how the aperture of faults and fractures, that lie at the interface between reservoir and caprock, change due to the increased pressure and decreased temperature of a CO_2 plume. Results show that during injection, the reservoir layer undergoes contraction due to cooling, which significantly increases the fault's aperture in the reservoir section. As the far-field stress is kept constant, the contraction of the reservoir layer applies additional compression to the surrounding layers, including the caprock. Thus, the fault's aperture reduces in sections located in the caprock.

Results also show that the thermo-elastic stresses dominate the reservoir deformation and the fault's aperture distribution within the reservoir, while the aperture in the caprock is controlled by poro-elastic deformations. Matrix contraction due to the injection of cold fluid in the reservoir layer induces compression on the caprock layer, which reduces the aperture of the faults within the caprock. Results show that injecting warmer fluid, or having a softer matrix (lower Young's modulus) reduces the thermo-elastic effects. The possible fracture growth is evaluated by computing stress intensity factors at the fault tips. Shearing of the existing fractures due to thermo-poro-elastic deformations is also investigated, and it is shown that the fractures are susceptible to shear under combined mode II and III due to the thermo-poro-elastic deformations.

A sensitivity analysis is performed to study the effect of the reservoir stiffness as well as the injection temperature. Softer reservoir rocks reduces the compaction due to the matrix contraction. Higher injection temperature (lower temperature difference) also applies lower contraction into the reservoir layer, and reduces the compaction. The shearing of the existing fractures is also studied using the Stress Intensity Factors (SIFs). The significantly different geomechanical effects observed in each geological unit underlines the importance of WP1's efforts towards understanding *in situ* reservoir conditions.

Results show that a combination of low friction and high *in situ* shear stress on the fracture surfaces may trigger fracture propagation under combined mode II and III in the reservoir layer or at the interface of the reservoir and caprock. This propagation is not observed when injection temperatures are increased to 40^oC. In fact, no propagation is predicted for any of the 40^oC injection cases. This highlights the importance of thermal effects when considering permeability changes in fractures, and in the deformation of reservoir-caprock containment structures. No tensile growth is observed in any of the modelled cases. The results of this study are published in the *IJGGC* (Salimzadeh *et al.*, 2018).

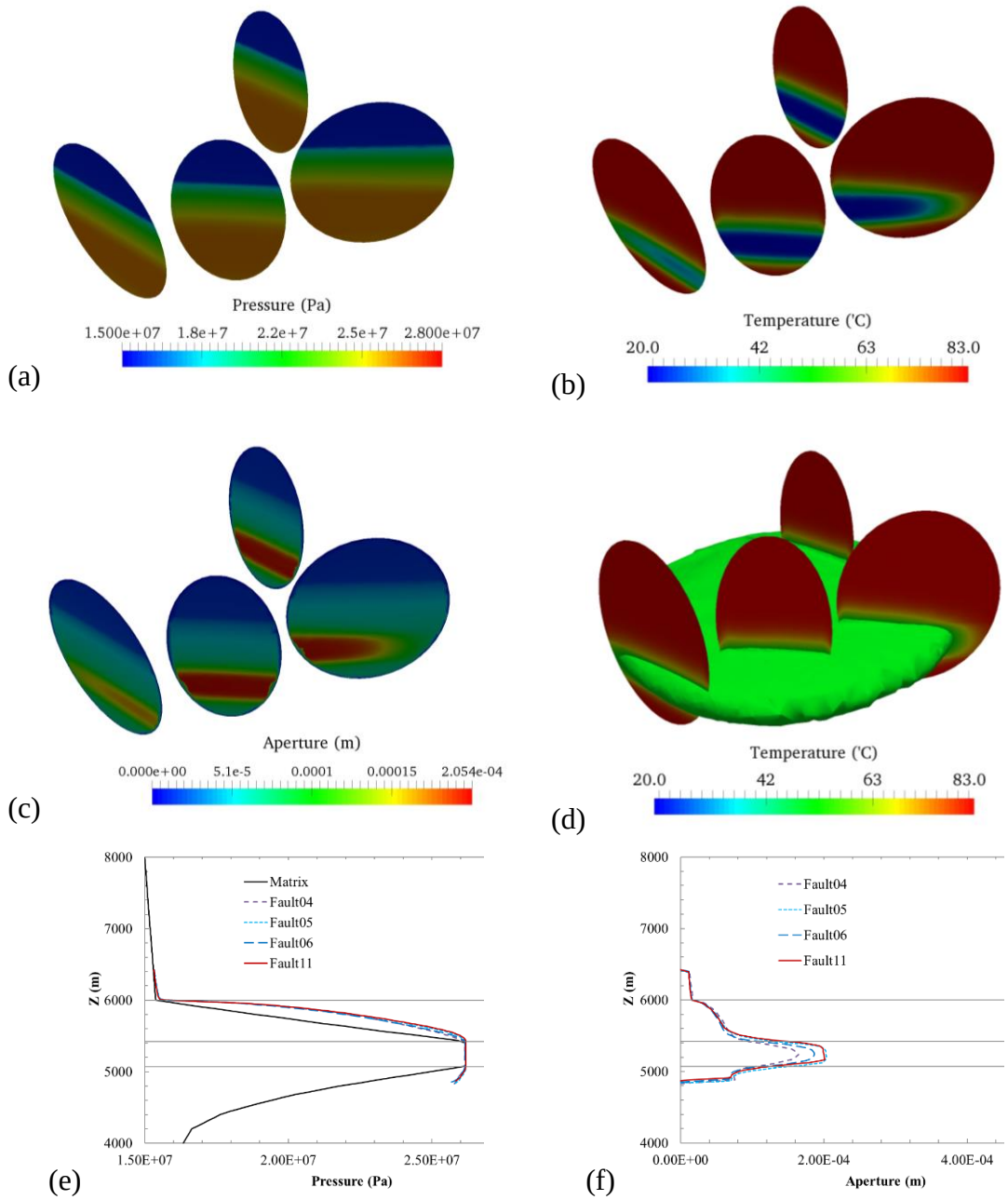

Figure 28 - The fluid pressure (a), temperature (b), and aperture distribution (c) on the faults, the temperature plume within the reservoir layer (d), pressure profile along a vertical line passing through faults (e), and the aperture profile along a vertical line passing through the centre of the faults (f), after 160 years for the case E = 10 GPa, T_{inj} = 20°C.

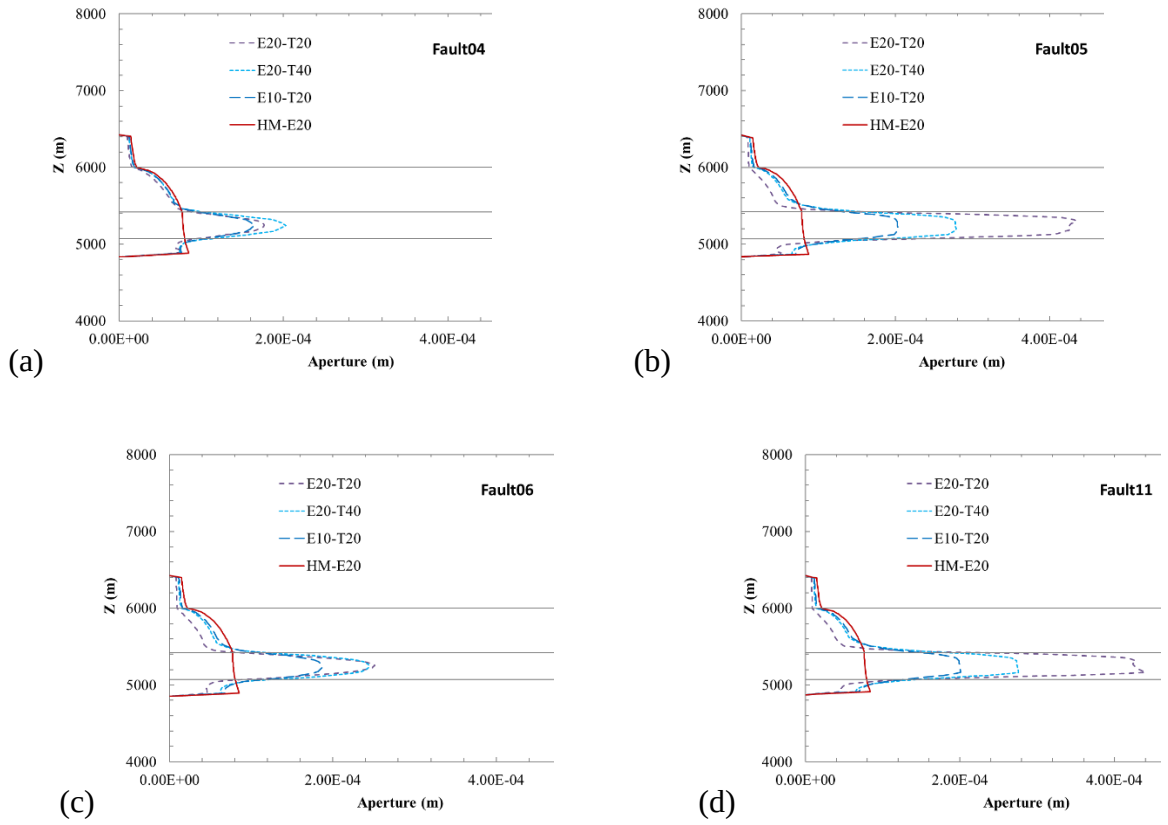

Figure 29 - Comparison of the aperture profiles on a vertical line passing through the centre of (a) Fault04, (b) Fault05, (c) Fault06, and (d) Fault11, for different cases. E20 amd E10 corresponds to a Young's modulus of 20 GPa and 10 GPa, respectively. HM refers to the isothermal case, as in hydro-mechanical only. And, T20 and T40 refer to the temperature of the injected CO_2.

3.5 UPSCALING OF GEOMECHANICS

One of the key aims of our contribution to CONTAIN was to incorporate multi-scale fracture modelling, wherein simulations contain both large discrete fractures and small fractures, without the requirement to mesh the smaller fractures in full detail. In this way, the geomechanical properties of the medium have been upscaled, significantly reducing the computational cost of simulations, whilst preserving the connectivity and anisotropy of the fractures in the. Two papers investigated the implemented damage model, comparing its performance to the discrete fracture model (Defoort *et al.*, *ARMA* 2016) and applying it to a simulation of caprock failure for the Goldeneye reservoir (Defoort *et al.*, *ARMA* 2015).

The double-notch specimen provided an ideal test case to compare both the discrete fracture and damage models to standard fracturing experiments. Figure 30 compares the results of experiments to the shape of the damage zone and geometry of discrete fractures. Significant heterogeneity of ±50% Young's modulus is required in order to have a noticeable impact on the geometry of the fractures. Higher heterogeneity induced higher crack roughness in the damage mechanics simulations, but has limited impact in the fracture mechanics simulations. In both approaches, heterogeneities seemed to decrease fracture interaction. Results show that damage occurs in the region between interacting cracks, which points to the importance of capturing non-linear behaviour in order to accurately model fracture interaction in the case of heterogeneous material.

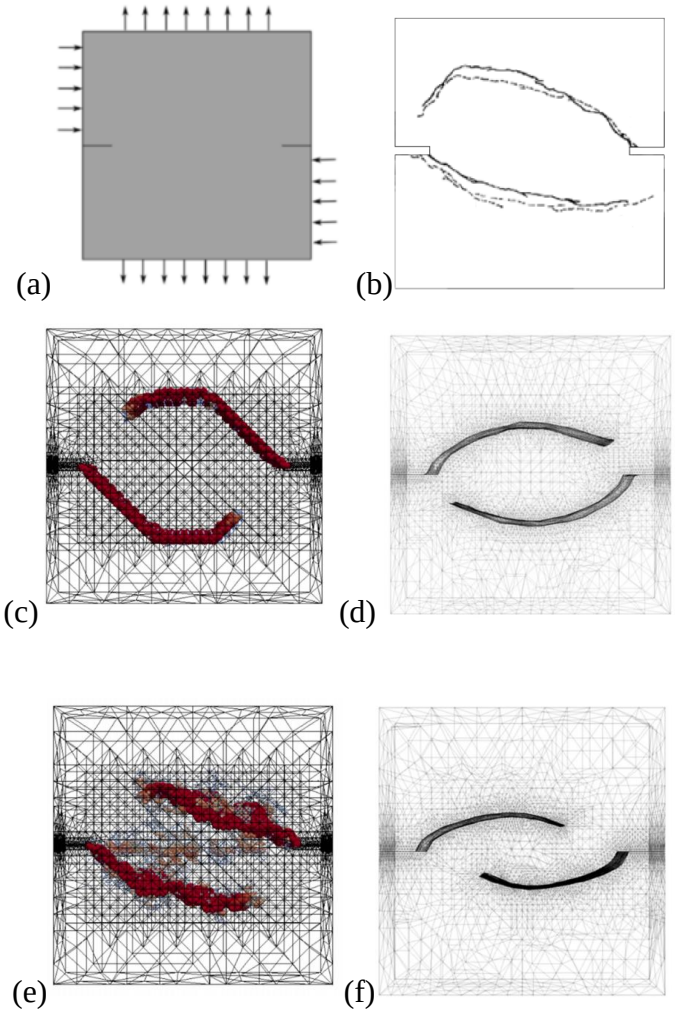

Figure 30 - Mixed mode fracture growth boundary conditions (a) and experimental fracture pattern results (b), simulated using isotropic damage (c, e) and discrete fracture growth (d, f), in homogeneous (c, d) and heterogeneous (e, f) materials. The heterogeneous case has ±50% stiffness/strength variation. Fully damaged elements in the isotropic damage models are represented by red spherical glyphs.

3.6 INTERACTION BETWEEN FRACTURES AND FAULTS

Activation of pre-existing faults in the caprock was considered by exploring and quantifying the change in stress at a fracture's tip due to the presence of other fractures. A quantitative method for defining the interaction that a fracture experiences was developed (Thomas *et al*., *JGR* 2017). In the process, the increase in stress between interacting fractures was validated against other semi-analytical and numerical methods. Three measures were developed to summarise the magnitude and type of interaction (shielding, amplification, or mixed shielding and amplification). This method was demonstrated for mutually interacting fractures under tension and compression, and can be readily extended for understanding the influence of changing material properties on the stress state at a fracture's tip. The spatial variation of the interaction measures was visualized by plotting the value between two fractures (see Figure 31).

The possible effects of interaction on the geometry of fractures, grown using the coupled poro-elastic component of the simulator, were also presented in the results of Salimzadeh *et al.* (*IJRMMS* 2017b). Results show that fluid-driven fractures tend to grow away from each other due to the shielding effect of nearby fractures (Figure 32), whereas the differential *in situ* stresses force the fracture to grow in a plane perpendicular to the minimum *in situ* stress. The interaction between two nearby fractures reduces by increasing spacing.

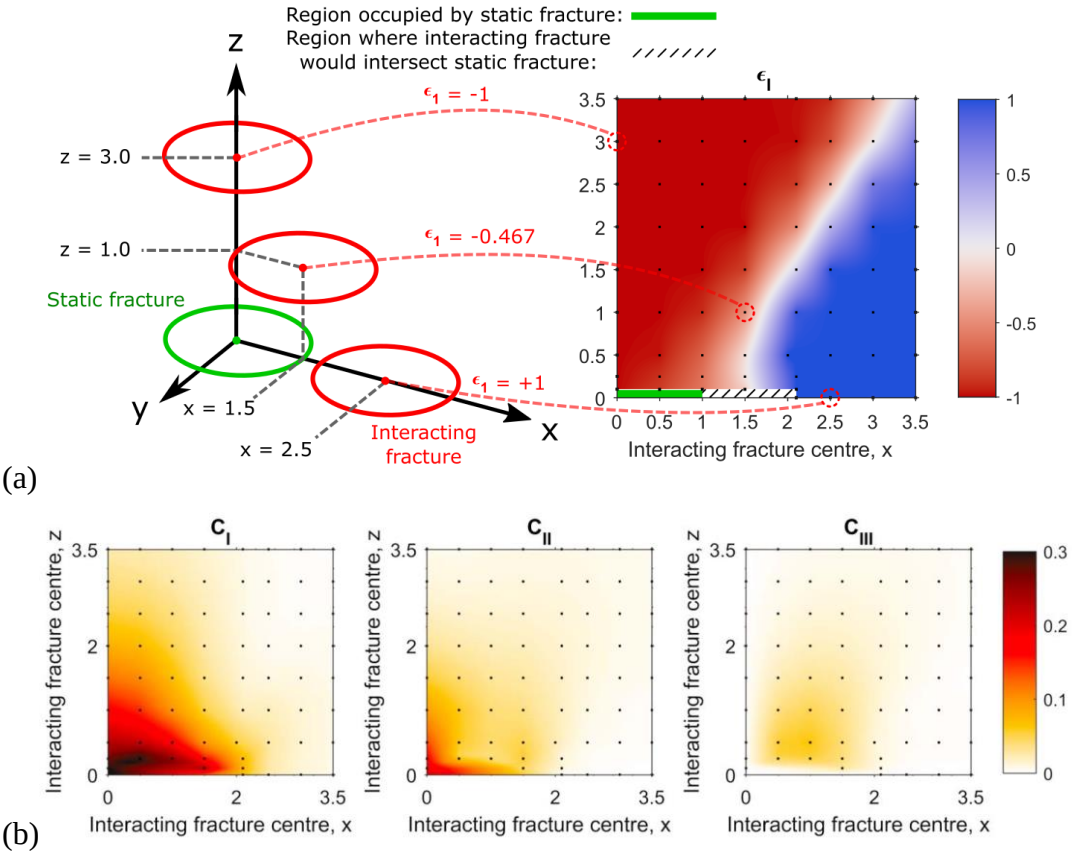

Figure 31 - (a) Methodology for constructing fracture interaction maps. The axes on the left show how three different fracture simulations are used to produce values of the interaction measures. The right shows how these values are combined with a grid of results to create an interaction map for two co-planar fractures under tension. A value of 1 means that the fractures interact only to amplify the stress at one another's tip. A value of -1 means they shield stress. Intermediate values mean that parts of the fracture are amplified and parts are shielded when the fractures overlap. (b) Fracture interaction maps quantifying the magnitude of interaction, independent of the type (amplification or shielding) for three modes. Higher values indicate that the SIFs have been changed more due to the interaction between two fractures.

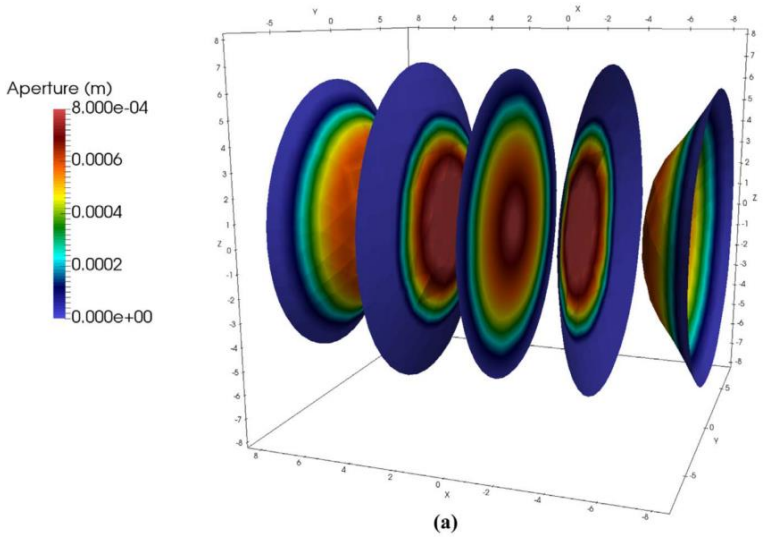

Figure 32 - Five fractures growing due to hydraulic stress in an isotropic stress field.

Poroelastic effects were also introduced to the hydraulic fracture interaction problem by comparing growth geometries under a range of matrix permeabilities and Biot coefficents. Low matrix

permeabilities have minimal effects on the propagation direction of fractures. In leakoff-dominated cases, poro-elastic effects are significant and affect the propagation direction of two interacting fractures. Additional compression from the expanded matrix pushes the fractures to propagate away from each other and that increases the curvature of the induced fracture. In contrast, fractures in toughness regime have lower interactions than those in viscosity regime. This can be explained by lower fracture aperture in fractures under toughness regime.

3.7 DISCUSSION AND FUTURE WORK

The incorporation of thermal and poro-elasticity into ICGT has enabled various insights into predicting the geomechanical effects that will arise during injection. The observation that thermal effects lead to contraction and reduction of fracture apertures in the caprock suggests fracturing would be shear induced rather than tensile. The results demonstrate that altering injection temperatures enables control over the thermo-elastic stresses in the reservoir, and therefore alter fracture apertures in the caprock. Lower fluid temperatures lead to reduced caprock fracture apertures, thereby resulting in reduced vertical caprock permeability. This final study provides a quantitative geomechanical assessment of the impact of CO_2 injection honouring statistics of the Goldeneye reservoir as provided by WP1. Additional work during the project on hydraulically induced fracture growth, fracture interaction, and damage models has provided new methodologies for understanding thermal and poro-elastic processes that take place in subsurface reservoirs.

3.8 SUMMARY OF PROJECT RESULTS

3.8.1 Lessons learned

- Accurately modelling the displacement effects following the depletion of the Goldeneye reservoir required the inclusion of discrete fractures.
- Fractures and faults are stressed in complex ways during production. A range of consistent effects were found across many fractures in the caprock, including:
    - Shear failure close to the injection region;
    - Tensile failure away from the injection region;
    - Higher stress at the reservoir-caprock interface during injection, which migrates to the top of the caprock in the period after injection;
    - Injection can cause both local and remote fractures to propagate.
- Fractures propagation is observed in regimes where poro-elastic effects are considered.
- Interaction between fractures and faults has a significant impact on fracture tip stress states, and may lead to the enhancement of growth of closely spaced fractures.
- Fracture apertures during injection are strongly localised within the reservoir, and exhibit a non-linear decrease into the caprock.
- Due to the strongly localised aperture increase, tensile growth due to injection is more likely within the reservoir than in the caprock. This may indicate that re-inflation deformation may be partially accommodated by fracture growth within the reservoir itself. Further studies within a wider parametric space should follow.
- Damage mechanics is a viable upscaling methodology for fracture mechanics in simplified geometries, but fails for larger systems.
- Discrete fracture mechanics is a viable caprock integrity methodology for small and large systems, of single and multiple geological layers.

3.8.2 List of technological advances

- Development of a fully-coupled, finite element-based thermo-hydro-mechanical model incorporating discrete fractures.
- Flexible scheme for propagating fractures due to hydraulic, thermal, and mechanical stresses, or a combination thereof.
- Mechanical upscaling alongside discrete fractures in simulations, via a distributed damage model.
- Methods for quantifying the magnitude and type of interaction between fractures.

These technological advances are thoroughly detailed in our papers to make them accessible and readily implementable into other contemporary simulators.

The research fellow working on this project, Adriana Paluszny, now will go on to develop this fracture analysis technology further, sponsored by a Royal Society University Research Fellowship. Post-doctoral researcher Saeed Salimzadeh will go on to develop this technology in the context of geothermal modelling, at CSIRO (Australia). Two post-doctoral research associates, Dr Vasia Tsaparli and Dr Pamela Tempone, who worked on CONTAIN, are now working in geomechanics-related industrial positions. During the last months of the project, research associate Robin Thomas will participate in CONTAIN by further applying fracture interaction principles to caprock integrity analysis. A further study of thermal-induced fracturing is being conducted using the developed technology with the Department of Mathematics at the University of Bergen.

4 Work Package 3 – Social understanding and acceptance of CCS storage proposals

4.1 INTRODUCTION

While CCS likely offers environmental and economic benefits, it remains controversial (van Egmond & Hekkert, 2012) and there has been high-profile public opposition to particular CCS developments (Oltra *et al.*, 2012). For example, public opposition to the CCS project in Barendrecht, near Rotterdam, where a total of 10 million tons of CO_2 were to be stored in a depleted oil field under a residential area, ultimately led to the project being cancelled (e.g., Bellona, 2010). As a result of public 'engagement failures' of this kind, it is increasingly accepted that public acceptance of CCS as a vital precondition for its rollout (RCUK, 2010; van Alphen *et al.*, 2007). For example, the coalition UK Government in 2012 concluded that '*CCS projects need to learn from experience to date which suggests that community engagement begins early and goes beyond the requirements under the regulatory regime'* (DECC, 2012).

The CONTAIN project therefore went beyond considering CCS and its risks from a geophysical perspective to examining how CCS, its risks and benefits are understood by the general public, and how this differs from expert views. In particular, WP3 aimed:

- To examine expert views on public engagement with CCS, including common barriers and possible solutions,
- To explore expert-public divergence in understanding CCS in order to inform public engagement efforts,
- To identify factors shaping public acceptance of CCS, and
- To develop guidelines for engaging the public with CCS.

Deliverables 7, 8 and 9, and Xenias & Whitmarsh (2017) detail our methods and results from WP3. Here we briefly describe the methods used and outline the key findings and implications.

4.2 OVERVIEW OF METHODS

The methods we used in CONTAIN WP3 included:

1) *Expert interviews.* Thirteen CCS experts were recruited for interview through Internet searches, colleague recommendations, and snowballing. Nine interviewees were based in the UK, one in Norway, and three in the Netherlands. Experts represented a range of relevant backgrounds and sectors. Questions addressed perceptions of barriers to CCS deployment in the UK, experiences with public engagement, challenges to public engagement with CCS and possible solutions, and the importance and utility of public engagement with CCS. Interviews lasted between 23 and 88 minutes; and were analysed using thematic coding. Further details can be found in D7.
2) *Expert survey.* A survey (N = 99) was undertaken of CCS experts from private, public and third sectors across Europe (almost half were academics). Forty-five per cent were from England; the remainder were from across Europe, Australia, North America, and India. Around half the sample had direct experience of engaging the public with CCS. The survey included questions about barriers to CCS roll-out, risks and benefits from CCS, factors

influencing public support for CCS, attitudes towards energy sources, and the role of CCS in climate change mitigation.

3) *Public survey.* Participants (N = 5,406) were recruited via Qualtrics, an online participant panel provider. Two samples in five countries (UK, USA, Canada, Norway, Netherlands) – a national sample and a local sample – in each country. National samples were demographically representative in terms of gender and age. Local samples were defined as living close to a current or proposed CCS processing, pipeline or storage sites. The survey comprised questions on support for energy sources, attitudes to CCS, benefit and risk perceptions, various psychological constructs (e.g., place attachment, technophilia, environmental identity, environmental worldview) and demography. Participants were assigned to one of three conditions which provided different messages about CCS – CCS without lifestyle change ('business as usual'); CCS with carbon dioxide utilisation (CDU); and CCS with lifestyle change – after which CCS support and attitudes were again measured. Further details of the survey methodology can be found in D8.

In addition, we undertook at extensive literature review of public perceptions (reported in D8) and collated recommendations for public engagement with CCS (see D9) that drew on expert interviews, expert survey and public survey.

4.3 OVERVIEW OF RESULTS

4.3.1 Public perceptions of CCS

Previous research highlights **low public awareness** of CCS across all countries (e.g., Demski *et al.*, 2013). In CONTAIN, we also found low levels of awareness of CCS, although there were cross-national differences, with Norway (where CCS technologies are more established) showing more awareness than elsewhere (see D8 and Figure 33).

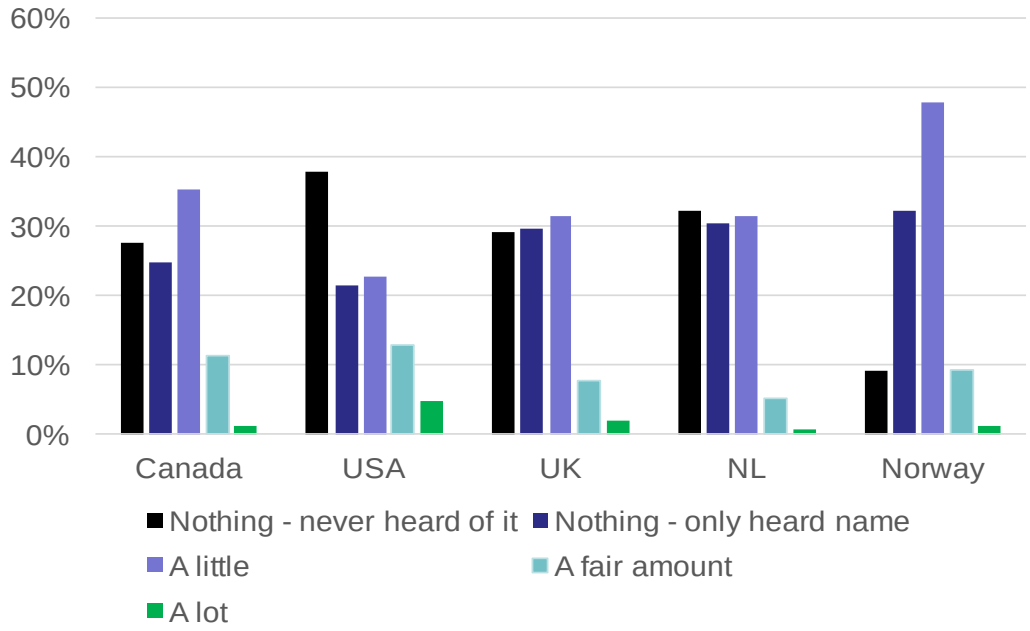

Figure 33 – Public awareness of CCS, by country. Note: Question wording was: 'How much would you say you know about 'carbon capture and sequestration' also known as 'carbon capture and storage' (or 'CCS')?'

Also consistent with previous work (Demski *et al.*, 2013), we found that attitudes to CCS are **mixed** though overall rather positive than negative (see D8 and Figure 34). For example, more of the public (approximately half the sample) agree that CCS should be implemented in their country than disagree (approximately one-quarter). While strongest agreement (over three-quarters of the sample) was on the risk of leaks ('CO_2 stored underground might leak back into the atmosphere'); reflecting the sample's ambivalence, almost the same proportion agreed that 'CCS helps to keep an important greenhouse gas out of the atmosphere'. There was also overall agreement that CCS is risky, that the risks are underestimated, but that it will also benefit the economy.

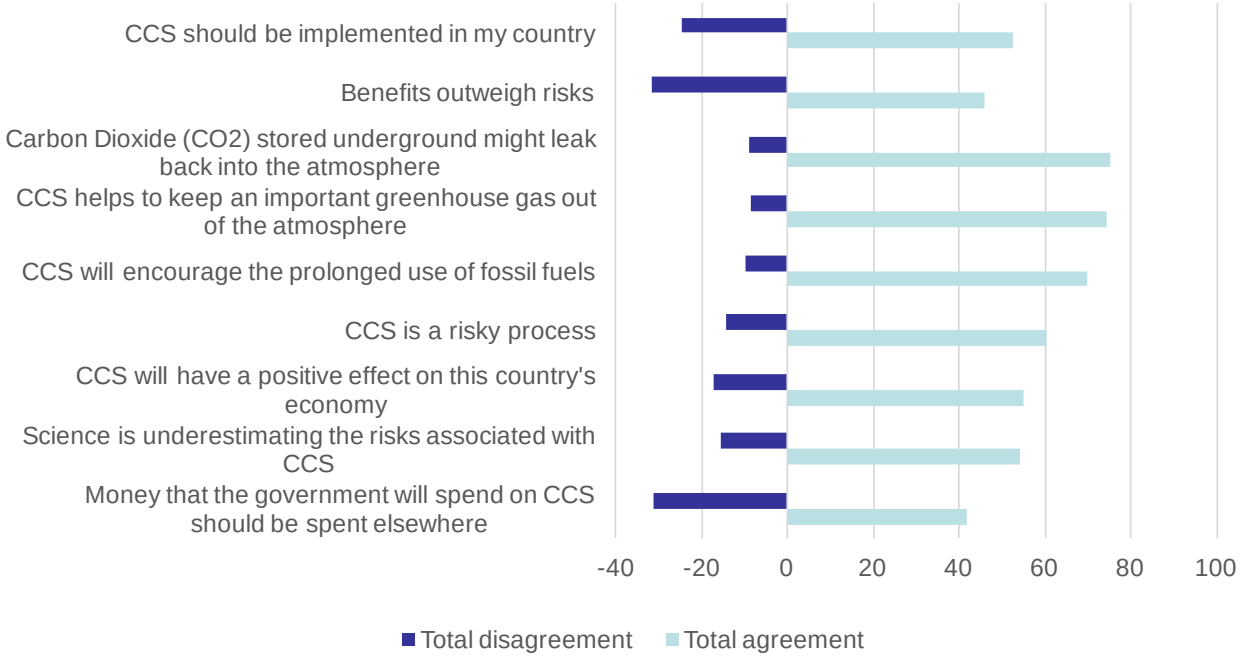

Figure 34 – Public attitudes to CCS.

Existing literature also shows that, when it comes to CCS perceptions, the public is highly **heterogeneous**. In CONTAIN, we found nationality was by far the strongest influence on CCS support (either before or after information provision). After nationality, the strongest predictors of CCS support were place attachment, climate change belief, technophilia, and environmental identity, as well as working in the energy industry, living near a CCS site, and age. Following provision of the CCS messages, we found environmental worldviews, education, rurality, gender, and left-wing ideology, become significant negative predictors (see D8).

The literature also shows areas of both convergence and divergence between **expert and public views** of CCS (e.g., Shackley *et al.*, 2007). While public support for CCS is generally lower than expert stakeholder acceptance both consider CCS to be a partial solution to climate change. In CONTAIN (see D8), we similarly found the public across the five surveyed countries are more supportive of renewable energy sources and reducing energy demand than of CCS; and nearly three-quarters agreed that 'CCS will encourage the prolonged use of fossil fuels'.

Furthermore, there is disparity in public perceptions between the **general public or specific local communities** likely to be affected by CCS (e.g., Huijts *et al.*, 2007). In CONTAIN, we also found differences in CCS attitudes between local communities living near current/proposed CCS sites, and the general public. However, overall, we found support was *stronger* at the local than national level, perhaps because of their history and dependence on energy industry for employment and

greater familiarity with the technology (cf. Parkhill *et al.*, 2010). Consistent with the literature, we also found these local-national differences varied by country; in particular, local communities in the UK (in and around Peterhead, Scotland) were more likely to be positive than local samples in the other counties (Figure 35).

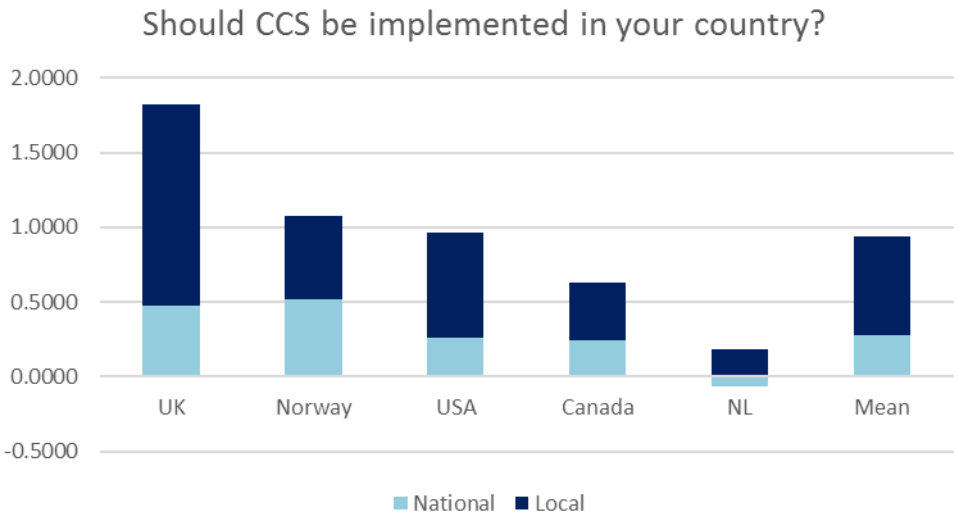

Figure 35 – National and regional differences in support for CCS implementation. Note: Question wording was 'Should CCS be implemented in [name of country]? With a 5-point response scale from 'Yes, definitely 2' to 'Definitely not -2' and 'I don't know' (removed for analysis).

Previous work has also found **cross-national differences** in attitudes to CCS, although this evidence is very limited (L'Orange Seigo *et al.*, 2014). In CONTAIN, we conducted one of the most detailed cross-national studies of CCS attitudes amongst the public, and found strong cross-national differences. Specifically, the UK showed much higher support for implementation, followed by Norway and the US (Figure 35). The Netherlands showed slight opposition overall to implementation, consistent with previous work (Ashworth *et al.*, 2013).

4.3.2 Engaging the public with CCS

Both the type of framing of CCS information and audience characteristics (e.g., knowledge, values) are strong influencers of public views on the technology (e.g., Yang *et al.*, 2016). Consequently, providing information about CCS does not always allay fears or change attitudes. In CONTAIN, we found that pairing CCS with biofuels led to higher acceptability, than asking about CCS alone; whereas pairing CCS with heavy industry or fossil fuels (especially, shale gas) led to lower acceptability (see D8).

Consistent with pervasive confirmation bias in information processing whereby initial beliefs or feelings filter whether or how further information is perceived (de Bruin & Wong-Parodi, 2014), information may also reinforce positive attitudes or exacerbate or confirm concerns. For example, framing CCS as dealing with 'waste' is more persuasive than framing it in terms of climate or economic benefits (Broecks *et al.*, 2016). We similarly found in CONTAIN that framing CCS as dealing with waste improved perceptions; specifically, when we discussed CCS in conjunction with **carbon dioxide utilisation** (CDU), we found a significant increase in support for CCS implementation in respondents' country (see D8 and Figure 36).

On the other hand, in CONTAIN, we also found differences when we introduced **information**

about the cost of CCS. Specifically, we provided information about current estimated costs of CCS per household (£6 - 12 per year) and the potential for future greater costs associated with climate change mitigation to be avoided if CCS was immediately implemented. Despite the focus on avoiding future, greater costs, compared to support for implementation before costs were mentioned, support for CCS actually reduced when we introduced the cost information (see D8 and Figure 37).

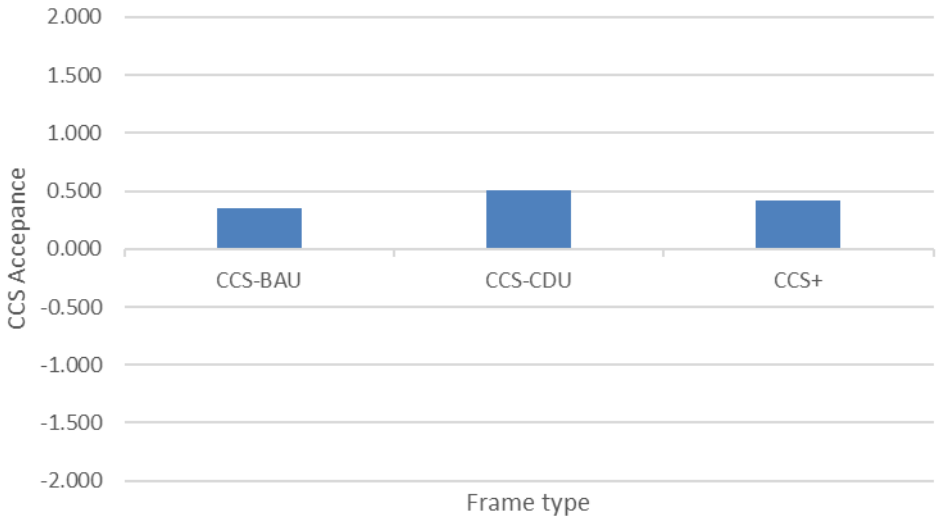

Figure 36 –Effect of different information frames on CCS support. Note: Dependent variable was the implementation question. CCS-BAU was the 'business as usual' CCS frame, stating lifestyles would not need to change; CCS-CDU included a description of CDU through which waste CO_2 would be recycled to make new products; CCS+ described CCS as part of a range of other changes, including lifestyle changes, to tackle climate change.

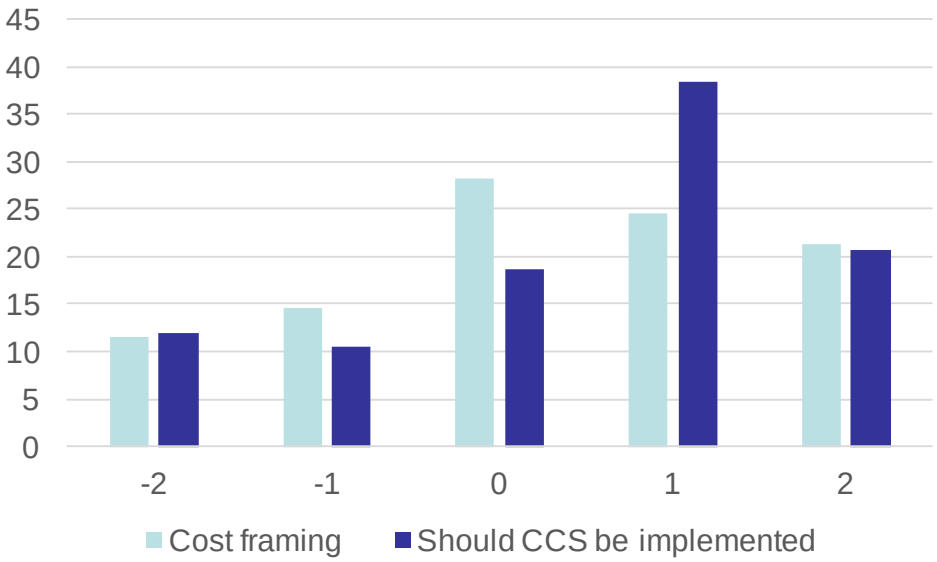

Figure 37 –Effect of cost information on CCS support. Note: Question wording was: 'Implementing CCS comes at a cost - currently estimated at £6 - £12 [or converted to local currencies] on the average household electricity bill per year. But if we do not implement CCS in this country now, energy bills could rise even more in the future (because more CO_2 mitigation measures would be necessary). How willing would you be to accept immediate implementation of CCS if this increase in bills was avoided?' with a 5-point response scale: 'Completely willing 4' to 'Not at all willing 0'. The implementation question was as in the previous figure.

As noted, a key factor influencing CCS attitudes is **trust** in industry developing CCS projects (e.g., de Best-Waldhober *et al.*, 2011). Indeed, L'Orange Seigo *et al.* (2014, p.31) conclude that *'trust plays a particularly important role for benefit perception in the case of CCS, more so than with other large technologies, whose benefits are more visible'*. Consistent with this, previous work also highlights that the **engagement process** can profoundly influence community perceptions of CCS (e.g., Oltra *et al.*, 2012). In particular, there are clear benefits of early and substantive engagement (see D8 and D9 for literature on engagement). In CONTAIN, we undertook a small-scale public engagement event with the general public (see Figure 38), rather than affected communities, and found visitors to our station were very interested in CCS as a potential climate change mitigation option; and often expanded their questions beyond technicalities, but were also interested in governance and societal issues (e.g., policy decsions about CCS; see D10 for details).

Figure 38 – Photos from the CONTAIN public engagement event at the Natural History Museum.

4.3.3 Expert views on engaging the public

Our work in CONTAIN also shed light on public engagement with CCS from the perspective of CCS experts – including those who directly engage the public with CCS as part of their work. The interviews and survey we conducted with experts (see D7; Xenias & Whitmarsh, 2017) indicated their views on CCS were more positive than the public's views on these technologies. Nevertheless, most felt that CCS was not the only climate change mitigation strategy required, and that it posed risks as well as benefits.

Experts highlighted that the public are largely unaware of CCS, its risks and benefits, and felt that misperceptions needed to be addressed. Many, though, noted that this needed to be sensitive to different audiences, using tailored approaches; and that visualisations and analogies can help communicate unfamiliar processes like CCS. They also felt that belief in and concern about climate change were 'gateway' beliefs to accepting CCS; that is, without accepting climate change as a problem, the purpose and benefits of CCS would not be appreciated. Indeed, this was supported by our public survey, as discussed above. Some went further to say that there should be a change in discourse from climate change issues to the broader vision of decarbonising society and contributing to healthier living (see D7).

Experts also felt that onshore CCS developments would always be more controversial and pose problems in terms of public engagement, compared to offshore developments, which would less directly affect communities. In as far as our public survey analysis shows, there appears to be some

support for this, as the two most positive countries were the UK and Norway, where CCS developments (actual or proposed) are offshore; whereas (somewhat) less support was seen for actual/proposed CCS sites in Canada, the US and (particularly) the Netherlands.

The need for trusted communicators and open, direct communication was also highlighted by interviewees (see D7). In particular, many found that the public see CCS as industry 'greenwash' and so express scepticism about it; using non-industry communicators to highlight its role in climate change mitigation was seen as important for effective engagement. At the same time, having strong government commitment, demonstration projects and consistent media messaging can signal to the public that CCS is important as part of the UK's response to climate change.

While many experts focussed more on one-way forms of communication; others stressed the need for early and sustained two-way engagement with the public (consistent with the broader literature). A variety of rationales for engagement were expressed – ranging from instrumental (to overcome opposition to CCS roll-out) to substantive and normative (e.g., for democratic public policy). However, most felt that public engagement was a lower priority for CCS implementation than policy support and investment (D7; Xenias & Whitmarsh, 2017).

In respect of our expert survey results, it appears that experts expressed more positive and unambiguous support for renewables over CCS, and for CCS over (unabated) fossil fuels, compared to the general public (see Xenias & Whitmarsh, 2017). Moreover, those who engage directly with the public seem to be even more convinced of the benefits of CCS than those who do not. That is, experts directly involved with publics perceived both local and global risks as lower than experts with no direct public exposure. The inverse was true about CCS benefits (i.e., higher perceptions for directly engaged experts; see Figure 39). This is an interesting finding, and may be due to the function of direct public communicators in 'convincing' publics about CCS – compared to experts who do not face publics directly.

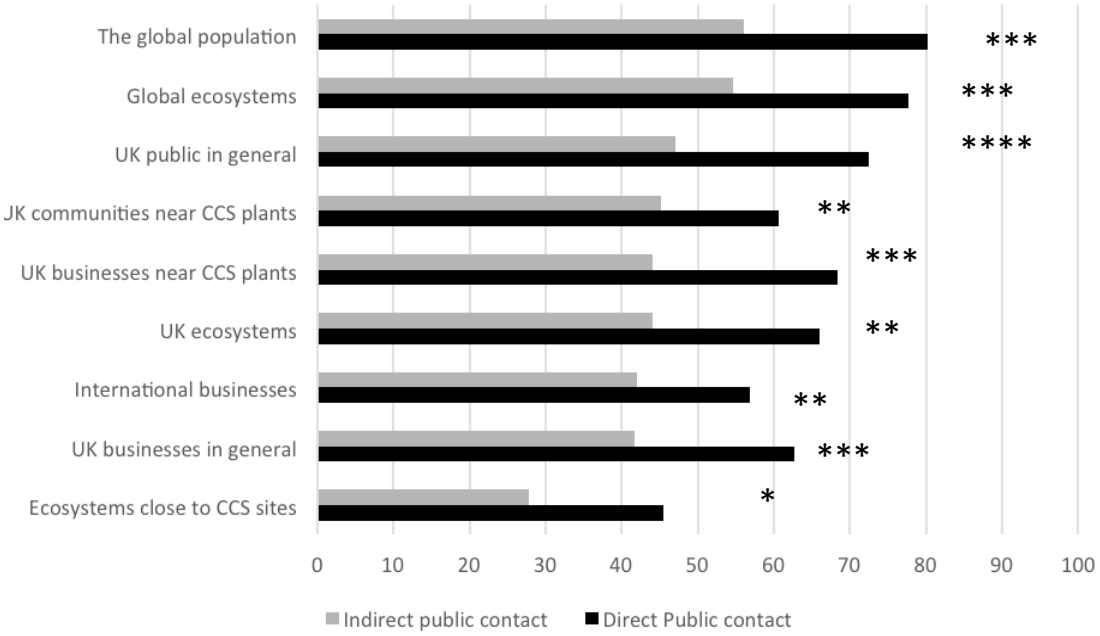

Figure 39 – Expert views on beneficiaries of CCS. Question wording: "To what extent will each of the following experience benefits from CCS developments?". * = p < 0.1; ** = p < 0.05; *** = p < 0.01; **** = p < 0.001.

CCS experts also generally recognise the importance of public engagement for the roll-out of CCS for both substantive and instrumental reasons, and are largely aware of the range of factors (knowledge, values, trust, etc.) influencing public engagement. Here there was again an important distinction between experts directly exposed to publics, who placed heavier emphasis on environmental values, knowledge of CCS and explaining the need to reduce emissions, and experts indirectly exposed to publics who placed heavier emphasis on financial compensation for communities as factors influencing public support for CCS (see Xenias & Whitmarsh, 2017).

Another interesting finding was that nearly half of all experts surveyed found that once the full CCS chain of technologies has been implemented, they should actively be ongoing for over 80 years or indefinitely. This contradicts the current view that CCS should be treated as a bridging technology that will temporarily aid decarbonisation of power generation and heavy industry and aid the transition to a low carbon future. It is not clear what drives such preference for an indefinite application of CCS, and this might merit further research.

Equally, further research and improvement is needed in engaging experts with best practice on public engagement: both our interviews and survey suggest that experts recognise the importance of engagement but only for instrumental reasons (e.g. removing obstacles/opposition) by those who do not engage publics directly. The relatively low salience of the need for early and substantive engagement amongst CCS experts suggests that there is room for improving the flow of learning from the public engagement research literature to those charged with delivering it.

4.4 IMPLICATIONS

Here, we summarise our key findings and their implications for engaging the public with CCS:

- *Basic awareness is limited:* Both the expert and public data show public awareness of CCS is low. Even in countries where this technology is most established (e.g., Norway), there is little self-reported knowledge beyond recognition of the term 'CCS'.
  This indicates a need to provide a range of information, including basic, policy, and technical information about CCS if the public are to be involved in decision-making about CCS investment, use and siting.
- *Framing effects are powerful:* Our research and previous studies show that the way in which CCS is presented and discussed (whether it is presented along with alternatives to mitigate climate change, as well as the nature and focus of the CCS information provided) can strongly shape people's attitudes towards it. Moreover, this information framing can interact with prior attitudes in ways that can polarise audiences. *For example, highlighting costs of CCS or pairing CCS with fossil fuels or industry seem to reduce support for CCS; while discussing CCS with CDU or with bioenergy increases support.* Other work shows that, for example, small-scale CCS sites are more supported than large-scale.
  It is critical, then, to carefully calibrate the CCS frames involved in a particular project, to the current discussions on siting particulars and benefits from CCS – which change and need to be updated from time to time.
- *Framing effects also depend on the broader context:* They include and depend on what alternatives are provided; and we and others have found that CCS is seen as a temporary, techno-fix solution to climate change that may prolong dependence on fossil fuels.
  It is therefore important to highlight the role of CCS in the context of a broader low-carbon societal transition.

- *Recognise diversity:* Our work adds to the broader evidence demonstrating the heterogeneity of audiences in relation to CCS attitudes. In particular, we found strong national variation in support, as well as local and demographic differences, and variation according to attitudes and values (e.g., climate change beliefs, environmental values, technophilia). This heterogeneity highlights the importance of understanding the local context in which information about CCS is provided or CCS developments proposed. Contrary to assumptions, local communities are not necessarily 'NIMBYs' (Not in My Backyard); rather, as we found, they may actually be strongly in favour of CCS implementation if they have positive experiences with similar technologies or the energy industry. Further, consistent with the persuasion literature (e.g., Petty & Cacioppo, 1986), targeting information to audience values is likely to be more effective than untargeted communication: technophiles and climate change believers are more likely to be receptive to CCS information, whereas those with 'deep green' values will tend to oppose it (however framed) as it does not offer deeper societal change believed to be required to tackle climate change.
  This places much emphasis on the importance of co-creation of communication materials, policies and even technology design, to address bespoke needs of individual communicates. Such co-created processes are likely to have higher chances of success as opposed to remotely developed, implemented strategies.
- *Engagement process is critical:* While we did not conduct face-to-face engagement with publics in CONTAIN, the literature and expert interviews show that the process of engaging communities or the general public with CCS can fundamentally shape acceptance of implementation. Two-way engagement (dialogue) is likely to more effective than one-way (information provision); furthermore, early and sustained engagement in which the public is substantively involved is likely to lead to more constructive and supported outcomes.
- *Trust is also important:* Trust is critical both to engagement processes, and to effective information provision: industry tends to be less trusted than scientists or environmental organisations, but trust in particular sources or organisations varies between communities and individuals (according to prior experiences and values).
- *Important parameters affecting trust are the perceived fairness or justice (both procedural and distributional) involved in proposed infrastructure projects including CCS projects. A fairly implemented project by a trusted organisation is more likely to succeed.*

In summary, project CONTAIN partly confirmed previous literature on public engagement with CCS; we also, more importantly, broke new ground in the field by comparing expert and lay opinions on CCS and engaging in the most extensive internationally comparative survey on CCS perceptions to date. Together, these elements advance a more global view on public engagement with CCS which we hope will help planners, practitioners and publics engage in meaningful co-design of climate mitigation projects now and in the future.

5 Conclusion

The three Work Packages of the CONTAIN project have delivered some major outcomes. WP1 outlines a phenomenological approach to assessing possible deformation during operation. WP2 expands this understanding by considering fractured caprock. WP3 offers new and valuable insight on future public awareness campaigns aimed at gaining acceptance of CCS. Project outcomes are summarised below:

- A valuable mechanical dataset has been acquired for Mercia Mudstone Group, Våle Shale, Sherwood Sandstone Group, and Bestwood Sandstone. This has been combined with new interpretations of data for Boom Clay, Callovo-Oxfordian mudstone, Penrith Sandstone, Darley Dale Sandstone, and Tennessee Sandstone.
- Critical state mechanics approach provides a robust framework that can be used to predict the onset of deformation in response to pore pressure changes during depletion and/or inflation.
- Four scenarios have been introduced based on strong/weak reservoirs and caprocks using drawdown and inflation scenarios for five North Sea fields.
- Weak caprocks are favourable as they can accommodate deformation, strong caprocks over a subsiding reservoir are subject to flexure forces that may result in fracturing.
- For CCS in virgin fields (saline aquifers), when deformation occurs this is likely to be through localised shear processes (fractures).
- Consideration has been given to varying degrees of available data:
    - A full suite of triaxial experiments is favourable
    - If core is limited, defining P^* and p'_c and assuming yield form is next preferable
    - Estimation of P^* from petrology and p'_c from burial history and assuming yield form is least preferable, but still applicable and requires conservatism.

- Discrete fracture mechanics is a viable caprock integrity methodology for small and large systems, of single and multiple geological layers.
- Accurately modelling the displacement effects following the depletion of the Goldeneye reservoir required the inclusion of discrete fractures.
- Fractures and faults are stressed in complex ways during production. A range of consistent effects were found across many fractures in the caprock.
- Due to the strongly localised aperture increase, tensile growth due to injection is more likely within the reservoir than in the caprock. This may indicate that re-inflation deformation may be partially accommodated by fracture growth within the reservoir itself. Further studies within a wider parametric space should follow.
- A new fully-coupled, finite element-based thermo-hydro-mechanical model incorporating discrete fractures has been developed.

- CONTAIN confirmed previous literature on public engagement with CCS. New ground was broken in the field by comparing expert and lay opinions on CCS and engaging in the most extensive internationally comparative survey on CCS perceptions to date.
    - Basic awareness is limited: Both the expert and public data show public awareness of CCS is low.
    - Framing effects are powerful: Our research shows that the way in which CCS is presented and discussed can strongly shape people's attitudes towards it.
    - Framing effects also depend on the broader context: They include and depend on what alternatives are provided.
    - Recognise diversity: Our work adds to the broader evidence demonstrating the heterogeneity of audiences in relation to CCS attitudes.

    - Engagement process is critical: Two-way engagement (dialogue) is likely to more effective than one-way (information provision)
    - Trust is also important: Trust is critical both to engagement processes, and to effective information provision:
- These elements advance a more global view on public engagement with CCS which will help planners, practitioners and public engage in meaningful co-design of climate mitigation projects now and in the future.

The integrated CONTAIN project has advanced our understanding of CCS during operation and the acceptability of CCS as a technological solution to climate change mitigation. The outcomes from the project will guide assessment of potential CCS sites and has highlighted areas of operation that require careful consideration.

6 Appendix

6.1 – CONTAIN OUTPUTS

Defoort, T., Paluszny, A., and Zimmerman, R.W. (2016) Comparison of fracture mechanics and damage mechanics approaches to simulate three-point bending and double-notch shear experiments on rock samples. Paper ARMA-2016-670. *50th U.S. Rock Mechanics/Geomechanics Symposium*, 26-29 June, Houston.

Defoort, T., Salimzadeh, S., Paluszny, A., and Zimmerman, R.W. (2015) A finite element geomechanical study of the brittle failure of a caprock due to deflation. Paper ARMA-2015-352. *49th U.S. Rock Mechanics/Geomechanics Symposium*, 28 June-1 July, San Francisco.

Dobbs, M.R., Cuss, R.J., Ougier-Simonin, A., Parkes, D., and Graham, C.C. (2018) Yield envelope assessment as a preliminary screening tool to determine carbon capture and storage viability in depleted southern north-sea hydrocarbon reservoirs. *International Journal of Rock Mechanics and Mining Sciences*, **102**, pp.15-27.

Dobbs, M.R., Ougier-Simonin, A., Graham, C.C., Cuss, R.J., and Harrington, J.F. (2015) CONTAIN: The geomechanics of candidate CCS reservoirs and seals *11th Euroconference on Rock Physics and Rock Mechanics.* Poster Session 2, board 09, 6 – 11 September 2015, Ambleside, UK.

Graham, C.C. (2014) Storing it under the seabed: Could we collect carbon dioxide in energy generation and store it underground in depleted oil and gas reservoirs? *Orkney Science Festival,* 9th September 2014.

Graham, C.C. (2015) CONTAIN Project. UKCCSRC Biannual Meeting, Cranfield, Invited talk.

Graham C.C., Harrington J.F., and Milodowski A.E. (2015) Experimentally Determined Transport and Consolidation Properties of the Mercia Mudstone Group. *Second EAGE Workshop on Geomechanics and Energy: Geomechanics for CO2 storage.* https://doi.org/10.3997/2214-4609.201414302.

Harrington, J.F. (2017) Hydromechanical properties of the Sherwood Sandstone. Database.

Harrington, J.F. (2017) Hydromechanical properties of the Mercia Mudstone Group. Database.

Harrington, J.F., Graham, C.C., Tamayo-Mas, E., and Parkes, D. (2018) Stress controls on transport properties of the Mercia Mudstone Group: Importance for hydrocarbon depletion and CO2 injection. *Marine and Petroleum Geology*, **93**, pp.391-408.

Paluszny, A., Salimzadeh, S., Tempone, P., and Zimmerman, R.W. (2017) Evaluating natural fracture growth in shale caprocks during cold CO_2 injection at the Heletz pilot site. ARMA 17-836. *51st U.S. Rock Mechanics/Geomechanics Symposium*, 25-28 June, San Francisco.

Paluszny, A., Thomas, R.N., and Zimmerman, R.W. (2018) Finite element-based simulation of the growth of dense three-dimensional fracture networks. ARMA 18–491. *52nd U.S. Rock Mechanics/Geomechanics Symposium*, 17–20th June, Seattle.

Parkes, D., Graham, C.C., Harrington, J.F., and Tamayo-Mas, E. (2016) Heterogeneity of the Mercia Mudstone Group: a review across the UK and influence on hydraulic properties. *UKCCSRC biannual meeting*, Edinburgh, poster presentation.

Salimzadeh, S., Paluszny, A., Nick. H.M., and Zimmerman, R.W. (2018) A three-dimensional coupled thermo-hydro-mechanical model for deformable fractured geothermal systems. *Geothermics*, **71**, 212-224.

Salimzadeh, S., Paluszny, A., and Zimmerman, R.W. (2017) Three-dimensional poroelastic effects during hydraulic fracturing in permeable rocks. *International Journal of Solids* and *Struct*ures, **108**, 153-163.

Salimzadeh, S., Paluszny, A., and Zimmerman, R.W. (2018) Effect of cold CO_2 injection on fracture apertures and growth. *International Journal of Greenhouse Gas Control*, **74**, 130-141.

Salimzadeh, S., Usui, T., Paluszny, A., and Zimmerman, R.W. (2017) Finite element simulations of interactions between multiple hydraulic fractures in a poroelastic rock. *International Journal of Rock Mechanics and Mining Sciences*, **99**, 9-20.

Thomas, R. N., Paluszny, A., and Zimmerman, R. W. (2017) Quantification of fracture interaction using stress intensity factor variation maps. *Journal of Geophysical Research: Solid Earth*, **122**(10), 7698–7717.

Thomas, R.N., Paluszny, A., and Zimmerman, R.W. (2018) Effect of fracture growth velocity exponent on fluid flow through geomechanically-grown 3D fracture networks. *2nd International Discrete Fracture Network Engineering Conference*. 20–22th June, Seattle.

Whitmarsh, L., Xenias, D., and Jones, R. (In Press). Framing effects on public support for carbon capture and storage. Submitted to *Nature Communications*

Xenias, D. (2016) Engaging the public with CCS: learning from experts. Presented at: *CCS in the UK: Moving forward*, Manchester, UK, 13-14th April 2016.

Xenias, D. (2016) Experts' views on engaging the public with CCS. Presented at: *SRA-Europe 2016 Conference*, Bath, UK, 20-22nd June 2016.

Xenias, D. (2017) Public engagement with CCS: barriers, key issues and ways forward. *Geophysical Research Abstracts*, **19**.

Xenias, D. and Whitmarsh, L. (2016) Learning from experts on public engagement with Carbon Capture and Storage. Presented at: *European Geosciences Union General Assembly 2016*, Vienna, Austria, 17-22nd April 2016.

Xenias, D. and Whitmarsh, L. (2017) Symposium: Carbon Capture, Utilisation and Storage (CCUS): perceptions and acceptance. Presented at: *International Conference of Environmental Psychology ICEP 2017*, A Coruna, Spain, 30 Aug - 1 Sept 2017.

Xenias, D. and Whitmarsh, L. (In Press). Carbon Capture and Storage (CCS) experts' attitudes to and experience with public engagement. *International Journal of Greenhouse Gas Control* (Accepted).

Project web page: https://www.bgs.ac.uk/co2contain/

6.2 APPENDIX 2: HYDRO-MECHANICAL DATA OF WP1

Material	Geotechnical Properties			
	Bulk Density	Dry Density	Porosity	Void Ratio
	Kg/m^3	Kg/m^3	%	
Captain Sandstone	2.15 - 2.70	1.89 - 2.69	1.0 - 27.7	0.001 - 0.383
Sherwood Sandstone Group (SSG1)	2.33 - 2.52	2.16 - 2.40	10.3 - 17.5	0.115 - 0.212
Sherwood Sandstone Group (SSG2)	2.09 - 2.10	1.75 - 1.78	32.3 - 34.0	0.478 - 0.515
Mercia Mudstone	2.30 - 2.35	2.07 - 2.11	22.4 - 23.8	0.288 - 0.313
Våle Shale	2.33 - 2.36	2.12 - 2.19	18.5 - 21.5	0.227 - 0.274
Callovo-Oxfordian	2.42	2.3	11.1 - 13.9	0.126 - 0.162

Table 1: Geotechnical properties of reservoir and caprock rock of WP1.

	Hydraulic Properties	Mechanical Properties							
Material	**Permeability**	**Poisson's Ratio**	**Young's Modulus**		**Bulk Modulus**	**Uniaxial Compressive Strength**	**Shear strength**	**Angle of friction**	**Grain crushing or preconsolidation stress**
	m^2	**-**	**Drained GPa**	**Undrained GPa**	**GPa**	**MPa**	**MPa**	**°**	**MPa**
Sherwood Sandstone Group (SSG1)	1.0×10^{-16}	0.27 - 0.31	24.79 - 36.95	/	21 – 23	101.2 - 117.6	26 - 35	28.4 - 37	170.5
Sherwood Sandstone Group (SSG2)	**/**	0.09 - 0.38	3.97 - 9.34	/	/	1.44 - 2.51	2.16	21.5	20.4
Mercia Mudstone	2.12×10^{-20} - 1.1×10^{-18}	0.25	/	/	0.92 - 3.74	/	/	/	30 - 37.1
Våle Shale	1.68×10^{-22} - 8.53×10^{-22}	0.22	/	1.99 - 2.36	1.48 - 5.28	23.59	16.55	5.5	33.8 - 43.0
Callovo-Oxfordian	**/**	0.3	/	/	1.52 - 7.76	/	/	/	/

Table 2: Hydro-mechanical properties of reservoir and caprock materials of WP1.

References

British Geological Survey holds most of the references listed below, and copies may be obtained via the library service subject to copyright legislation (contact libuser@bgs.ac.uk for details). The library catalogue is available at: http://geolib.bgs.ac.uk.

Armitage, P.J., Worden, R.H., Faulkner, D.R., Butcher, A.R. and Espie, A.A. (2016). Permeability of the Mercia Mudstone: suitability as caprock to carbon capture and storage sites. Geofluids, 16(1), pp.26-42.

Armitage, P.J., Worden, R.H., Faulkner, D.R., Aplin, A.C., Butcher, A.R. and Espie, A.A. (2013). Mercia Mudstone Formation caprock to carbon capture and storage sites: petrology and petrophysical characteristics. Journal of the Geological Society, 170, 119-132.

Arts RJ, Chadwick RA, Eiken O, Thibeau S, Nooner S. Ten years' experience of monitoring CO_2 injection in the Utsira Sand at Sleipner, offshore Norway. First Break. 2008; 26: 65–72.

Atkinson, J.H.and Bransby, P.L. (1978). The Mechanics of Soils: An Introduction to Critical State Soil Mechanics. McGraw-Hill, London.

Baud P, Vajdova V, Wong T-F. Shear-enhanced compaction and strain localization: Inelastic deformation and constitutive modeling of four porous sandstones. Journal of Geophysical Research: Solid Earth. 2006; 111: B12

Baud, P., Klein, E. and Wong, T.F., 2004. Compaction localization in porous sandstones: spatial evolution of damage and acoustic emission activity. *Journal of Structural Geology*, *26*(4), pp.603-624.

Bentham M. An assessment of carbon sequestration potential in the UK – Southern North Sea case study. Norwich, UK: Tyndall Centre for Climate Change Research, University of East Anglia, Working Paper 8; 2006.

Bentham M, Williams G, Vosper H, et al. Using pressure recovery at a depleted gas field to understand saline aquifer connectivity. Energy Proc. 2017;114:2906–2920.

Bickle MJ. Geological carbon storage. Nature Geoscience. 2009; 2: 815–18.

Biot, M.A. (1941). General theory of three-dimensional consolidation. Journal of Applied Physics, 12, 155 –164.

Boulin, P.F., Bretonnier, P., Vassil, C., Samouillet, A., Fleury, M. and Lombard, J.M. (2013). Sealing efficiency of caprocks: Experimental investigation of entry pressure measurement methods. Marine and Petroleum Geology, 48, 20-30.

British Standards Institution. 1990. BS 1377-2:1990. Methods of test for soils for civil engineering purposes. Classification tests. British Standards Institution, London.

Brook, M, Shaw, K, Vincent, C, Holloway, S. 2003. Storage and Potential of the Bunter Sandstone in the UK sector of the southern North Sea and the adjacent onshore area of Eastern England. *British Geological Survey Commissioned Report*, CR/03/154. 37pp

Cameron, TDJ, Crosby, A, Balson, PS, Jeffery, DH, Lott, GK, Bulat, J, And Harrison, DJ. 1992. *United Kingdom offshore regional report: the geology of the southern North Sea* (London: HMSO for the British Geological Survey)

Chadwick RA, Williams GA, Williams JDO, Noy DJ. Measuring pressure performance of a large saline aquifer during industrial-scale CO_2 injection: The Utsira Sand, Norwegian North Sea. International Journal of Greenhouse Gas Control. 2012; 10: 374-88.

Cooke-Yarborough.P The Hewett Field, Blocks 48/28-29-30, 52/4a-5a, UK North Sea *in Abbots, I.L. (ed.), 1991 United Kingdom Oil and Gas Fields, 25 Years Commemorative Volume, Geological Society Memoir No. 14, pp.433-442.*

Cuss R.J, Rutter EH, Holloway RF. The Application of Critical State Soil Mechanics to the Mechanical Behaviour of Sandstone. Int. J. of Rock Mech. and Min. Sci. 2003; 40: 847-62. DOI: 10.1016/S1365-1609(03)00053-4

Cuss, R.J., Harrington, J., Giot, R., and Auvray, C. (2014) Experimental observations of mechanical dilation at the onset of gas flow in Callovo-Oxfordian claystone. In: *Clays in Natural and Engineered Barriers for Radioactive Waste Confinement*; Norris, A., Bruni, J., Cathelineau, M., Delage, P., Fairhurst, C., Gaucher, E.C., Hohn, E.H., Kalinichev, A., Lalieux, P, and Sellin, P. (Eds), **400,** *Geological Society Special Publications*: London, United Kingdom, Geological Society of London, pp. 507-519, doi:10.1144/SP400.26

DECC. CCS Roadmap: Supporting deployment of Carbon Capture and Storage in the UK. London: Department of Energy and Climate Change; 2012.

DiMaggio FL, Sandler IS. Material model for granular soils. J. Eng. Mech. Div., Am. Soc. Civ. Eng. 1971; 97: 935-50

Dobbs, M.R., Cuss, R.J., Ougier-Simonin, A., Parkes, D. and Graham, C.C., 2018. Yield envelope assessment as a preliminary screening tool to determine carbon capture and storage viability in depleted southern north-sea hydrocarbon reservoirs. *International Journal of Rock Mechanics and Mining Sciences*, *102*, pp.15-27.

Downing RA, Burgess WG, Smith IF, Allen DJ, Price M and Edmunds WM (1982). Investigation of the geothermal potential of the UK; Geothermal aspects of the Larne No 2 Borehole London Institute of Geological Science NERC report.

Economides, MJ, Ehlig-Economides CA. Sequestering Carbon Dioxide in a Closed Underground Volume. Journal of Petroleum Science and Engineering. 2010; 70: 123–30.

Egermann, P., Lombard, J.M., Bretonnier, P. 2006. A fast and accurate method to measure threshold capillary pressure of caprocks under representative conditions. SCA 2006.

Engelder, T. (1992). Stress regimes in the lithosphere. Princeton University Press

Fortin, J., Stanchits, S., Dresen, G. and Guéguen, Y., 2006. Acoustic emission and velocities associated with the formation of compaction bands in sandstone. *Journal of Geophysical Research: Solid Earth*, *111*(B10).

Harrington, J.F., Birchall, D.J., Noy, D.J. and Cuss, R.J. (2007). Consolidation and mass transport properties of the Nordland Shale. *British Geological Survey Commissioned Report*. **CR/07/210**.

Harrington, J.F., Cuss, R.J., and Talandier, J. (2017[b]) Gas transport properties through intact and fractured Callovo-Oxfordian mudstones. In Rutter, E.H., Mecklenburgh, J. & Taylor, K.G. (eds) Geomechanical and Petrophysical Properties of Mudrocks. Geological Society, London, Special Publications, 454, https://doi.org/10.1144/SP454.7

Harrington, J.F., Cuss, R.J., Wiseall, A.C., Daniels, K.A., Graham, C.C., and Tamayo-Mas, E. (2017[a]) Scoping study examining the behaviour of Boom Clay at repository depths of interest to OPERA. *OPERA-PU-BGS523&616*, 215pp.

Harrington, J.F., Graham, C.C., Tamayo-Mas, E. and Parkes, D., 2018[a]. Stress controls on transport properties of the Mercia Mudstone Group: Importance for hydrocarbon depletion and CO2 injection. Marine and Petroleum Geology, 93, pp.391-408.

Harrington, J.F., Cuss, R.J., Wiseall. A.C., Dobbs, M., Daniels, K.A., Graham, C.C., Parkes, D., (2018[b]) CONTAIN: Experimental Investigation into hydro-mechanical properties of North Sea caprocks with respect to Carbon Capture Storage. BGS Open Report OR/18/037.

Haszeldine RS. Carbon capture and storage: How green can black be? Science. 2009; 325(5948): 1647–52.

Hobbs P R N, Hallam J R, Forster A, Entwisle D C , Jones L D, Cripps A C, Northmore K J, Self S J, Meakin J L (2002) *Engineering geology of British rocks and soils - Mudstones of the Mercia Mudstone Group.* British Geological Research Report, RR/01/02. 106pp.

Hoek E, Carranza-Torres C, Corkum B. Hoek-Brown Failure Criterion – 2002 Edition. In: Proceedings of the. NARMS-TAC Conference. University of Toronto, Toronto; 10 July 2002. pp. 267–73.

Hoek E, Diederichs MS. Empirical estimation of rock mass modulus. Int. J. of Rock Mech. & Min. Sci. 2006; 43: 203–15

Holloway S, Vincent CJ, and Kirk KL. Industrial carbon dioxide emissions and carbon dioxide storage potential in the UK. Keyworth, Nottingham: British Geological Survey, CR/06/185N; 2006.

Horseman, S.T., Higgo, J.J.W., Alexander, J. and Harrington, J.F. (1996). Water, gas and solute movement in argillaceous media. Rept. No. CC-96/1 to OECD/NEA Working Group on Measurement and Physical Understanding of Groundwater Flow through Argillaceous Media. Nuclear Energy Agency, OECD, Paris.ISBN 92-64-1488-1.

Horseman, S.T., Winter, M.G., Entwistle, D.C. (1993). Triaxial experiments on Boom Clay. In: Cripps, J.C., Coulthard, J.M., Culshaw, M.G., Forster, A., Hencher, S.R., Moon, C.F. (Eds.). The Engineering Geology of Weak Rock. Balkema, Rotterdam, 36–43.

Horseman, S.T., Harrington, J.F., Birchall, D.J., Noy, D.J. and Cuss, R.J. (2005). Consolidation and rebound properties of Opalinus Clay: A long term fully-drained test. British Geological Survey Commissioned Report. CR/05/128. 60pp.

Hvorslev, M.J. (1937). Uber die fesigkeitseigenshaften gestorter bindinger boden, Ingvidensk. Skr., 45.

Johnson H, Leslie AB, Wilson CK, Andrews IJ and Cooper RM (2005). Middle Jurassic, Upper Jurassic and Lower Cretaceous of the UK Central and Northern North Sea. British Geological Survey Research Report, RR/03/001. 42pp.

Klein, E., Baud, P., Reuschlé, T. and Wong, T.F., 2001. Mechanical behaviour and failure mode of Bentheim sandstone under triaxial compression. *Physics and Chemistry of the Earth, Part A: Solid Earth and Geodesy*, *26*(1-2), pp.21-25.

Louis, L., Baud, P. and Wong, T.F., 2009. Microstructural inhomogeneity and mechanical anisotropy associated with bedding in Rothbach sandstone. *Pure and applied geophysics*, *166*(5-7), pp.1063-1087.

Mathieson A, Midgley J, Dodds K, Wright I, Ringrose P, Saoul N. CO_2 sequestration monitoring and verification technologies applied at Krechba, Algeria. The Leading Edge. 2010; 29(2): 216-22.

Noy, D.J.; Holloway, S.; Chadwick, R.A.; Williams, J.D.O.; Hannis, S.A.; Lahann, R.W (*2012*) Modelling large-scale carbon dioxide injection into the Bunter Sandstone in the UK Southern North Sea. *International Journal of Greenhouse Gas Control*, *9. 220-233.*

Parkes D, Graham C C, Harrington J F, Cuss R J, Ougier-Simonin A, (2014). *CONTAIN D1: Identification of candidate geologies and experimental approach.* British Geological Survey Open Report, OR/15/008. 93pp.

Pinnock S J, and Clitheroe A R J, (1997). *The Captain Field, UK North Sea: appraisal and development of a viscous oil accumulation.* Petroleum Geoscience, 3, 305-312.

Roscoe, K.H., Schofield, A. and Wroth, C.P. (1958). On the yielding of soils. Géotechnique, 8, pp. 22-53.

Rose (1999). *Reservoir characterization in the Captain Field: integration of horizontal and vertical well data,* in Fleet A J, and Boldy S A R, (eds) Petroleum Geology of Northwest Europe: Proceedings of the 5th Conference, 1101-1113.

Ruistuen, H., Teufel, L.W. and Rheff, D. (1999). Influence of reservoir stress path on deformation and permeability of weakly cemented sandstone reservoirs, Society of Petroleum Engineers Reservoir Evaluation and Engineering, 2(3), 266-272.

Rutter, E.H. and Glover, C.T., 2012. The deformation of porous sandstones; are Byerlee friction and the critical state line equivalent?. *Journal of Structural Geology*, *44*, pp.129-140.

SCCS (2015). Optimising CO2 storage in geological formations; a case study offshore Scotland.

Schofield, A., and Wroth, C.P. (1968) Critical State Soil Mechanics. London, McGraw-Hill, 310 pp.

Scott, C. R. (1980). An Introduction to Soil Mechanics and Foundations. 3rd Edition. Applied Science Publishers LTD.

Sheldon, H.A., Barnicoat, A.C. and Ord, A. (2006). Numerical modelling of faulting and fluid flow in porous rocks: an approach based on critical state soil mechanics. Journal of Structural Geology, 28(8), pp.1468-1482.

Shell. Geomechanics Summary Report. Scottish Power CCS Consortium, UK Carbon Capture and Storage Demonstration Competition Report, UKCCS-KT-S7.19-Shell004; 2011.

Ulusay R, Hudson JA, eds. The Complete ISRM Suggested Methods for Rock Characterization, Testing and Monitoring: 1974-2006. Ankara, Turkey: Commission on Testing Methods, International Society of Rock Mechanics; 2007:2007.

Van Thienen-Visser K, Breunese JN. Induced seismicity of the Groningen gas field: History and recent developments. The Leading Edge. 2015; 34(6): 664-71.

Verdon JP, Kendall JM, Stork AL, Chadwick RA, White DJ, Bissell RC. Comparison of geomechanical deformation induced by megatonne-scale CO_2 storage at Sleipner, Weyburn, and in Salah. Proceedings of the National Academy of Sciences. 2013; 110(30): E2762-71.

Wenk, H.-R., Voltolini, M., Mazurek, M., Van Loon, L.R. and Vinsot, A. (2008) Preferred Orientations and Anisotropy in Shales: Callovo-Oxfordian Shale (France) and Opalinus Caly (Switzerland), *Clays and Clay Minerals*, **56**, pp 285-306.

Whitlow, R. (2001). Basic soil mechanics. Pearson Prentice Hall, fourth edition, ISBN 0582-38109-6.

Williams, J.D.O., Jin, M., Bentham, M., Pickup, G.E., Hannis, S.D. and Mackay, E.J., 2013. Modelling carbon dioxide storage within closed structures in the UK Bunter Sandstone Formation. *International Journal of Greenhouse Gas Control*, *18*, pp.38-50.

Wilson M, Monea M. IEA GHG Weyburn CO_2 monitoring & storage project. Summary report 2000-2004. Regina, SK, Canada: Petroleum Technology Research Centre; 2004.

Wiseall, A.C., Graham, C.C., Zihms, S.G., Harrington, J.F., Gregory, S., Shaw, R.P. (2015). Properties and Behaviour of the Boom Clay Formation within a Dutch Repository Concept, COVRA comimissioned report BGS, OPERA-PU-BGS615.

Wong T-F, David C, Zhu W. The transition from brittle faulting to cataclastic flow in porous sandstones mechanical deformation. J. Geophys. Res. B. 1997; 102(2): 3009–25.

Wong, T.F. and Baud, P., 2012. The brittle-ductile transition in porous rock: A review. *Journal of Structural Geology*, *44*, pp.25-53.

Zhu W, Wong T-F. Shear-enhanced compaction in sandstone under nominally dry and water-saturated conditions. Int. J. Rock Mech. Min. Sci. 1997; 34: 372.

Zhu, W. and Wong, T.F., 1997. The transition from brittle faulting to cataclastic flow: Permeability evolution. *Journal of Geophysical Research: Solid Earth*, *102*(B2), pp.3027-3041.

Zoback MD, Gorelick SM. Earthquake triggering and large-scale geologic storage of carbon dioxide. Proc. Natl. Acad. Sci. USA. 2012; 109(26): 10164–68.

Zoback, M. D. (2010). Reservoir geomechanics. Cambridge University Press.

Zoback, MD, Zinke JC. Production-induced normal faulting in the Valhall and Ekofisk oil fields. In: The Mechanism of Induced Seismicity, CI Trifu, editor. Basel: Birkhäuser; 2002. pp. 403-20.